Spot Pricing Principles in Distribution Grids: From Local Market Organization to Multi-regional Coordination

Kai Zhang, M. Sc.

Vollständiger Abdruck der von der Fakultät für Elektrotechnik und Informationstechnik der Technischen Universität München zur Erlangung des akademischen Grades eines

Doktor-Ingenieurs (Dr.-Ing.)

genehmigten Dissertation.

Vorsitzender:

Prof. Dr.-Ing. habil. Erwin Biebl

Prüfer der Dissertation:

1. Prof. Dr. rer. nat. Thomas Hamacher

2. Prof. Jalal Kazempour, Ph.D.

Die Dissertation wurde am 17.08.2020 bei der Technischen Universität München eingereicht und durch die Fakultät für Elektrotechnik und Informationstechnik am 03.08.2021 angenommen.

Abstract

Given recent discussions of forming a liberalized market at the distribution grid level, this dissertation focuses on the coordinated market framework. Based on spot pricing principles, the market framework comprises market structures and pricing schemes that allow greater economic efficiency and continued satisfactory operation of the distribution grid in a decentralized manner. We focus on the following research areas at two hierarchical levels. At a lower level, a market framework that comprises a coordinated market-clearing model for i) a centralized distribution grid operator (DSO) market for ancillary services (ASs) in distribution grids and, ii) a fully decentralized market for peer-to-peer (P2P) energy trade. The P2P market enables the bilateral transaction between prosumers, whereas the ASs market is supposed to procure sufficient resources for improving the local/upstream grid stability. This is because the grid constraint violation is the major challenge for P2P energy sharing in the low-voltage (LV) distribution grid, despite its appealing perspective in enabling a consumer-centered market. To mitigate the grid-constraint-violation issue, we envision that the AS market can be organized by DSO that utilizes distributed energy resources (DERs) to improve economic efficiency. To regulate and encourage the market participants in the P2P market towards "grid-friendly" behavior, a grid usage pricing (GUP) scheme is developed to interlink the decoupled markets. By calculating the decomposable distribution locational marginal prices (DLMPs), the essential price information of providing ASs can be recovered to allocate the grid usage cost to each P2P transaction. By examining the composition of GUPs, we show that it serves as price signals to incentivize the P2P market to support the grid operation in terms of loss reduction, voltage support and congestion management. The duality analysis of the coordinated market-clearing model provides the analytical results for the composition of P2P trading prices and their interpretations. Moreover, a numerical analysis demonstrates the effectiveness of the market design to support grid operational objectives of loss reduction, congestion management, and voltage control. At a higher level, the region-to-region coordination between the local distribution grid markets is proposed. In principle, each distribution grid regional operators maximizes its social-welfare, which is the local (regional) version of the overall social-welfare maximization problem. The individual problem incorporates the coupled physical information (voltage magnitude, angles and line flows) from its neighboring regions. The consensus regarding these state variables of all regions is enforced through the proposed **C**onsensus-**A**lternating direction method of multipliers **S**tructured **T**rust-**r**egion (CAST) algorithm. On convergence, DLMPs are recovered for each region, which is novel in the sense that on one hand they are computed in a distributed manner, i.e. with preserving local information, and, on another side, they accurately represent loss allocation from the neighboring regions. The framework hierarchically coordinates information, while aiming to achieve consensus by sharing physically coupled information among multiple regional operators. The proposed methodologies are further validated with numerical examples.

Zusammenfassung

Dieser Arbeit konzentriert sich auf den koordinierten Ordnungsrahmen für die Aufstellung eines liberalisierten Marktes im Verteilungsnetz. Auf der Grundlage von Spot-Pricing-Grundsätzen umfasst der vorgeschlagen Ordnungsrahmen die Marktstruktur und Preisschema, die eine höhere Wirtschaftlichkeit und einen weiterhin zufriedenstellenden dezentralen Betrieb des Verteilungsnetzes ermöglichen. Die folgende Forschungsbereiche auf zwei hierarchischen Ebenen werden untersucht. Auf der niedrigeren Ebene, der Ordnungsrahmen umfasst ein koordiniertes Marktbereinigungsmodell für i) einen zentral oganisierten DSO-Markt für Systemdienstleistungen (ASs) in Verteilungsnetzen und ii) einen vollständig dezentralisierten Markt für Peer-to-Peer (P2P) Energiehandel. Der P2P-Markt ermöglicht die bilaterale Transaktion zwischen Prosumern, während der AS-Markt aus Gründen der lokalen/globalen Netzstabilität ausreichende Ressourcen beschaffen soll. Dies liegt daran, dass der Verstoß gegen die Netzbeschränkung die grösste Herausforderung für den P2P Energiehandel im Niederspannungsverteilungsnetz darstellt, obwohl die Ermöglichung eines verbraucherorientierten Marktes attraktiv ist. Um das Problem des Verstoßes gegen die Netzbeschränkung zu mindern, schlagen wir vor, dass der AS-Markt vom DSO organisiert werden kann, der verteilte Energieressourcen (DERs) koordiniert, um die Wirtschaftlichkeit zu verbessern. Um die Marktteilnehmer im P2P-Markt zu "netzfreundlichem" Verhalten zu animieren, wird ein Netznutzungspreis (GUP) entwickelt, der die entkoppelten Märkte miteinander verknüpft. Durch die Berechnung der zerlegbaren Distribution Location Marginal Prices (DLMPs) können die wesentlichen Preisinformationen für die Bereitstellung von ASs wiederhergestellt werden, um die Netznutzungskosten jeder P2P-Transaktion zuzuordnen. Anhand der Zusammensetzung der GUPs zeigen wir, dass sie als Preissignale dienen, um den P2P-Markt anzuregen, den Netzbetrieb in Bezug auf Verlustreduzierung, Spannungsunterstützung und Engpassmanagement zu unterstützen. Die Dualitätsanalyse des koordinierten Marktbereinigungsmodells liefert die Ergebnisse für die Zusammensetzung der P2P-Handelspreise und deren Interpretation, während eine numerische Analyse die Wirksamkeit des Marktdesigns zur Unterstützung der Netzbetriebsziele (Verlustminderung, Engpassmanagement und Spannungsregelung) demonstriert. Auf der höheren Ebene wird die regionale Koordinierung zwischen den lokalen Verteilnetzmärkten untersucht. Grundsätzlich maximiert jeder regionale Verteilungsnetzbetreiber seine gesamtwirtschaftliche ökonomische Wohlfahrt, was die lokale (regionale) Version des allgemeinen Problems der Maximierung der ökonomischen Wohlfahrt darstellt. Das individuelle Problem bezieht die gekoppelten physikalischen Informationen (Spannungsgrösse, Spannungswinkel und Lastfluss) aus seinen Nachbarregionen ein. Der Konsens von diesen Zustandsvariablen aller Regionen wird durch die vorgeschlagene Methode **C**onsensus-**A**lternating direction method of multipliers **S**tructured **T**rust-**r**egion (CAST) erzwungen. Bei Konvergenz wird der DLMP für jede Region erhalten. Dies ist insofern neu, als er einerseits verteilt berechnet wird, d.h. unter Beibehaltung lokaler Informationen, und andererseits die Verlustverteilung aus verschiedenen Nachbarregionen darstellt. Die Ordnungsrahmen koordiniert Informationen hierarchisch und strebt gleichzeitig einen Konsens an, indem physisch gekoppelte Informationen zwischen mehreren regionalen Betreibern ausgetauscht werden. Die vorgeschlagenen Methoden werden in der numerischen Analyse validiert.

Acknowledgements

I would like to express my sincere gratitude to the many people who have dedicated their time to help me to complete this work at hand. I feel very fortunate to be supervised by Dr. Thomas Hamacher, who has provided me with supportive guidance and thoughtful inspirations throughout my four years' time at TUMCREATE. I am also grateful for the valuable assistance and advice provided by Dr. Tobias Massier as well as the opportunity to conduct my research work in Singapore.

I am very thankful for the numerous discussions with Dr. Sarmad Hanif and Sebastian Troitzsch. I am very fortunate to have them to solve problems together when encountering bottlenecks and issues. There have been many colleagues and PhD students, whom I've been working with in this work. These include Andrej Tropovski, Soner Candas and many others. The experience to share the knowledge are very beneficial and essential to orient myself in the research work. Furthermore, Dr. Christoph Hackl's instructions have provided me with strong foundations in numeric modeling.

As the time of writing, I have begun with my marriage life. I will express my deepest gratitude to my families. I will forever remain indebted for their selfless dedication. At last, I gratefully acknowledge that this work was financially supported by the Singapore National Research Foundation under its Campus for Research Excellence And Technological Enterprise (CREATE) programme.

Contents

List of Figures

List of Tables

List of Algorithms

Nomenclature

Scalars are denoted with lower-case letters, i.e., x, whereas vectors and matrices are in bold letters, i.e., $\mathbf{x}, \mathbf{X}$. We specify the entries of a matrix $\mathbf{X}$ by x_{ij} and the entries of a vector $\mathbf{x}$ by x_i. For multiple regions in distribution grids, the regional version of a variable/parameter $\mathbf{x}$ i is indexed as $\mathbf{x}_i$. Conjugates of a complex scalar, vector or matrix are denoted with underline, i.e., $\underline{x}, \underline{\mathbf{x}}, \underline{\mathbf{X}}$. The obtained optimal solutions are denoted as $x^*, \mathbf{x}^*$. For complex scalars, vectors or matrices, $\Re(), \Im()$ are used to extract the real and imaginary part. The transpose of a vector or matrix is denoted by $()^\intercal$ and diag$(\mathbf{x})$ constructs a diagonal matrix using vector $\mathbf{x}$ as the diagonal elements. $|x|$,$|\mathbf{x}|$ is for extracting the magnitude of a complex quantity. Note tuning parameters in various algorithms are excluded here. Terms "bus" and "node" are interchangeable throughout of the work. $\jmath$ is the imaginary unit with $\jmath^2 = -1$ (where ":=" means "is defined as").

Number Sets

$\mathbb{C}$	Complex Numbers
$\mathbb{R}$	Real Numbers
$\mathcal{B}$	Buyer Nodes, $\mathcal{B} := \{1, 2, ..., b\}$
$\mathcal{F}$	Flexible loads (FLs), $\mathcal{F} := \{1, 2, ..., fl\}$
$\mathcal{G}$	Distributed generators (DGs), $\mathcal{G} := \{1, 2, ..., g\}$
$\mathcal{H}$	Grid lines, $\mathcal{H} := \{1, 2, ..., h\}$
$\mathcal{L}$	PQ Nodes, $\mathcal{L} := \{1, 2, ..., n\}$
$\mathcal{N}$	All Grid Nodes, $\mathcal{N} := \{0, 1, 2, ..., n\}$
$\mathcal{S}$	Seller Nodes, $\mathcal{S} := \{1, 2, ..., s\}$

Constants

η^{ch}	Charge efficiency factor
η^{d}	Discharge efficiency factor
b	Buyers number
fl	FL number

g DG number

h Grid lines number

n Grid nodes number (excluding root-node)

r Regions number in distribution grids

s Sellers number

sl Static (non-elastic) loads number

Model Parameters

$\mathbf{A}^{\mathsf{x}}$ Mapping matrices to grid nodes, $\mathbf{A}^{\mathsf{x}} \in \mathbb{R}^{x\times(n+1)}, \mathsf{x} \in \{\mathsf{g}, \mathsf{fl}, \mathsf{sl}\}$

$\mathbf{C}^{\mathsf{f}}, \mathbf{C}^{\mathsf{t}}$ Mapping matrices of "from"/"to" nodes to grid nodes, $\mathbf{C}^{\mathsf{f}}, \mathbf{C}^{\mathsf{t}} \in \mathbb{R}^{h\times(n+1)}$

$\mathbf{c}^{\mathsf{x}}$ Cost coefficient of market bids, $\mathbf{c}^{\mathsf{x}} \in \mathbb{R}^{x}, \mathsf{x} \in \{\mathsf{g}, \mathsf{fl}\}$

$\mathbf{d}^{\mathsf{x}}$ Cost coefficient of market bids, $\mathbf{c}^{\mathsf{x}} \in \mathbb{R}^{x}, \mathsf{x} \in \{\mathsf{g}, \mathsf{fl}\}$

$\mathbf{m}_{\mathcal{L}}^{\mathsf{pp}}$ Senstivity matrix of slack node active power injection with respect to active power injections at PQ buses $\mathbf{m}_{\mathcal{L}}^{\mathsf{pp}} \in \mathbb{R}^{1\times n}$

$\mathbf{m}_{\mathcal{L}}^{\mathsf{pq}}$ Senstivity matrix of slack node active power injection with respect to reactive power injections at PQ buses $\mathbf{m}_{\mathcal{L}}^{\mathsf{pq}} \in \mathbb{R}^{1\times n}$

$\mathbf{m}_{\mathcal{L}}^{\mathsf{qp}}$ Senstivity matrix of slack node reactive power injection with respect to active power injections at PQ buses $\mathbf{m}_{\mathcal{L}}^{\mathsf{qp}} \in \mathbb{R}^{1\times n}$

$\mathbf{m}_{\mathcal{L}}^{\mathsf{qq}}$ Senstivity matrix of slack node reactive power injection with respect to reactive power injections at PQ buses $\mathbf{m}_{\mathcal{L}}^{\mathsf{qq}} \in \mathbb{R}^{1\times n}$

$\mathbf{M}_{\mathcal{L}}^{\mathsf{vp}}$ Sensitivity matrix of voltage magnitudes w.r.t. active power injections at PQ nodes, $\mathbf{M}_{\mathcal{L}}^{\mathsf{vp}} \in \mathbb{R}^{n\times n}$

$\mathbf{M}_{\mathcal{L}}^{\mathsf{vq}}$ Sensitivity matrix of voltage magnitudes w.r.t. reactive power injections at PQ nodes, $\mathbf{M}_{\mathcal{L}}^{\mathsf{vq}} \in \mathbb{R}^{n\times n}$

$\mathbf{m}_{\mathcal{L}}^{\mathsf{vv}}$ Senstivity matrix of voltage magnitudes at PQ nodes with respect to slack node voltage magnitude, $\mathbf{m}_{\mathcal{L}}^{\mathsf{vv}} \in \mathbb{R}^{n\times 1}$

$\mathbf{M}_{\mathcal{L}}^{\theta\mathsf{p}}$ Sensitivity matrix of voltage angles w.r.t. active power injections at PQ nodes, $\mathbf{M}_{\mathcal{L}}^{\theta\mathsf{p}} \in \mathbb{R}^{n\times n}$

$\mathbf{M}_{\mathcal{L}}^{\theta\mathsf{q}}$ Sensitivity matrix of voltage angles w.r.t. reactive power injections at PQ nodes, $\mathbf{M}_{\mathcal{L}}^{\theta\mathsf{q}} \in \mathbb{R}^{n\times n}$

$\mathbf{m}_{\mathcal{L}}^{\theta\mathsf{v}}$ Senstivity matrix of voltage angles at PQ nodes with respect to slack node voltage magnitude, $\mathbf{m}_{\mathcal{L}}^{\theta\mathsf{v}} \in \mathbb{R}^{n\times 1}$

$\mathbf{Q}$ Battery capacity vector

$\mathbf{Y}$ Nodal admittance matrix, $\mathbf{Y} \in \mathbb{C}^{(n+1)\times(n+1)}$

$m^{\mathsf{pv}} \in \mathbb{R}$ Senstivity of slack node active power injections with respect to slack node voltage magnitudes, $m^{\mathsf{pv}} \in \mathbb{R}$

$m^{\mathsf{qv}} \in \mathbb{R}$ Senstivity of slack node reactive power injections with respect to slack node voltage magnitudes, $m^{\mathsf{qv}} \in \mathbb{R}$

y_{ij} Admittance of line (i, j)

Primal Variables

$\boldsymbol{\theta}$ Voltage angle vector, $\boldsymbol{\theta} \in \mathbb{R}^{n+1}$

$\mathbf{E}$ Energy transfer matrix between seller and buyer node in P2P trade, $\mathbf{E} \in \mathbb{R}^{s \times b}$

$\mathbf{p}$ Active power nodal injection, $\mathbf{p} \in \mathbb{R}^{n+1}$

$\mathbf{p}^{\mathsf{x}}$ Active power injection from DGs, FLs, static loads, sellers, buyers, $\mathbf{p}^{\mathsf{x}} \in \mathbb{R}^{x}, \mathsf{x} \in \{\mathsf{g}, \mathsf{fl}, \mathsf{sl}, \mathsf{s}, \mathsf{b}\}$

$\mathbf{q}$ Reactive power nodal injection, $\mathbf{q} \in \mathbb{R}^{n+1}$

$\mathbf{q}^{\mathsf{g}}$ Reactive power injection from DGs, $\mathbf{q}^{\mathsf{g}} \in \mathbb{R}^{g}$

$\mathbf{s}$ Complex nodal injection, $\mathbf{s} = \mathbf{p} + \jmath\mathbf{q} \in \mathbb{R}^{n+1}$

$\mathbf{s}^{\mathsf{f/t}}$ Complex "from"/"to" line flow, $\mathbf{s}^{\mathsf{f/t}} = \mathbf{p}^{\mathsf{f/t}} + \jmath\mathbf{q}^{\mathsf{f/t}} \in \mathbb{C}^{h}$

$\mathbf{u}$ Complex voltage vector $\mathbf{u} := \mathbf{v}\mathbf{e}^{\jmath\boldsymbol{\theta}} \in \mathbb{C}^{n+1}$

$\mathbf{v}$ Voltage magnitude vector, $\mathbf{v} \in \mathbb{R}^{n+1}$

p^{loss} Active power loss, $p^{\mathsf{loss}} \in \mathbb{R}$

q^{loss} Reactive power loss, $q^{\mathsf{loss}} \in \mathbb{R}$

Dual Variables

λ Dual variables for equality constraints

Λ, Φ Energy exchange prices for P2P trade

μ, ν Dual variables for inequality constraints

Π Grid usage prices for P2P trade

π Distribution locational marginal prices

π^{c} Distribution locational marginal prices: congestion part

π^{e} Distribution locational marginal prices: energy part

π^{e} Distribution locational marginal prices: loss part

π^{v} Distribution locational marginal prices: voltage part

Chapter 1

Introduction

1.1 Background

1.1.1 Discussions on transactive energy paradigm in distribution grid

Due to its convenience to transfer energy, electricity has been adapted in vast, growing applications in our daily life and becomes the backbone of the economy and technology. Power system is built to supply, transfer and utilize electric power. The system has been continuously growing ever since its emergence during the second industrial revolution. In the past, electric power systems used to contain a few large-scale generation facilities that supplied energy to the passive loads. Recently, due to the renewable integration and market liberalization, this arrangement is slowly transforming into a multiple-layered, cyber-physical intelligent grid with active loads and small-scale renewable generators. In view of the evolution of the electricity market, the integration of the distributed resources and installation of new demand-side management technologies are the cornerstones that pave way for the decarbonization of the electricity sector, where the distribution grid is likely to accommodate the distributed energy resources (DERs). This entails new control technologies along with market frameworks for their cost-effective integration.

In line with the DER integration and market deregulation process, there is an increasing interest in proposing decentralized grid operation, e.g., microgrids [3], virtual power plant (VPP) [4]. The technologies provide opportunities for demand-side-management in the distribution grids. By enabling the decentralized operations, the vision of smart grids on the market liberalization process promises new market and regulatory paradigms for efficient energy markets at the distribution grid level, which ends the monopoly of the electricity utility company. From the bulk system operation's perspective, the distribution grids cannot be simply integrated in the current transmission level markets [5]. Fundamentally, the difficulty originates from the fact that distribution grids have i) higher nonlinearities in the power flow due to the high R/X ratio, and ii) larger number of nodes compared to transmission grids. This brings practical challenges to the grid operation, which necessitate different forms of services such as voltage control and congestion management (conventionally provided by Distribution System Operator (DSO)). With the integration of DERs, there is a potential to use market mechanisms to procure the grid operation services from DERs, which eventually leads to more efficient grid management and

lower prices of electricity.

In light of this, this fundamental transformation towards the distribution grid market shall be accompanied by the evolution of DSO model. Conventionally, the power system is organized to facilitate the energy flow from the high-voltage transmission system to low-voltage distribution grid and then to the end-customers and DSOs are the asset owners and the grid operators that maintain the local distribution grid stability. In line with the discussion on transactive energy paradigm (see, e.g., [6, 7]), an independent DSO model is introduced that is envisioned to have the function of both grid operator and market operator. In the aspect of the grid operation function, it is supposed to be an independent, not-for-profit entity to coordinate, control and monitor the local distribution systems. For market operation function, DSO is assumed to operate the energy market and the ancillary service (AS) market in different time scales to achieve a cost-effective allocation of grid operation resources. With the development of these new concepts, technologies and mechanisms, the electricity market at the distribution grid will be undergoing significant structural changes in the coming decades.

1.1.2 Spot pricing principles and distribution grids operation

In the transmission grid, the electricity spot markets have been established since the 1980s when the electricity pricing theory was introduced by Fred C. Schweppe et al in the work "Spot Pricing of Electricity" [8]. The introduced pricing concept is termed as "spot pricing principle" and later on implemented to liberalize the electricity sector in various countries. Markets that adopt the spot pricing principles are established around the globe and may varying implementation in different countries, e.g., the North America market and Nord Pool in Europe.

Based on spot pricing theory, rules for optimal short-run decisions and long-run actions, e.g., system planning, can be derived. The general procedure to derive spot prices is based on solving the social welfare optimization problem subject to energy balance and network constraints. Then the resulting spot prices can be explicitly given as [9]:

$$\begin{aligned}\text{Optimum Spot Price} = &\text{Marginal Generator Cost}\\ &+ \text{Energy Balance Quality of Supply Premium}\\ &+ \text{T\&D Network Quality of Supply Premium},\end{aligned} \tag{1.1}$$

where the Marginal Generator Cost[1] is the incremental fuel cost of the marginal generator. Energy Balance Quality of Supply Premium is the premium to reduce the demand or increase the supply to maintain the energy balance constraint. The premium is equal to zero when there is a surplus generation or tie-line capacity. T&D Network Quality of Supply Premium is the price signal (non-negative when the network constraints are binding) sent to customers so that they can adjust their consumption behavior to remove the line congestion and voltage violations. The location-specific cost are also termed as locational marginal price (LMP).

Based on the spot pricing principle, a typical market design in the current wholesale market implementation can be followed by step i) the submission of supply

[1] It is also termed as marginal fuel cost in [9]

offers by electricity generators, step ii) the submission of (fixed) demand by load aggregators, and step iii) the aggregation of supply offers to form a system dispatch curve based on their merit order and clearance of the market at the point, where the dispatch curve intersects the (fixed) level of demand by the transmission grid operator. Those generators with supply offers below the market-clearing point are dispatched while those with supply offers above the market clearing point are not dispatched. Given no tie-line congestion, all the generator facilities upon market-clearing will get paid by the same marginal price. When there is transmission congestion, the marginal cost of meeting demand in one location will be different from the marginal cost of meeting demand in another location due to the different costs and supply offers by generators. The spot pricing principle is not only used for the procurement of electricity but also can be used to procure the ASs like reserves for frequency control and ramping support. The financial settlement for the some types of ASs can be calculated by T&D Network Quality of Supply Premium in (1.1) in an integrated market environment. One example that adopts the integrated market design is the California market (CalPX) [10, 11].

With the shift of generation and active demand-side management to the distribution system, notable effort in the research community to extend the current wholesale market is made for the distribution grid context. Fundamentally, the driving forces for the increasing propositions to extend the spot pricing principles to distribution grid are:

- the decreasing grid inertia at the bulk system level due to the integration of renewable energy resources shifts some of the grid operation tasks, e.g., provision of reserve capacity, to the distribution grid,
- the continuous improvement of communication infrastructure and the deployment of enabling technologies such as IoT (Internet-of-Things) devices, smart meters and advanced control devices for demand-side management,
- the need of incentives provision for the aggregation of the DERs to respect the local distribution system constraints.

To this end, the coordination mechanism between different system levels such as transmission grid, distribution grids, and DERs needs to be developed. Particularly, in the center of the enabling technology is the concept of active distribution grid, which is envisioned to be a smart low-voltage grid that is capable of real-time monitoring of its feeding area and utilizes the flexibility of DERs to enhance the hosting capacity of the network [12]. With the advanced data analysis and control capability, the active distribution grid is essential to fulfill the promise of transactive energy in the future.

1.1.3 Distribution grid market through DLMPs

With the deployment of enabling technologies and regulatory frameworks, a generic distribution grid market can be cast as in Fig. 1.1. In essence, the DSO procures energy and ASs either from upstream wholesale market or from local DERs. After the local grid demand is satisfied, DSO can make additional capacity available to the transmission grid. This kind of organization introduces the interface of DSO

between small-scale DERs and the bulk system. Note that different coordination schemes can be organized between DSO and transmission system operator (TSO) level, which has been a study object for a notable number of projects and proposals (see, e.g., [13, 5, 14, 15]).

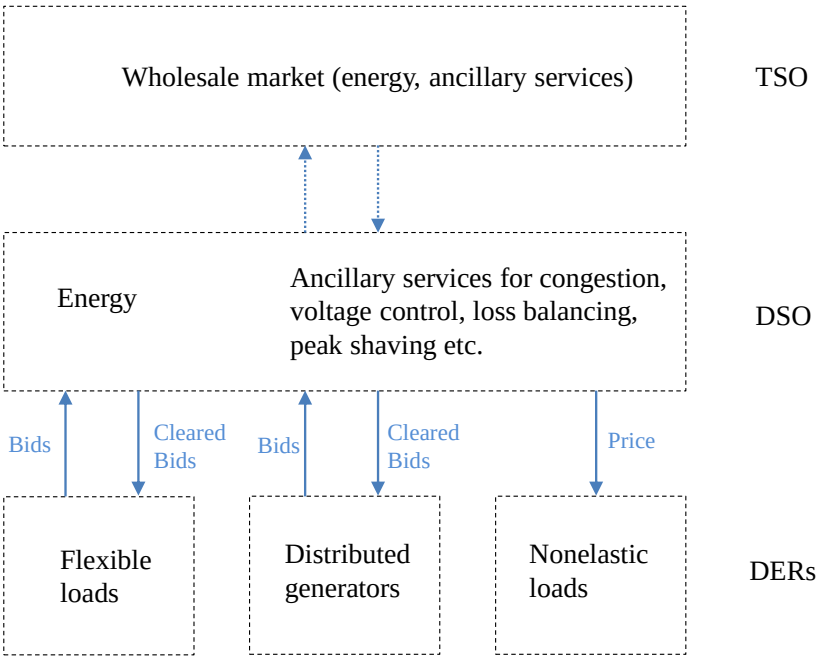

Fig. 1.1: Overview of market layers.

Specific to the DSO market, the market-clearing process can be generally provided by the following steps. First, the DERs submit their bids in the DSO market. Then the DSO clears the market and sends the cleared bids (may include market-clearing price and quantity) to the DERs. The pricing mechanism that achieves the market equilibrium can be based on the same spot pricing principles as in Equation (1.1). This pricing scheme, which is a variant of LMP in transmission grid, is termed as distribution LMP (distribution locational marginal price (DLMP)) that can achieve accurate cost allocation, DSO budget balance and optimal grid operation. Overall, the DLMP-based market mechanism coordinates the goal of DSO and its underlying market participants like flexible loads (FLs), distributed generators (DGs) and conventional loads (nonelastic load), and is the cornerstone to achieve different coordination scheme between entities, regulatory bodies and DERs aggregators.

Although DLMP shows promising prospects for the DER integration, some practical aspects of applying such a scheme are still under investigation. Phenomena like price volatility and price differentiation create acceptability issues as conventional electricity users are lacking in knowledge or equipment to react on quick time-varying price signals. Investment in advanced communication infrastructure is generally expensive and therefore, designing incentives for investment and its underlying market structure is the research interest of a considerable number of proposals (see e.g., [16, 17]). In view of the transactive energy mechanisms, these investment questions may be tackled by promoting the decentralized grid opera-

tion in distribution grids. Compared to the centralized system, decentralized grid operation is proved advantageous in terms of computation efficiency, modularity, scalability, and privacy [3]. Moreover, emerging technologies like microgrids and VPPs introduce consumer-friendly interfaces between energy market and small-scale prosumers, which provides opportunities for decentralized/distributed frameworks to operate a cluster of geographically-closed DGs, energy storage units and, small residential loads.

An important part of these frameworks is also a proposal to encourage the decentralized energy trading [13]. Yet, the nature of energy trade between market participants can be very distinctive, and therefore their respective regulatory frameworks should be designed accordingly. For example, a number of prosumers can initiate an "energy community" that establishes a local market to exchange energy. The regulatory works, hence, needs to take into account the selfishness of the participants, particularly in the case of some participants having the market power. On the other hand, suppose two geographically-separated distribution grid to exchange power. The exchange prices can be negotiated by the regional grid operators in a way to be aligned to the collective objective (maximization of the social welfare). In relevance to this, DSO-operated market need to be accompanied by the concept of regional DSOs, independent entities, with the task of operating their local regions safely and securely and monitoring their power flows from the neighboring regions. This kind of regional coordination between DSOs can potentially encourage the physical energy and ASs trade between different regional distribution grids.

1.2 Motivation

In this work, aiming to form efficient and consumer-centered distribution grid markets, the research questions arise in i) how to develop the coordination scheme between DSO-operated market and alternative transactive platforms using spot pricing principles (DLMPs), and ii) how to achieve the regional coordination between interconnected spot markets at the distribution grid level. Details for each research question are provided in the following.

1.2.1 Coordination between potential markets

The current discussion on distribution grid market liberalization focuses on two types of mechanisms that can be potentially implemented to enable the participation of small-scale energy prosumers. The first option is to form a spot market that resembles the structure of the current wholesale market at transmission level as a natural extension to the distribution system (e.g., [13, 2]). As an alternative way, a bilateral market, also termed as peer-to-peer (P2P) electricity market, can be introduced (see also [18]). The P2P energy trade requires the market participants to settle bilateral energy transactions without any third-party supervision [18] and therefore enables a consumer-centric market that allows small and medium-sized prosumers to trade energy based on their preferences. On the other hand, the spot market mechanism is closely coupled with introducing an independent body that operates the market (similarly as Regional Transmission Operator (RTO)/ independent system operator (ISO)). The spot market is centrally operated market.

Therefore, the market operation function is commonly suggested to be realized by DSO that monitors and ensures the grid stability while operating the market.

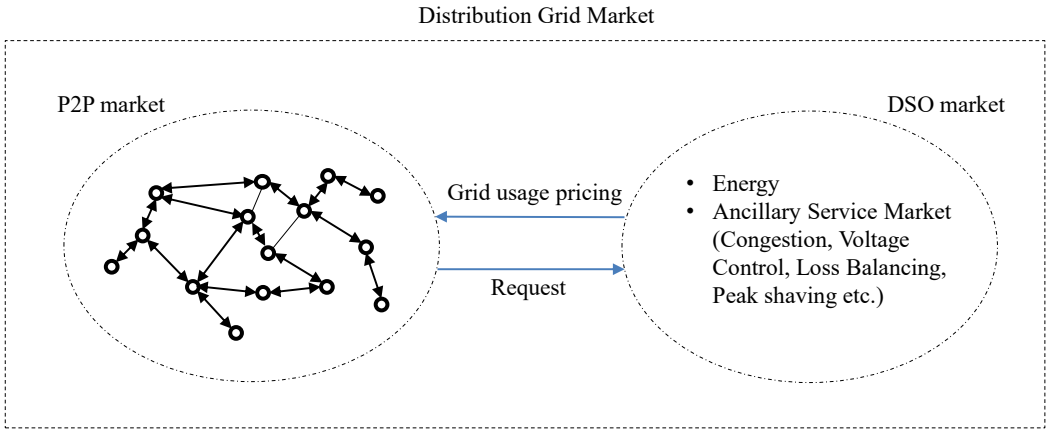

Fig. 1.2: Overview of distribution grid market organization.

A fundamental challenge to implement such P2P energy trade is the necessity to respect electric grid constraints while transporting the energy from the seller to the buyer in a bilateral transaction [19, 20]. This issue may not be significant if the P2P energy market platform is a relatively small compared to the size of the wholesale market. However, if bilateral energy trade becomes a widespread practice, the assumption of minor impact may no longer be valid. This is because, unlike the exchange of conventional goods, the transport of electricity based on a P2P transaction is governed by nonlinear power flow equations for the current electricity infrastructure. To this end, the routing of energy transfer for a given P2P transaction cannot be imposed straightforwardly.

In the context of transmission grid, existing practice for bilateral/multilateral transactions is to form Genco-Disco pair in the transmission system [21], where the traded quantities and prices agreed upon are negotiated on a bilateral basis and not a matter for the system operators. Note that this coincides with the idea of P2P energy trade that the transaction is made without third-party intervention and the transmission grid operator only provides power transport facilities and essential ASs. Then the P2P transaction should be reported to the balancing authorities to be taken into account for in the grid operations and the final cost settlement. However, this practice may not be applicable in distribution grids. The difficulty exists in i) higher dynamic of distribution system compared to transmission system and ii) potentially large number of small prosumers. One potential solution can be reflected in the transmission grid market, where the network constraints are explicitly considered by applying the spot market pricing principles. Specifically, the agents in the P2P energy trade can be enforced to respect the network constraints by imposing a mandatory energy transport price. This concept is depicted in Fig. 1.2. It requires a coordinated optimization between centralized DSO market and the decentralized P2P market to determine the grid usage price (GUP) while the P2P energy exchange can be incentivized to behave in a “grid-friendly” manner. In this work, we intend to provide such a coordinated optimization model and the underlying GUP formulation.

1.2.2 Multi-regional distribution grid operation

In resemblance to the existing market operation at the transmission grid level, where multiple RTOs operate their regional transmission grid while exchanging energy and ASs to maximize the social welfare of the overall system (see also [22, 23]), market-clearing procedures can be coordinated between interconnected distribution grids. In the envisioned market integration in Fig. 1.3, the regional DSO is held responsible to support the energy/ASs exchange between two hierarchical levels (upstream wholesale market and neighboring DSO markets).

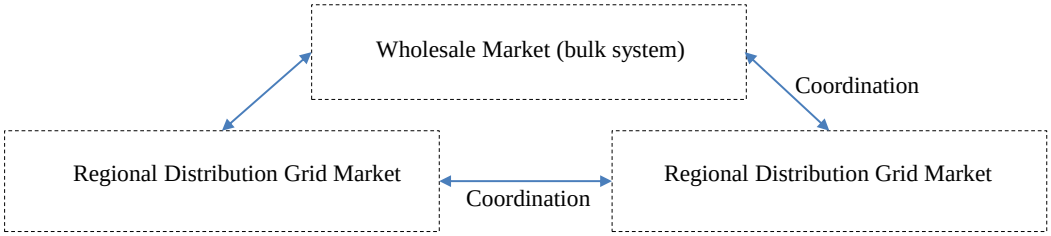

Fig. 1.3: Overview of multi-regional concept.

Based on the argument that distribution grids are more dynamic and sensitive compared to the bulk transmission system, the coordination of two interconnected distribution grids is considered to be difficult. Particularly, the cost allocation in grid operation for coupled distribution systems should be carefully treated. Towards the envisioned decentralized grid operation, two research questions are further specified in the following.

- What is the suitable coordination mechanism for market-clearing purpose between regional DSO markets?
- How to achieve the financial settlement for energy exchange between neighboring distribution grid regions in a cost-effective manner?

1.3 State-of-the-art market frameworks

Grid usage pricing

The idea of introducing transport cost for energy transfer in a bilateral contract is not new. In the transmission grid, earlier work [11] has formulated prices for point-to-point transfer in an auction-based transmission grid market using LMPs. In the context of distribution grid operation, however, studying the cost allocation for such a service using a dynamic pricing model is still a new subject in the research community. For example, P2P energy trade are assumed to be practiced at the energy community basis which is supposed to be realized by advanced power-routing technologies [24]. Hence, the electric grid constraints are neglected. Work [25] addresses the grid-constraints-violation issue by suggesting the DSO in the P2P-clearing process to check for constraint violations and calculate power flow equations in real-time. In [26], it utilizes a system-centric design for P2P transactions, which in principle relies on the DSO to collect the bids and clear the P2P market in a centralized way. These proposals suffer from drawbacks in the aspects, where,

i) the system-centric P2P framework resembles the current wholesale market design and contradicts the fundamental idea of the P2P market to remove third-party supervision and ii) there is no economic incentive for the DSO to deliver such a service for checking constraint violations. As an alternative, reference [27] addresses this by proposing the transformation of the DSO into an energy transport service provider for the P2P energy trade and a cost allocation scheme is designed to charge the P2P transactions for their electric grid usage with a uniform GUP prior to the trade settlement. However, the adoption of a DC power flow model limits the scope to transmission grid operation, and GUP requirements at the distribution grid level such as voltage support and loss compensation are excluded from the discussion.

In fact, GUP has been conceptualized and implemented in the transmission grid market for a long time, where it is evaluated by the nodal price difference between two transactive nodes in a bilateral agreement [11]. In line with this approach, reference [28] proposes a method for calculating the GUP through the DLMP based on a second-order conic programming (SOCP) formulation in the distribution grid context, focusing on the comparison of different market-clearing configurations and architectures. This approach is appealing as the DLMP formulation and exact power flow can be used to recover the exact grid operational cost. However, the DLMP formulation in [28] from relaxation-based optimal power flow (OPF) is non-intuitive which results in the difficulty to decouple GUP for various cost-centers to collect the payment. As the GUP is a derivative of the DLMP, the interpretation of the DLMP plays a key role in understanding the behavior of the GUP. In light of this, earlier work [5] has shed light on this issue, where the SOCP-based formulation and two alternative DLMP models including the implicit-function-based formulation and marginal losses are analyzed. It generally turned out that the relaxation-based AC optimal power flow (AC-OPF) results in a recursive formula that potentially leads to a non-intuitive interpretation of marginal changes in a radial network and the implicit-function-based formulation provides the most accurate interpretation. To this end, I derived the GUP, which is inherited from the implicit-function-based DLMP formulation, to obtain the desirable P2P market equilibrium point from the grid operation perspective. As the time of writing, a very recent work [29] investigated the integration of DLMP in the P2P energy trade, where probabilistic DLMPs are developed to charge the P2P market participants for their grid usage. The idea coincides with the proposed framework in the sense that the implicit-function-based formulation are adopted in both works.

Ancillary service market with DLMPs

Another development is the increasing trends in proposing AS market in distribution grid. Traditionally, grid stability is ensured by the DSO, which in the past means that the distribution grid equipment is sufficiently sized for peak load conditions. The load flexibility and DGs, either locally utilized or provided to upstream or downstream grid operators, presenting great potential to increase the grid inertia to prevent cascade failure. In the scope of P2P energy trade, while the GUP provides an incentive for P2P market participants to prefer transactions that will improve the grid conditions, this incentive does not guarantee feasible grid conditions alone. To address the economical aspects of providing such services, a notable number of

research effort, e.g., [13, 14, 30] propose the introduction of an AS market into the distribution system that adopts a similar approach to the existing frameworks at the transmission system level.

In the AS market, reserve capacities of local DERs are dispatched in such a way that voltage constraints are maintained, grid congestion is removed and power losses are balanced. In [13, 14, 2], the AS market was proposed as a complement to a energy spot market at the distribution system level rather than a P2P energy market. In line with the transactive energy paradigm development, recent proposals for P2P market designs also include a two-stage market-clearing structure of forward and real-time market to accommodate uncertainties [31] and differentiation among prosumers based on their heterogeneous preferences [32]. Nevertheless, the settlement of losses and other ASs are assumed to be accounted for by a separate process in these works and a coordinated market-clearing model to underpin these potential markets has received limited attention in the literature.

DLMPs for multi-regional operation

In view of DLMP for multi-regional operation, it essentially involves the calculation of DLMP in a distributed way. For the calculation of accurate and interpretable DLMP, the state-of-the-art work mainly focuses on the centralized methods for computation, composition and interpretation of DLMP [5]. Since the transformation of DSO model to an independent market operator is under discussion, the majority of the literature for distribution grid market naturally assigns the DSO to operate the distribution grid market and maximize social welfare (see e.g., [5, 33, 16, 2, 34]). In terms of centralized DLMP calculation, references [34, 35] provide a DLMP model obtained from a linearized OPF with features such as congestion management and a multi-period energy-dispatch model for a day-ahead market. However, power flow linearization in [34, 35] inflicts an error in calculating DLMPs, removed in [2] by using a trust-region algorithm. Moreover, it is shown that the trust-region based methodology yields a tractable solution along with DLMP decomposition into loss, congestion and voltage components. Alternative DLMP models are proposed in [36, 37, 13] using convexified load-flow models which suffer from the drawbacks of lack of straight-forward interpretation as discussed in [5, 2]. More specifically, the DLMP decomposition based on the formulation of the relaxation of AC-OPF results in a recursive formula that potentially leads to non-intuitive interpretations of marginal change in distribution grids.

For the multi-regional operation purpose, it entails a distributed DLMP scheme that can protect the regional operation autonomy. In this scope, a price-based control framework has been proposed earlier in [38, 39, 40], where the subgradient algorithm is adopted to achieve a distributed implementation to protect the information privacy of market participants. However, with a direct-current power-flow model, it inflicts a large error in low voltage networks. This is important since the power flow parameters like voltages are strongly coupled between distribution grid portions. The work in [40] uses a distributed online pricing scheme using the primal-dual method, where the prices are devised as the online incentive control signal. To our knowledge, the authors in [40] (i) used a static linear approximation of power flow and (ii) organized the framework in terms of only an operator and end consumers. Both considerations come with drawbacks. The first drawback is related

to the fact that static linear approximations inflict errors as compared to the actual power flow [2, 34, 35]. Another drawback arises from the fact that no coordination is provided when the grid is operated by multi-region DSOs, which only have access to local information and physically connected neighbors. Reference [37] proposed a three-level hierarchical market framework consisting of a TSO, DSOs and local aggregators without the coordination of operators in the distribution grid being handled. The work in [13] has to be mentioned, where the distributed calculation of DLMP is proposed by using convexified load flow models. Nevertheless, all these works [40, 37, 13] do not address the effect on the price due to physically connected neighboring regions, i.e., the effect of coupled losses and the associated cost allocations between distribution grid regions. In light of the aforementioned challenges, methods for accurate and scalable DLMP calculations need to be addressed.

1.4 Technical Contributions

In view of above research gaps in the previous works, the technical contributions of this work are outlined as follows.

- We propose a coordinated market design including two emerging markets at the distribution grid level (AS and P2P) with a simultaneous market-clearing model, aiming to provide a DLMP-based common tool to direct DERs towards “grid-friendly" behavior;
- An interpretable GUP scheme is derived based on implicit function formulation, wherein the GUPs lend themselves as price signals because they are naturally decomposable into price signals for voltage support, congestion management, and loss compensation. This GUP scheme can be utilized for DSO to allocate its cost, which is also shown to effectively incentivize the P2P market participants to reduce the grid operation cost in various scenarios;
- We propose an alternating direction method of multipliers (ADMM)-based regional coordination scheme together with the accurate cost-allocation for interconnected distribution grids. The DLMP calculation has been fully distributed into each region while only limited information exchange is required. We derive the multi-regional injection sensitivity to describe the influence between regions to achieve the distributed DLMP computation. The derived sensitivity only reveals the physical information on the coupled buses between regions. Therefore, the regional operation autonomy is preserved.

1.5 Assumptions

In light of the solution methodologies and their application perspectives, it is important to have a brief discussion of the assumptions of the mathematical tools that have been utilized in this work.

Duality-based Pricing

As DLMP is used as the main coordination mechanism between the market operator and participants in this work, it is worth mentioning that the duality theory

(detailed in Chapter 3) serves as the theoretical foundation to derive various optimal prices in this work. Hence, it is essential to be aware of the assumptions and requirements to underpin the functionality of the duality-based pricing, which are summarized in the following.

First, convexity is the backbone of duality-based pricing. This is because, convex problem formulation provides strong duality, whereas in the cases of non-convex problems and local optimal solutions, the dual variables as prices signals may not be support the market participants to make the social optimal decisions [41]. Second, individual agent is assumed to be economical rational, which means the agents are able to make optimal decisions given limited information and time. Third, spot pricing principles is derived based on the assumption of price-taking agents, which means the market participants' awareness of the effects of their decision on the market-clearing outcome is not taken into account. It is worth noticing that for the market design that adopts the spot-pricing principle, Lagrangian duality plays a vital role to translate the OPF solutions into prices to incentivize selfish agents to behave in a social-economic way. This mathematical realization, however, may never fully apply in reality [41].

Distributed Optimization

In this work, there are some settings, where distributed optimization techniques are shown to be useful. For example, in distribution grids, a large number of DERs are embedded in the low-voltage feeder, where the individual DER is constrained by their communication, computation and information capabilities. Under the assumption of the agents to be collaborative, distributed optimization can be utilized in this context to organize the agents towards the collective objective while entailing necessary information exchange between agents. Note that it is necessary for the individual agent to fully comply with the protocol predefined by distributed optimization methods to reach the collective objectives.

Another setting is to utilize distributed optimization as a market-clearing mechanism to solve the optimal exchange problems, e.g., settling the P2P energy trade. It is worth noticing that the adoption of distributed optimization only is applicable for non-strategic agent behavior. This assumption is realistic for the case that the market place is sufficient competitive and the agents can only behave as price takers. It is also similar to assumption to adopt the duality-based pricing, where each individual agent is assumed to fully comply to the protocol and not aware of its effects on the market outcome and their profitability. We contrast this to the game-theoretical approaches where each agent optimizes their decisions by estimating the other agents' decisions and gains additional profits than usual. Note that game-theoretical approaches remove the price-taker assumptions in duality-based pricing, which may be more realistic in some scenarios (see, e.g., presence of market power [42]), it does not come without drawbacks. The assumptions of fully rational market participants may crumble as the anticipation of market outcome is generally very difficult and considered to be out of reach for ordinary people. On the other side, the computational complexity of game theory makes the approach intractable compared to optimizations. It is important to emphasize that we limit ourselves to price-taker assumptions in this proposal for elaborating on the market structures and organizations. Nevertheless, the compatibility of game theory to

distributed optimization is briefly discussed in Chapter 4 in the P2P energy trade context, which may provide some technical details required for the future extension of the current proposal.

1.6 List of Publications

For the proposed market framework, following publications are made, which directly and indirectly contribute to the problem formulation and solution methodologies that are proposed in this dissertation.

Journal Publications

- K. Zhang, S. Troitzsch, S. Hanif, and T. Hamacher. "Coordinated Market Design for Peer-to-Peer Energy Trade and Ancillary Services in Distribution Grids". In: *IEEE Transactions on Smart Grid* 11.4 (2020), pp. 2929–2941. DOI: doi:10.1109/TSG.2020.2966216

- K. Zhang, S. Hanif, C. M. Hackl, and T. Hamacher. "A Framework for Multi-Regional Real-Time Pricing in Distribution Grids". In: *IEEE Transactions on Smart Grid* 10.6 (Nov. 2019), pp. 6826–6838. DOI: 10.1109/TSG.2019.2911996

- S. Hanif, K. Zhang, C. M. Hackl, M. Barati, H. B. Gooi, and T. Hamacher. "Decomposition and Equilibrium Achieving Distribution Locational Marginal Prices Using Trust-Region Method". In: *IEEE Transactions on Smart Grid* 10.3 (May 2019), pp. 3269–3281. ISSN: 1949-3053. DOI: 10.1109/TSG.2018.2822766

Refereed Conference Publications

- S. Troiztsch, M. Grussmann, K. Zhang, and T. Hamacher. "Distribution Locational Marginal Pricing for Combined Thermal and Electric Grid Operation". In: *2020 IEEE Innovative Smart Grid Technologies - Europe (ISGT Europe)*. accepted. 2020

- S. Candas, K. Zhang, and T. Hamacher. "A Comparative Study of Benders Decomposition and ADMM for Decentralized Optimal Power Flow". In: *2020 IEEE Power Energy Society Innovative Smart Grid Technologies Conference (ISGT)*. to be published. 2020

- K. Zhang, S. Hanif, and T. Hamacher. "Decentralized Voltage Support in a Competitive Energy Market". In: *2019 IEEE Power Energy Society Innovative Smart Grid Technologies Conference (ISGT)*. Feb. 2019, pp. 1–5. DOI: 10.1109/ISGT.2019.8791571

- S. Hanif, K. Zhang, and T. Hamacher. "Coordinated Market Mechanism for Economic Dispatch in Active Distribution Grids". In: *2019 IEEE Power Energy Society General Meeting (PESGM)*. Aug. 2019, pp. 1–5. DOI: 10.1109/PESGM40551.2019.8973817

- K. Zhang, S. Hanif, S. Troitzsch, and T. Hamacher. “Day-ahead Energy Trade Scheduling for Multiple Microgrids with Network Constraints”. In: *2019 IEEE Power Energy Society General Meeting (PESGM)*. Aug. 2019, pp. 1–5. DOI: 10.1109/PESGM40551.2019.8973609
- S. Troitzsch, S. Hanif, K. Zhang, A. Trpovski, and T. Hamacher. “Flexible Distribution Grid Demonstrator (FLEDGE): Requirements and Software Architecture”. In: *2019 IEEE Power Energy Society General Meeting (PESGM)*. Aug. 2019, pp. 1–5. DOI: 10.1109/PESGM40551.2019.8973567
- K. Zhang, D. Recalde, T. Massier, and T. Hamacher. “Charging Demonstrator for Ancillary Service Provision in Smart Grids”. In: *2018 IEEE Innovative Smart Grid Technologies - Asia (ISGT Asia)*. May 2018, pp. 988–993. DOI: 10.1109/ISGT-Asia.2018.8467795
- K. Zhang, D. Recalde, T. Massier, and T. Hamacher. “Fast Online Distributed Voltage Support in Distribution Grids using Consensus Algorithm”. In: *2018 IEEE Innovative Smart Grid Technologies - Asia (ISGT Asia)*. May 2018, pp. 350–355. DOI: 10.1109/ISGT-Asia.2018.8467821
- D. Recalde, A. Trpovski, S. Troitzsch, K. Zhang, S. Hanif, and T. Hamacher. “A Review of Operation Methods and Simulation Requirements for Future Smart Distribution Grids”. In: *2018 IEEE Innovative Smart Grid Technologies - Asia (ISGT Asia)*. May 2018, pp. 475–480. DOI: 10.1109/ISGT-Asia.2018.8467850
- K. Zhang, S. Hanif, and D. Recalde. “Clustering-based decentralized optimization approaches for DC optimal power flow”. In: *2017 IEEE Innovative Smart Grid Technologies - Asia (ISGT-Asia)*. Dec. 2017, pp. 1–6. DOI: 10.1109/ISGT-Asia.2017.8378334

1.7 Outline

The dissertation is structured as follows. In Chapter 2 and Chapter 3, we introduce the theoretical basis of optimal power flow models and spot pricing principles. As an essential tool, the duality analysis and distributed optimization solution methodologies are interlinked and introduced in Chapter 3, which are the key enablers to derive the coordination schemes by using their economic interpretations. Furthermore, as the main body of this dissertation, the solution methodologies to address the research questions are proposed in Chapter 4 and Chapter 5, respectively, together with their numerical validation, limitations and potential extensions. Finally, discussions on the proposals in the dissertation and interesting future works will be presented in Chapter 6.

Chapter 2

System Modeling

In this chapter, we derive the system models and basic concepts that lay the cornerstone for the coordinated market mechanisms. We start with the DER models with their linear approximations and integrate them into the load flow models. The variety of solution methodologies for OPF problems with an emphasis on nonlinear programming technique and their respective model accuracy are discussed in the second half of this chapter. Note that the dissertation views power system through linearization-colored glasses, so to say, with the chapter dedicated to linear-approximation-based distribution system optimization.

2.1 Distributed energy resources modeling

2.1.1 Distributed generator model

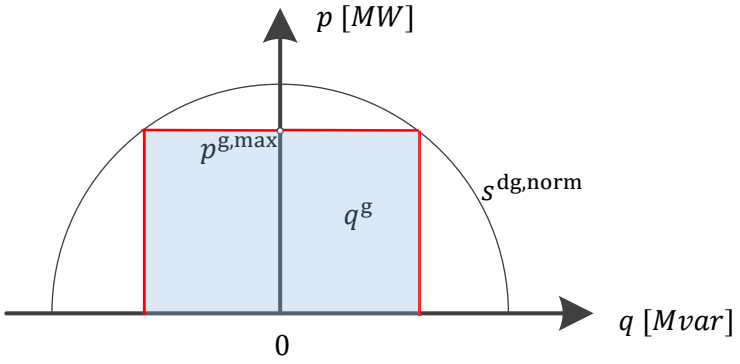

Fig. 2.1: The range of dispatchable q^{g} in dependence of p^{g} and the nominal power $s^{\mathrm{dg,nom}}$ for photovoltaic generators [55].

The DG model, e.g., PV or wind turbine systems, for real-time market participation is considered to be equipped with a full-scale grid-side inverter. The inverter allows the reactive power to be controlled independently from the active power within the DG's power rating [56, ch. 3]. To facilitate DG aggregator to be able to follow the power generation trajectory in a single market interval, it is assumed that the energy

storage systems is part of the DG system that buffers the renewable energy output and reduces the uncertainty [57].

The dispatchable region of the inverter-interfaced DGs is considered as follows. In principle, the DG reactive power output is supposed to be time-invariant that is restricted by a ratio κ to its nominal apparent power of the DG system denoted as $\mathbf{s}^{\mathsf{dg,nom}}$, i.e., $[-\kappa\mathbf{s}^{\mathsf{dg,nom}}, \kappa\mathbf{s}^{\mathsf{dg,nom}}]$. In Fig. 2.1, we illustrate the dispatchable reactive power for a typical DG. The reactive power capability of a DG unit (e.g. photovoltaic generators) is in general dependent by its nominal apparent power capability $\mathbf{s}^{\mathsf{dg,nom}}$ as well as the instantaneous time-varying active power p^{g} (i.e. $q^{\mathsf{g}} \leq \sqrt{(s^{\mathsf{dg,nom}})^2 - (p^{\mathsf{g}})^2}$), which makes the reactive power injection time-varying and complicates the optimization problem. To tackle this, the nominal apparent power capability $\mathbf{s}^{\mathsf{dg,nom}}$ of the inverter is advocated to be larger than the maximal active power $p^{\mathsf{g,max}}$, such that enough freedom can be provided for reactive power dispatch in most cases [55, 58]. Since the nominal apparent power $s^{\mathsf{dg,nom}}$ is preset to a value which is larger than the maximally admissible value of the active power $p^{\mathsf{g,max}}$, a time-invariant set for the reactive power (as approximation), i.e. $q^{\mathsf{g}} \leq \sqrt{(s^{\mathsf{dg,nom}})^2 - (p^{\mathsf{g,max}})^2} := \kappa s^{\mathsf{dg,nom}}$ is obtained. A reasonable value for oversizing the inverter can be set as $\mathbf{s}^{\mathsf{dg,nom}} = 1.1p^{\mathsf{g,max}}$, which gives $q^{\mathsf{g}} \leq 0.45p^{\mathsf{g,max}}$ [55]. With a *time-invariant* approximation, the feasible region of the dispatchable reactive power q^{g} is obtained as a constrained area regardless of the active power injections of the DG unit.

2.1.2 Flexible load model

A generic FL model is considered in this work, which captures the nature of heating, ventilation, and air conditioning (HVAC) system, charging system for electrical vehicles (EVs). The characteristic of these systems are described by the concept of virtual battery (VB) [59]. Let fl denote the number of FLs, the dynamic of the FLs can be essentially described by a linearized state of charge (SOC) model:

$$\mathbf{soc}_t = \mathbf{soc}_0 - \mathsf{diag}^{-1}(\mathbf{Q}) \sum_{k=1}^{t} (\frac{1}{\eta^d}\mathbf{p}_k^{\mathsf{d}} - \eta^{ch}\mathbf{p}_k^{\mathsf{ch}})\Delta t, \tag{2.1}$$

where $\mathbf{soc}_t \in \mathbb{R}^{fl}$ denote the SOC of the VB at time step t, $\eta^{ch}, \eta^d \in \mathbb{R}$ represent the charge and discharge efficiency and Δt represents the market period duration, $\mathbf{Q} \in \mathbb{R}^{fl}$ denotes the battery capacity, and $\mathbf{p}^{\mathsf{d}}, \mathbf{p}^{\mathsf{ch}} \in \mathbb{R}^{fl}$ denote the discharge and charge power. The parameters can be determined based on recent works using techniques like machine learning [60] or linear regression [61]. Note that the charge and discharge power are limited at each time intervals, which can be modeled by box constraints during their market participation.

2.2 Distribution grid modeling

2.2.1 Load flow models - steady state

We consider a balanced low-voltage distribution grid with a radial network topology. In reality, however, most of distribution feeders are three-phase and even unbalanced. For the sake of notational simplicity, we derive the main body of the

framework based on balanced network. Extensions to unbalanced three-phased are covered by work [62, 63, 64].

The distribution feeder has a root node with index 0, which is modeled as a slack node. This node refers to the power supply point (PSP) connected to the transmission grid, whereby its voltage is considered as a control variable. This is realized by voltage regulation devices like on load tap changer (OLTC) transformers, which are usually operated by DSOs. The rest of the nodes are modeled as PQ buses contained in the set $\mathcal{L} := \{1, 2, ..., n\}$. For all grid nodes we obtain the set $\mathcal{N} := \mathcal{L} \cup \{0\}$. For all grid nodes, we have complex injections and voltage as $\mathbf{s} := \mathbf{p} + \jmath\mathbf{q}$ and $\mathbf{u} := \mathbf{v} \cdot \mathbf{e}^{\jmath\boldsymbol{\theta}}$ all with size $\mathbb{C}^{n+1}$, where vectors that are associated to PQ buses are given as $\mathbf{s}_{\mathcal{L}}, \mathbf{u}_{\mathcal{L}} \in \mathbb{C}^n$ and the individual node $i \in \mathcal{N}$ defines $s_i := p_i + \jmath q_i$ and $u_i = v_i e^{\jmath\theta_i}$. Note that active and reactive power for the entire grid consists of $\mathbf{p} = (p_0, \mathbf{p}_{\mathcal{L}}^{\intercal})^{\intercal}$, $\mathbf{q} = (q_0, \mathbf{q}_{\mathcal{L}}^{\intercal})^{\intercal}$.

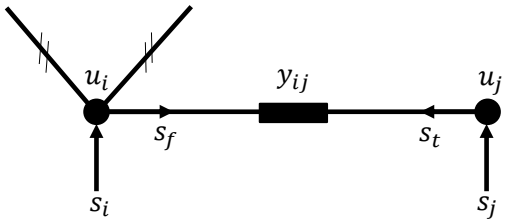

Fig. 2.2: Nodal injection model.

For energy balance of node i, the nodal injection s_i equals to the collective branch flows to the neighboring nodes, i.e.,

$$s_{ij} = \sum_{j \neq i} u_i (\underline{u}_i - \underline{u}_j) \underline{y}_{ij}, \tag{2.2}$$

where y_{ij} is the admittance of the lines, u_i, u_j are the complex voltage at these nodes, respectively. The above relations extend to the whole distribution system by defining the following system admittance matrix. Let $i \sim j$ denote if node i is connected to node j. The admittance matrix $\mathbf{Y} \in \mathbb{C}^{(n+1)\times(n+1)}$ is defined as follows[1]:

$$Y_{i,j} = \begin{cases} \sum_{k \sim j} y_{ik} & \text{if } i = j \\ -y_{ij} & \text{if } i \sim j \\ 0 & \text{if } i \nsim j \end{cases}. \tag{2.3}$$

Hence, the following nodal injection model is to be satisfied for the distribution grid:

$$\mathbf{s} = \mathbf{p} + \jmath\mathbf{q} = \text{diag}(\mathbf{u})\underline{\mathbf{Y}}\,\underline{\mathbf{u}}. \tag{2.4}$$

We are also interested in the collective active/reactive power losses on the lines since in the spot pricing theory, the power losses is used to formulate the global power balance equation (with the nodal prices derived for nodal balance equations at each grid node). The power balance equation is provided as:

$$s_0 + \mathbf{s}_{\mathcal{L}} = s^{\text{loss}}. \tag{2.5}$$

[1] Note that shunt admittance is neglected in the grid modeling.

with the total power losses on the lines calculated as the $s^{\text{loss}} = \sum_{i \in \mathcal{N}} s_i$. It gives

$$s^{\text{loss}} = p^{\text{loss}} + \jmath q^{\text{loss}} = \mathbf{u}^{\mathsf{T}} \underline{\mathbf{Y}}\, \underline{\mathbf{u}}. \tag{2.6}$$

Furthermore, we define the "forward"/"to" directions for a line as in Fig. 2.2, which is important to capture the thermal limits of the power flow on the distribution lines. Hence the thermal limit can be defined for the squared magnitude of $|\mathbf{s}^{\text{f}}|^2, |\mathbf{s}^{\text{t}}|^2$. Note that exceeding the thermal limit is termed as line congestion in this dissertation. The expression of $|\mathbf{s}^{\text{f}}|^2, |\mathbf{s}^{\text{t}}|^2$ can be given in a similar form as in nodal injection model, i.e., eq. (2.4), which can be found in references [65, 66].

In essence, eq. (2.4) is a nonlinear equation that can be solved by methods like Newton-Rapson iterations [67], where linearization of the nonlinear equations at a given operating point are necessary at each Newton-Rapson step. Also, the feasibility of the solutions for such a equation can not be guaranteed at all times. This subject has been intensively studied in the past years (see e.g. [68]). Recent expositions focus on fixed point method to provide existence conditions for balanced and unbalanced networks. For power system optimization problems, power flow linearizations and the sensitivity analysis lay the foundations for applying optimization methods. Particularly, the structural information like gradients, Hessians and sparsity plays a key role in the representation and interpretation of the LMPs and DLMPs. In the following, we briefly cover the topic of power flow linearization in an explicit-function form.

2.2.2 Explicit distribution grid power flow linearization

This section presents the power flow linearization for the slack bus, PQ buses and the power loss. The considered control variables are the nodal injections at PQ buses, i.e. $\mathbf{p}_{\mathcal{L}}$ and $\mathbf{q}_{\mathcal{L}}$ and voltage at the slack bus v_0 by assuming OLTCs located at the PSPs. The linearization is considered as "'explicit' since all linearized terms are parameterized regarding the predefined control variables $\mathbf{p}_{\mathcal{L}}$, $\mathbf{q}_{\mathcal{L}}$ and v_0, which can be contrasted to the implicit linearization methods in [63].

PQ buses

For a given operating point $(\hat{\mathbf{v}}_{\mathcal{L}}, \hat{\boldsymbol{\theta}}_{\mathcal{L}})$, the linear estimate of $(\tilde{\mathbf{v}}_{\mathcal{L}}, \tilde{\boldsymbol{\theta}}_{\mathcal{L}})$ is obtained as

$$\begin{bmatrix} \tilde{\mathbf{v}}_{\mathcal{L}} \\ \tilde{\boldsymbol{\theta}}_{\mathcal{L}} \end{bmatrix} = \begin{bmatrix} \hat{\mathbf{v}}_{\mathcal{L}} \\ \hat{\boldsymbol{\theta}}_{\mathcal{L}} \end{bmatrix} + \begin{bmatrix} \mathbf{M}_{\mathcal{L}}^{\mathsf{vp}} & \mathbf{M}_{\mathcal{L}}^{\mathsf{vq}} \\ \mathbf{M}_{\mathcal{L}}^{\theta\mathsf{p}} & \mathbf{M}_{\mathcal{L}}^{\theta\mathsf{q}} \end{bmatrix} \begin{bmatrix} \Delta\mathbf{p}_{\mathcal{L}} \\ \Delta\mathbf{q}_{\mathcal{L}} \end{bmatrix} + \begin{bmatrix} \mathbf{m}_{\mathcal{L}}^{\mathsf{vv}} \\ \mathbf{m}_{\mathcal{L}}^{\theta\mathsf{v}} \end{bmatrix} \Delta v_0, \tag{2.7}$$

where $\Delta\mathbf{p}_{\mathcal{L}} := \tilde{\mathbf{p}}_{\mathcal{L}} - \hat{\mathbf{p}}_{\mathcal{L}}$, $\Delta\mathbf{q}_{\mathcal{L}} := \tilde{\mathbf{q}}_{\mathcal{L}} - \hat{\mathbf{q}}_{\mathcal{L}}$ are the active/reactive power injection variations, respectively. Sensitivity matrices $\mathbf{M}_{\mathcal{L}}^{\mathsf{vp}}, \mathbf{M}_{\mathcal{L}}^{\mathsf{vq}}, \mathbf{M}_{\mathcal{L}}^{\theta\mathsf{p}}, \mathbf{M}_{\mathcal{L}}^{\theta\mathsf{q}}$ translate the impact of PQ injections $\mathbf{p}_{\mathcal{L}}$ and $\mathbf{q}_{\mathcal{L}}$ to the voltage and angle variations and are given analytically in [63, Proposition 1]. The sensitivity vectors $\mathbf{m}_{\mathcal{L}}^{\mathsf{vv}}, \mathbf{m}_{\mathcal{L}}^{\theta\mathsf{v}}$ translate the impact of the slack bus voltage to the voltage and angles at PQ buses. The nodal injection model is complex and nonlinear. We adapt the first-order linearization of (2.4) as in [63, Proposition 1].

$$\begin{bmatrix} \mathbf{M}_{\mathcal{L}}^{\mathsf{vp}} & \mathbf{M}_{\mathcal{L}}^{\mathsf{vq}} \\ \mathbf{M}_{\mathcal{L}}^{\theta\mathsf{p}} & \mathbf{M}_{\mathcal{L}}^{\theta\mathsf{q}} \end{bmatrix} = \Big[\Big(\langle [\underline{\mathbf{Y}}\mathbf{u}] \rangle + \langle \mathsf{diag}(\mathbf{u}) \rangle \mathbf{N} \langle \mathbf{Y} \rangle \Big) R(\mathbf{u}) \Big] \tag{2.8}$$

with following operators defined:

$$\mathbf{N} := \begin{bmatrix} \mathbf{I}_{n\times n} & \mathbf{0} \\ \mathbf{0} & -\mathbf{I}_{n\times n} \end{bmatrix}, \langle \mathbf{X} \rangle := \begin{bmatrix} \Re(\mathbf{X}) & -\Im(\mathbf{X}) \\ \Im(\mathbf{X}) & \Re(\mathbf{X}) \end{bmatrix},$$

$$R(\mathbf{u}) := \begin{bmatrix} \mathsf{diag}(\cos(\boldsymbol{\theta})) & -\mathsf{diag}(\mathbf{v})\mathsf{diag}(\sin(\boldsymbol{\theta})) \\ \mathsf{diag}(\sin(\boldsymbol{\theta})) & -\mathsf{diag}(\mathbf{v})\mathsf{diag}(\cos(\boldsymbol{\theta})) \end{bmatrix}.$$

To derive the sensitivity $\mathbf{m}_{\mathcal{L}}^{\mathsf{vv}}, \mathbf{m}_{\mathcal{L}}^{\theta\mathsf{v}}$, it is assumed that the power injection of all PQ buses are not affected by their voltage, i.e., $s_{\mathcal{L}}$ is independent of $v_{\mathcal{L}}$. We rewrite (2.4) for $i \in \mathcal{L}$, (PQ nodes) in the following scalar form:

$$s_i = u_i \sum_{j\in\{0\}\cup\mathcal{L}} \underline{\mathbf{Y}}_{i,j}\underline{u}_j. \tag{2.9}$$

The partial derivative of s_i with respect to v_0 is given as

$$\frac{\partial s_i}{\partial v_0} = \frac{\partial u_i}{\partial v_0} \sum_{j\in\{0\}\cup\mathcal{L}} \underline{\mathbf{Y}}_{i,j}\underline{u}_j + u_i \sum_{j\in\{0\}\cup\mathcal{L}} \underline{\mathbf{Y}}_{i,j}\frac{\partial \underline{u}_j}{\partial v_0}. \tag{2.10}$$

Consider replacing the complex voltage in polar coordinate system, where we have $u_i = v_i e^{\jmath\theta_i}$. It gives

$$\frac{\partial u_i}{\partial v_0} = e^{\jmath\theta_i}\frac{\partial v_i}{\partial v_0} + v_i\theta_i e^{\jmath\theta_i}\jmath\frac{\partial \theta_i}{\partial v_0}. \tag{2.11}$$

Equation (2.11) can be further simplified for the case of slack node $i = 0$, where

$$\frac{\partial u_0}{\partial v_0} = 1. \tag{2.12}$$

Recall the assumption of PQ nodes, where $\partial s_i/\partial v_k = 0$. Substitute it with (2.12) into (2.10), we have (2.10) reformulated as

$$-u_i\underline{\mathbf{Y}}_{i,0} = \frac{\partial u_i}{\partial v_0} \sum_{j\in\{0\}\cup\mathcal{L}} \underline{\mathbf{Y}}_{i,j}\underline{u}_j + \sum_{j\in\mathcal{L}} \underline{\mathbf{Y}}_{i,j}\frac{\partial \underline{u}_j}{\partial v_0}. \tag{2.13}$$

We rewrite it in a matrix form. More specifically, a total number of n equations can be written for (2.13) for all PQ nodes $i \in \mathcal{L}$. Note that we also have $\partial v_{\mathcal{L}}/\partial v_0 \in \mathbb{R}^n$ and $\partial\theta_{\mathcal{L}}/\partial v_0 \in \mathbb{R}^n$ (a total number of $2n$) as unknowns. By rewriting (2.13) into real and imaginary part (a number of $2n$), we can obtain the solutions for $\partial\mathbf{v}_{\mathcal{L}}/\partial v_0$ and $\partial\boldsymbol{\theta}_{\mathcal{L}}/\partial v_0$. We define the following matrices $\mathbf{A}, \mathbf{B} \in \mathbb{R}^{n\times n}$,$\mathbf{C} \in \mathbb{R}^{n\times 1}$ to write the solutions in a compact form:

$$\mathbf{A}_{i,l} = \begin{cases} \underline{u}_i\underline{\mathbf{Y}}_{i,i}e^{\boldsymbol{\jmath}\theta_i} + e^{\boldsymbol{\jmath}\theta_i}\sum_{j\in\{0\}\cup\mathcal{L}}\underline{\mathbf{Y}}_{i,j}\underline{u}_j & \text{if } i = l \\ \underline{u}_i\underline{\mathbf{Y}}_{i,l}e^{\boldsymbol{\jmath}\theta_l} & \text{if } i \neq l \end{cases} \tag{2.14}$$

$$\mathbf{B}_{i,l} = \begin{cases} u_i\theta_i\boldsymbol{\jmath}(\sum_{j\in\{0\}\cup\mathcal{L}}\underline{\mathbf{Y}}_{i,j}\underline{u}_j + \underline{u}_i\underline{\mathbf{Y}}_{i,j}) & \text{if } i = l \\ \underline{u}_i\underline{\mathbf{Y}}_{i,j}u_j\theta_j\boldsymbol{\jmath} & \text{if } i \neq l \end{cases} \tag{2.15}$$

$$\mathbf{C}_{i,l} = -u_i e^{\boldsymbol{\jmath}\theta_l}\underline{\mathbf{Y}}_{i,l} \tag{2.16}$$

The final result of $\begin{bmatrix}\mathbf{m}_{\mathcal{L}}^{\mathsf{vv}} \\ \mathbf{m}_{\mathcal{L}}^{\theta\mathsf{v}}\end{bmatrix} \in \mathbb{R}^{2n\times 1}$ is obtained as:

$$\begin{bmatrix}\mathbf{m}_{\mathcal{L}}^{\mathsf{vv}} \\ \mathbf{m}_{\mathcal{L}}^{\theta\mathsf{v}}\end{bmatrix} = \begin{bmatrix}\Re(A) & \Re(B) \\ \Im(A) & \Im(B)\end{bmatrix}^{-1} \begin{bmatrix}\Re(C) \\ \Im(C)\end{bmatrix}. \tag{2.17}$$

Since the matrix is invertible, the above linearization result is unique [69, Theory 1].

Slack bus

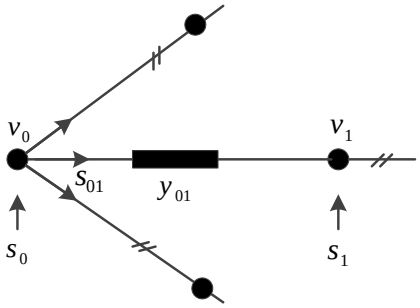

Fig. 2.3: Slack bus nodal injection.

For the slack (root) node, voltage v_0 are considered to be adjustable, whereas angle θ_0 is fixed quantity. The power flow linearization is obtained as the slack nodal injections with respect to the changes of PQ nodal injections and slack node voltage magnitude, i.e.,

$$\begin{bmatrix}\tilde{p}_0 \\ \tilde{q}_0\end{bmatrix} = \begin{bmatrix}\hat{p}_0 \\ \hat{q}_0\end{bmatrix} + \begin{bmatrix}\mathbf{m}_{\mathcal{L}}^{\mathsf{pp}} & \mathbf{m}_{\mathcal{L}}^{\mathsf{pq}} \\ \mathbf{m}_{\mathcal{L}}^{\mathsf{qp}} & \mathbf{m}_{\mathcal{L}}^{\mathsf{qq}}\end{bmatrix} \begin{bmatrix}\Delta\mathbf{p}_{\mathcal{L}} \\ \Delta\mathbf{q}_{\mathcal{L}}\end{bmatrix} + \begin{bmatrix}m^{\mathsf{pv}} \\ m^{\mathsf{qv}}\end{bmatrix} \Delta v_0, \tag{2.18}$$

where $\mathbf{m}_{\mathcal{L}}^{\mathsf{pp}} \in \mathbb{R}^{1\times n}$ given as

$$\begin{aligned}\mathbf{m}_{\mathcal{L}}^{\mathsf{pp}} = \sum_{k=1}^{n} \{&(-\Re(v_0\underline{\mathbf{Y}}_{0,k})\cos(\theta_k) + \Im(v_0\underline{\mathbf{Y}}_{0,k})\sin(\theta_k))\mathbf{M}_{\mathcal{L}}^{\mathsf{vp}}\mathbf{e}_k \\ &+ (\Re(v_0\underline{\mathbf{Y}}_{0,k})\sin(\theta_k) - \Im(v_0\underline{\mathbf{Y}}_{0,k})\cos(\theta_k))v_k\mathbf{M}_{\mathcal{L}}^{\theta\mathsf{p}}\mathbf{e}_k\}.\end{aligned} \tag{2.19}$$

$\mathbf{e}_i \in \mathbb{R}^n$ is defined as a vector with i-th entry equal to 1 and rest of the entries equal to 0. Similar results can be found for $\mathbf{m}_{\mathcal{L}}^{pq}$, $\mathbf{m}_{\mathcal{L}}^{qp}$, $\mathbf{m}_{\mathcal{L}}^{qq} \in \mathbb{R}^{1\times n}$, where their representation are excluded here.

The derivation is provided in the following. In Figure 2.3, the nodal injection at the slack bus is equal to the branch flow, i.e., $s_0 = \sum_{k=1}^{n} s_{0k}$. Consider the first-order derivative of slack nodal injection with respect to PQ nodal injection, which

gives

$$\frac{\partial p_0}{\partial \mathbf{p}_{\mathcal{L}}} = \frac{\partial \Re(\sum_{k=1}^{n} s_{0k})}{\partial \mathbf{p}_{\mathcal{L}}} \tag{2.20}$$

$$= \frac{\partial}{\partial \mathbf{p}_{\mathcal{L}}} \Re \sum_{k=1}^{n} (u_0(\underline{u_0} - \underline{u_k})\underline{\mathbf{Y}}_{0,k}). \tag{2.21}$$

By substituting $u_i = v_i e^{j\theta_i}$ into (2.20) and extracting the real part, we obtain the analytical form of $\mathbf{m}_{\mathcal{L}}^{\mathsf{pp}}$ as in (2.19). Alternative vectors $\mathbf{m}_{\mathcal{L}}^{\mathsf{pq}}$, $\mathbf{m}_{\mathcal{L}}^{\mathsf{qp}}$, $\mathbf{m}_{\mathcal{L}}^{\mathsf{qq}} \in \mathbb{R}^{1\times n}$ can be derived in a similar manner.

The sensitivity of slack bus injections with respect to slack bus voltage $m^{\mathsf{pv}}, m^{\mathsf{qv}}$ are derived as follows. From the power balance equation (2.5), we have

$$\frac{\partial s_0}{\partial v_0} + \frac{\partial \mathbf{s}_{\mathcal{L}}}{\partial v_0} = \frac{\partial s^{\mathsf{loss}}}{\partial v_0}. \tag{2.22}$$

With the PQ nodal injections remaining unchanged, i.e., $\frac{\partial \mathbf{s}_{\mathcal{L}}}{\partial v_0} = \mathbf{0}$ we have

$$\frac{\partial s_0}{\partial v_0} = \frac{\partial s^{\mathsf{loss}}}{\partial v_0}. \tag{2.23}$$

Recalling the loss representation in (2.6) we obtain

$$\frac{\partial s_0}{\partial v_0} = \frac{\partial(\mathbf{u}^{\intercal}\underline{\mathbf{Y}}\,\underline{\mathbf{u}})}{\partial v_0} = \frac{\partial \mathbf{u}^{\intercal}}{\partial v_0}\underline{\mathbf{Y}}\,\underline{\mathbf{u}} + \mathbf{u}^{\intercal}\underline{\mathbf{Y}}\frac{\partial \underline{\mathbf{u}}}{\partial v_0}$$

$$= (\frac{\partial \mathbf{v}}{\partial v_0}e^{j\boldsymbol{\theta}} + j\mathbf{u}\boldsymbol{\theta}\frac{\partial \boldsymbol{\theta}}{\partial v_0})^{\intercal}\underline{\mathbf{Y}}\,\underline{\mathbf{u}} \tag{2.24}$$

$$+ \mathbf{u}^{\intercal}\underline{\mathbf{Y}}(\frac{\partial \mathbf{v}}{\partial v_0}e^{-j\boldsymbol{\theta}} - j\mathbf{u}\boldsymbol{\theta}\frac{\partial \boldsymbol{\theta}}{\partial v_0}). \tag{2.25}$$

Note that $\frac{\partial \mathbf{v}}{\partial v_0}, \frac{\partial \boldsymbol{\theta}}{\partial v_0}$ is the voltage and angle sensitivity with respect to v_0, i.e., $\mathbf{m}_{\mathcal{L}}^{\mathsf{vv}}, \mathbf{m}_{\mathcal{L}}^{\theta\mathsf{v}}$. Hence the slack-bus injection with respect to slack-bus voltage is given as

$$[m^{\mathsf{pv}}, m^{\mathsf{qv}}] = [\Re(\frac{\partial s_0}{\partial v_0}); \Im(\frac{\partial s_0}{\partial v_0})]. \tag{2.26}$$

losses

For loss linearization $\tilde{p}^{\mathsf{loss}}$ and $\tilde{q}^{\mathsf{loss}}$, we have

$$\begin{bmatrix}\tilde{p}^{\mathsf{loss}} \\ \tilde{q}^{\mathsf{loss}}\end{bmatrix} = \begin{bmatrix}\hat{p}^{\mathsf{loss}} \\ \hat{q}^{\mathsf{loss}}\end{bmatrix} + \begin{bmatrix}\mathbf{m}_{\mathcal{L}}^{\mathsf{pl,p}} & \mathbf{m}_{\mathcal{L}}^{\mathsf{pl,q}} \\ \mathbf{m}_{\mathcal{L}}^{\mathsf{ql,p}} & \mathbf{m}_{\mathcal{L}}^{\mathsf{ql,q}}\end{bmatrix} \begin{bmatrix}\Delta\mathbf{p}_{\mathcal{L}} \\ \Delta\mathbf{q}_{\mathcal{L}}\end{bmatrix}. \tag{2.27}$$

Specifically, $\mathbf{M}_{\mathcal{L}}^{\mathsf{loss}} \in \mathbb{R}^{2\times 2n}$ consists of four parts with respect to active power and reactive power:

$$\mathbf{M}_{\mathcal{L}}^{\mathsf{loss}} := \begin{bmatrix}\mathbf{m}_{\mathcal{L}}^{\mathsf{pl,p}} & \mathbf{m}_{\mathcal{L}}^{\mathsf{pl,q}} \\ \mathbf{m}_{\mathcal{L}}^{\mathsf{ql,p}} & \mathbf{m}_{\mathcal{L}}^{\mathsf{ql,q}}\end{bmatrix}, \tag{2.28}$$

where it can be calculated as [2]:

$$\mathbf{M}_{\mathcal{L}}^{\mathsf{loss}} = \big(\langle(\mathbf{Y}\,\hat{\mathbf{u}}_{\mathcal{L}})^{\intercal}\rangle + \langle\hat{\mathbf{u}}_{\mathcal{L}}^{\intercal}\rangle\mathbf{N}\langle\mathbf{Y}\rangle\big)R(\hat{\mathbf{u}}_{\mathcal{L}})\mathbf{M}_{\mathcal{L}}^{\mathsf{PQ}}(\hat{\mathbf{u}}_{\mathcal{L}}). \tag{2.29}$$

Remark (Correlation between power loss sensitivities and slack node sensitivities). Loss linearization can be related to slack bus injection linearization by the power balance equations, i.e., $p_0 + \mathbf{1}_n^\mathsf{T}\mathbf{p}_\mathcal{L} = p^{\text{loss}}$. By taking the first-order derivative on both sides of the equation, we obtain

$$\frac{\partial p_0}{\partial \mathbf{p}_\mathcal{L}} + \mathbf{1}_n = \frac{\partial p^{\text{loss}}}{\partial \mathbf{p}_\mathcal{L}}. \tag{2.30}$$

Note that the loss sensitivity is usually very small. Hence, intuitively, for small-scale networks, by increasing/reducing the power injections at PQ buses, similar amount of power will be reduced/increased at the slack bus, i.e., $\frac{\partial p_0}{\partial \mathbf{p}_\mathcal{L}} \approx -\mathbf{1}_n$.

Extension to unbalanced system

The extension to unbalanced system can be followed by two steps. First, the admittance matrix should be constructed for each phase by using unbalanced system modeling. Techniques can be found in e.g., [69, 70]. Second, repeat the same load flow linearization and OLTC linearization steps as above. There are existing works that focus on the load flow linearization for three-phase unbalanced network, e.g., [62]. Note that because of the nature of three-phase OLTC, the slack node voltage magnitudes of all phases are considered as control variables.

2.2.3 Linearized nodal injection model at flat voltage - a special case

In general, to calculate and update the sensitivity matrices is a tedious job. For some applications like voltage control, an approximation of load flow based on pre-defined operating point may achieve a good trade-off between accuracy and algorithmic tractability. Now assume that the nodal angle differences are very small throughout the network and use the flat voltage at the linearization point, we substitute $\boldsymbol{\theta} \approx \mathbf{0}, \mathbf{v} \approx \mathbf{1}$ into (2.8) and obtain the following linearized power injection model [63, 68]

$$\begin{bmatrix}\mathbf{p}\\ \mathbf{q}\end{bmatrix} = \begin{bmatrix}\Re(\mathbf{Y}) & -\Im(\mathbf{Y})\\ -\Im(\mathbf{Y}) & -\Re(\mathbf{Y})\end{bmatrix}\begin{bmatrix}\mathbf{v}\\ \boldsymbol{\theta}\end{bmatrix}. \tag{2.31}$$

The above approximate model has shown to perform reasonably well in voltage estimation (0.25% error for 5% voltage variation from the nominal voltage [71]) while neglecting the higher order active/reactive loss terms. We show in the following, the model (2.31) is indeed equivalent to the linearized DistFlow model, which is more interpretable.

Equivalence to linearized DistFlow model

The nodal injection model (2.4) is not the only model to describe the power flow. DistFlow model, as an alternative, may provide a better physical insights compared to the compact representation of the nodal injection model. Given a branch (i, j) connecting bus i and j, the network branch flow can be described using the LinDist

flow model [72].

$$p_j = p_{ij} - r_{ij} l_{ij} + \sum_{(i,j)\in\mathcal{H}} p_{jk} \tag{2.32}$$

$$q_j = q_{ij} - x_{ij} l_{ij} + \sum_{(i,j)\in\mathcal{H}} q_{jk} \tag{2.33}$$

$$v_j^2 = v_i^2 - 2(r_{ij} p_{ij} + x_{ij} q_{ij}) + (r_{ij}^2 + x_{ij}^2) l_{ij} \tag{2.34}$$

$$l_{ij} = \frac{p_{ij}^2 + q_{ij}^2}{v_i} \tag{2.35}$$

with $p_{ij}, q_{ij}, l_{ij} \in \mathbb{R}$ denoting the branch active/reactive flow and the branch current magnitude. r_{ij}, x_{ij} are the branch resistance and reactance respectively. Now neglecting the higher-order loss terms $r_{ij} l_{ij}, x_{ij} l_{ij}$ and $(r_{ij}^2 + x_{ij}^2) l_{ij}$ in (2.32) to (2.34) and applying a flat voltage profile approximation that $v_j^2 - v_i^2 = (v_j + v_i)(v_j - v_i) = 2(v_j - v_i)$, we obtain

$$p_j = p_{ij} + \sum_{(i,j)\in\mathcal{H}} p_{jk} \tag{2.36}$$

$$q_j = q_{ij} + \sum_{(i,j)\in\mathcal{H}} q_{jk} \tag{2.37}$$

$$v_j = v_i - (r_{ij} p_{ij} + x_{ij} q_{ij}) \tag{2.38}$$

which is a linearized DistFlow model. We use the resistance and reactance matrix $\mathbf{R}, \mathbf{X} \in \mathbb{C}^{(n+1)\times(n+1)}$ to model the grid, hence we can rewrite the above equation (2.36) to (2.38) in a compact form as:

$$\mathbf{v} = \mathbf{v_0} + \mathbf{R}\mathbf{p} + \mathbf{X}\mathbf{q} \tag{2.39}$$

where $\mathbf{v_0} \in \mathbb{R}^{n+1}$ is a vector with all the entries equal to v_0 (slack bus). The linearized DistFlow model is essentially equivalent to the linearized nodal injection model at flat voltage in (2.31) since both model are based on the assumption of substitution of flat voltage into different forms of power flow representations [63].

Linearized line current magnitude model

For the linearized DistFlow model, we consider the following linearized line current model to constrain the line flow not to exceed the thermal limit. Defining the line current between node i and node j as $l_{ij} \in \mathbb{C}$, thermal limits are usually defined as line current magnitude $|l_{ij}|$, which is directly related to the conductor's temperature. For brevity, assuming no shunt admittance exists, we obtain line current magnitude as

$$\begin{aligned} |l_{ij}| &= \sqrt{l_{ij}\underline{l}_{ij}} \\ &= \sqrt{(u_i - u_j) y_{ij} (\underline{u}_i - \underline{u}_j) \underline{y}_{ij}} \\ &= \sqrt{|y_{ij}|^2 (v_i^2 + v_j^2 - v_i v_j e^{(\theta_i - \theta_j)\jmath} - v_i v_j e^{(\theta_j - \theta_i)\jmath})} \end{aligned} \tag{2.40}$$

Based on the same assumption of small angle variance, i.e., $\theta_i - \theta_j = 0$, we obtain

$$|l_{ij}| = |y_{ij}||v_i - v_j|. \tag{2.41}$$

Interestingly, the results coincide with the linear line flow in [73]. Note that simple extension of this formulation also exists to include shunt admittance. The linearized line current is a conservative estimation of line current flow by neglecting the active/reactive power losses on the lines. We further validate the accuracy of the model with a test feeder.

We now rewrite (2.41) in a compact form using the admittance matrix $\mathbf{Y}^{\text{line}} \in \mathbb{C}^{h\times h}$ and the from/to mapping matrix $\mathbf{C}^{\text{f}}, \mathbf{C}^{\text{t}} \in \mathbb{R}^{h\times(n+1)}$ [74]. The basic idea of representing in from/to quantities is illustrated in Fig. 2.2, where each line segment is assigned a from/to direction from the start/end node to the end/start node. Hence, $\mathbf{C}^{\text{f}}/\mathbf{C}^{\text{t}}$ maps each line segment to the corresponding node index. $\mathbf{Y}^{\text{line}}$ is defined as a matrix with its diagonal terms equal to the line admittance and the off-diagonal terms equal 0. We obtain the line current magnitude vector $|\mathbf{l}| \in \mathbb{R}^h$ represented as

$$|\mathbf{l}| = |\mathbf{Y}^{\text{line}}||\mathbf{C}^{\text{f}}\mathbf{v} - \mathbf{C}^{\text{t}}\mathbf{v}|, \tag{2.42}$$

where $|\mathbf{Y}^{\text{line}}| \in \mathbb{R}^{h\times h}$ extracts the magnitude of the matrix $\mathbf{Y}^{\text{line}}$. Consider the thermal constraint that $|\mathbf{l}| \leq |\bar{\mathbf{l}}|$; an equivalent box constraint is obtained as

$$-|\bar{\mathbf{l}}| \leq |\mathbf{Y}^{\text{line}}|(\mathbf{C}^{\text{f}} - \mathbf{C}^{\text{t}})\mathbf{v} \leq |\bar{\mathbf{l}}| \tag{2.43}$$

144-bus network example for linearized DistFlow model

The linearized power flow model and current magnitude model is evaluated using the test network in [75] with the results plotted in Fig. 2.4. The voltage estimation error is very small, which verifies the claims from [71] whereas the current magnitude estimation achieves similar accuracy. Nevertheless, it is worth noticing that the error of the current magnitude estimation at the root node is the largest. This is because the deviation physically represents the loss quantities being neglected that is at its the largest near the root node for a distribution feeder. The average estimation error for active/reactive power branch flow is plotted in Fig. 2.4 for the loading factor range between 0.1 and 1.5. The estimation error increases with increasing load, whereas the maximum error is around 0.5 % for a loading factor of 1.5.

2.3 Optimal power flow

Optimal power flow serves as a fundamental tool for power system planning, operation and control. Since its introduction, it is applied for long-term planning, day-hour-minute scheduling, pricing and real-time control by system operators. Mathematically speaking, the objective of optimal power flow is to find a feasible power flow solution that can minimize user-defined cost function subject to the state variables of power system (voltage, angle, active/reactive power, current), which can

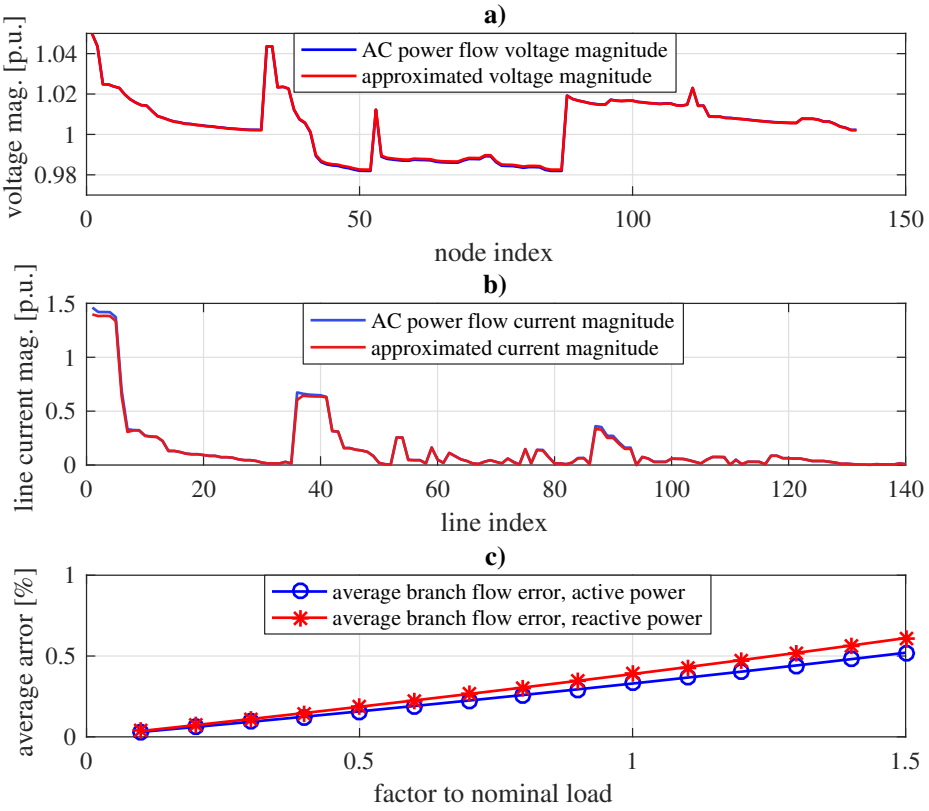

Fig. 2.4: a) - b) linearized voltage and current magnitude compared to AC power flow under nominal loading; c) average error of active/reactive branch flow under different loading conditions (factor to nominal load varies from 0.1 to 1.5).

be over a single or multiple time period. We briefly recapture the basic formulation of the optimal power flow problem as the following optimization problem

$$\min \quad f(\mathbf{p}, \mathbf{q}, \mathbf{v}) \tag{2.44a}$$

s.t.

$$\mathbf{p} + \jmath\mathbf{q} = \text{diag}(\mathbf{u})\underline{\mathbf{Y}}\,\underline{\mathbf{u}} \tag{2.44b}$$

$$\underline{\mathbf{p}} \leq \mathbf{p} \leq \overline{\mathbf{p}} \tag{2.44c}$$

$$|\mathbf{s}^{\mathbf{f}}|^2 \leq |\overline{\mathbf{s}}^{\mathbf{f}}|^2 \tag{2.44d}$$

$$|\mathbf{s}^{\mathbf{t}}|^2 \leq |\overline{\mathbf{s}}^{\mathbf{t}}|^2 \tag{2.44e}$$

$$\underline{\mathbf{q}} \leq \mathbf{q} \leq \overline{\mathbf{q}} \tag{2.44f}$$

$$\underline{\mathbf{v}} \leq \mathbf{v} \leq \overline{\mathbf{v}}, \tag{2.44g}$$

where the objective function is assumed to be a convex function that might represent one of the following objectives: i) the cost of power generation, ii) the overall losses on the lines, iii) penalty cost of system state variables (e.g. voltage deviations to the flat voltages). The optimal power flow model is a steady-state based formulation, which means the system dynamics in transient state and

harmonics are neglected. In the context of distribution grid, the control variables are considered to be the nodal injections and the slack node voltage (controlled by tap changers at the PSP). The capacitor bank switch is not considered in this highly simplified OPF model.

Discussion on solution methodologies for OPF problems

The problem given by (2.44) is a nonconvex and nonlinear problem due to the nature of power flow constraint in Eq. (2.44b), which makes the problem difficult to solve. In the power system research community, solving the optimal power flow has become a frequent optimization routine with the solution methodologies mainly categorized into: i) linearized optimal power flow, ii) convex relaxations of optimal power flow and iii) nonlinear programming algorithms. From the perspective of model applicability, a linearized optimal power flow model, despite their successful deployment in transmission grid operation, may not deliver sufficient model accuracy for the highly dynamic distribution grid physics. Hence, the subsequent resource allocation may not be optimal. On the other hand, the category ii) relaxation-based optimal power flow is proved to solve the OPF problem accurately, particularly in the case of the radial network topology [76], while a number of nonlinear programming (NLP) algorithms in category iii) are developed as exact, non-convex OPF models. Both category ii) and iii) show similar model accuracy while the convex-relaxation-based methods are computationally most intensive. The central motif of the dissertation is to impose certain economic interpretations and intuitions when addressing the solutions to the research questions.

In this regard, we limit our discussions in this work to the linearization-based approaches and nonlinear programming-based optimization without including the relaxations-based approaches in our discussion in great detail. This is based on the argument that relaxed-OPF-based DLMP models may not be the most intuitive one to be interpreted. More specifically, the SOCP-based formulation and other alternative relaxation-based DLMP models in comparison to the implicit-function-based formulation (corresponds to the category of LP and NLP) are analyzed in [5] and it generally turned out that the relaxation-based AC-OPF results in a recursive formula that potentially leads to a non-intuitive interpretation of marginal changes in a radial network and the implicit-function-based formulation provides the most accurate interpretation. Note that most NLP methods are based on newton's steps. Hence linearization is involved in NLP steps. In the following, we focus on one NLP method to form the basis for further discussions. On the other hand, the generic NLP methods generally reveals only Karush-Kuhn-Tucker (KKT) points. Yet, the hope is, the NLP converges to the global optimal point in the context of the distribution grid (radial topology), which has been reported in several references including [77, 2]. For meshed networks, there is no consensus in the research community about the solution methods to underpin the convexity and strong duality.

2.3.1 Nonlinear programming of optimal power flow

The NLP algorithms can be generally categorized into Newton-based method, which often involve the calculation of the Jacobian and Hessian to determine the search

direction and approximate the power flow constraint. As discussed previously, the advantage of NLP algorithms is that they provably converge to exact power flow solutions. We focus on trust-region method in this work to solve optimal power flow problems and motivate the adoption of NLP for the market-clearing purpose. Compared to the alternative NLP methods, e.g., primal-dual Interior Point Method (IPM), the benefits gained by trust-region method are twofold. First, a feasible power flow solution is guaranteed at each step. Second, the implicit computation of power flow sensitivities can be utilized for efficient DLMP calculations to enable online implementation.

Generic NLP problem

$$\min \quad f(\mathbf{x}) \tag{2.45a}$$

s.t.

$$g_i(\mathbf{x}) \leq 0, \quad i = 1, ..., m \tag{2.45b}$$
$$h_i(\mathbf{x}) = 0, \quad i = 1, ..., p, \tag{2.45c}$$

where the feasible set $\mathcal{X}$ of $\mathbf{x} \in \mathbb{R}^n$ is given as a continuous set that is defined by the inequality and equality equations (2.45b) and (2.45c). Depending on the availability of first-order derivative information of the functions f and g_i, the above definition can be categorized into i) smooth, and ii) non-smooth optimization problems. Since the derivative information is available on the functions f and g_i in the generic OPF problems as discussed in Section 2.2.2, we limit our context in the smooth optimization. To this end, a generic structure can be cast for formulating NLP algorithms to find a optimal solution for the problem as

Algorithm 1 Generic nonlinear programming [1]

while *converged?* **do**
  $k := k + 1$;
  determine search direction $\mathbf{r}(k)$;
  next iteration is $\mathbf{x}(k+1) := \mathbf{x}(k) + \text{diag}(\boldsymbol{\lambda}(k)) \cdot \mathbf{r}(k)$.
end

Note that λ is the step-size that can be time-invariant when adjusting the step sizes in the iterations. Variable $\mathbf{r}$ is the search direction determined by the gradient information of the constraint and objective function. Under this structure, a number of algorithms and variants are developed, including trust-region method [78], primal-dual IPM [79]. An interesting feature of trust-region method is the exactness of power flow solution, where the ability of online applications in close-to real-time operation can be exploited. The adoption of trust-region to solve the OPF problem is given in the following.

2.3.2 Trust-region algorithm in solving optimal power flow problem

The core idea of handling the power flow constraint (2.44b) in trust-region algorithm is to create an approximate model (e.g., linear model) for the initial operating

point within a feasible region (trust region). The approximate model should be sufficiently accurate so that one can "trust" the model for finding the objective decent direction within the "trust-region". With the help of the minimization step, the steepest descent direction along the objective function can be found. In a new iteration, the linearized model is then updated using the new operating point projected to the AC power flow model (by solving the nonlinear functions with the new decision variables). The algorithm repeats the steps until no further improvement can be found within the next minimization step. Note that the trust region is adjusted from iteration to iteration, i.e., the trust region will be enlarged if the approximate model represents the original problem well and vice versa.

Recall the OPF problem in (2.44), the power flow equations are replaced by its first-order approximations. More specifically, the nonlinear equation (2.44b) are approximated by using linear estimates:

$$\begin{bmatrix} \tilde{\mathbf{v}}_{\mathcal{L}} \\ \tilde{\boldsymbol{\theta}}_{\mathcal{L}} \end{bmatrix} = \begin{bmatrix} \hat{\mathbf{v}}_{\mathcal{L}} \\ \hat{\boldsymbol{\theta}}_{\mathcal{L}} \end{bmatrix} + \begin{bmatrix} \mathbf{M}_{\mathcal{L}}^{\mathsf{vp}} & \mathbf{M}_{\mathcal{L}}^{\mathsf{vq}} \\ \mathbf{M}_{\mathcal{L}}^{\theta\mathsf{p}} & \mathbf{M}_{\mathcal{L}}^{\theta\mathsf{q}} \end{bmatrix} \begin{bmatrix} \Delta\mathbf{p}_{\mathcal{L}} \\ \Delta\mathbf{q}_{\mathcal{L}} \end{bmatrix} + \begin{bmatrix} \mathbf{m}_{\mathcal{L}}^{\mathsf{vv}} \\ \mathbf{m}_{\mathcal{L}}^{\theta\mathsf{v}} \end{bmatrix} \Delta v_0, \tag{2.49}$$

and

$$\begin{bmatrix} \tilde{p}_0 \\ \tilde{q}_0 \end{bmatrix} = \begin{bmatrix} \hat{p}_0 \\ \hat{q}_0 \end{bmatrix} + \begin{bmatrix} \mathbf{m}_{\mathcal{L}}^{\mathsf{pp}} & \mathbf{m}_{\mathcal{L}}^{\mathsf{pq}} \\ \mathbf{m}_{\mathcal{L}}^{\mathsf{qp}} & \mathbf{m}_{\mathcal{L}}^{\mathsf{qq}} \end{bmatrix} \begin{bmatrix} \Delta\mathbf{p}_{\mathcal{L}} \\ \Delta\mathbf{q}_{\mathcal{L}} \end{bmatrix} + \begin{bmatrix} m^{\mathsf{pv}} \\ m^{\mathsf{qv}} \end{bmatrix} \Delta v_0, \tag{2.50}$$

where a *new* operating point $(\tilde{\mathbf{v}}_{\mathcal{L}}, \tilde{\boldsymbol{\theta}}_{\mathcal{L}}, \tilde{p}_{0,i}, \tilde{q}_{0,i}, \tilde{v}_{0,i})$ is approximated by the given (old) operating point $(\hat{\mathbf{v}}_{\mathcal{L}}, \hat{s\boldsymbol{\theta}}_{\mathcal{L}}, \hat{p}_{0,i}, \hat{q}_{0,i}, \hat{v}_{0,i})$ using the linearization coefficient matrices or vectors denoted by $\mathbf{M}_{\mathcal{L}}^{\mathsf{vp}}, \mathbf{M}_{\mathcal{L}}^{\mathsf{vq}}, \mathbf{M}_{\mathcal{L}}^{\theta\mathsf{p}}, \mathbf{M}_{\mathcal{L}}^{\theta\mathsf{q}} \in \mathbb{R}^{n\times n}, \mathbf{m}_{\mathcal{L}}^{\mathsf{pp}}, \mathbf{m}_{\mathcal{L}}^{\mathsf{pq}}, \mathbf{m}_{\mathcal{L}}^{\mathsf{qp}}, \mathbf{m}_{\mathcal{L}}^{\mathsf{qq}} \in \mathbb{R}^{1\times n}$, $\mathbf{m}_{\mathcal{L}}^{\mathsf{vv}}, \mathbf{m}_{\mathcal{L}}^{\theta\mathsf{v}} \in \mathbb{R}^{n\times 1}$, $m^{\mathsf{pv}}, m^{\mathsf{qv}} \in \mathbb{R}$. Based on this, the trust-region is formed using the linear estimates. Hence, a quadratic problem can be formulated in each step that searches for the optimal solution within the trust region. Let the decision variables for node i denoted by $\boldsymbol{\chi}_i := [p_i, q_i, v_i] \in \mathbb{R}^3$, the detail of trust-region algorithm is given in Algorithm 2. Note that a feasible power flow solution is recovered in step 1.3, which can be used to form a feed-back control loop to enable the online implementation.

Three-bus network example

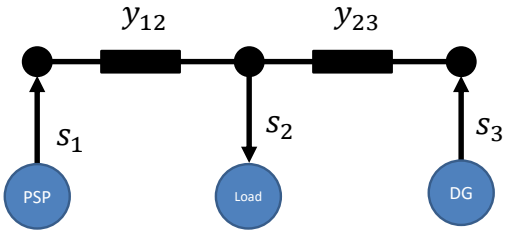

Fig. 2.5: Three-bus network example.

We illustrate the trust-region with a numerical example in the following. The test case is based on a three-bus network depicted in Fig. 2.5 with the network configuration provided in Table 2.1. In principle, two energy sources, i.e., PSP and DG,

Algorithm 2 Trust-region Algorithm of Solving OPF [2]

Input: $\hat{\boldsymbol{\chi}}_{\mathcal{L}_i}(0)$ - initial feasible state variable, $f_i(\hat{\boldsymbol{\chi}}_{\mathcal{L}_i}(0))$ - initial local objective value
Parameters: ϵ - termination tolerance, $\varphi_i(k)$ - trust-region radius; $\varphi_{\max}$ - maximal trust-region radius; η, β, $\gamma \in (0,1)$ - trust-region constants;

Step 1. (Local minimization with trust-region algorithm)

1.1 Choice of linearized model: to construct/update the sensitivity matrix for linearized power flow model at operating point $(\hat{u}(k), \hat{s}_0(k))$, i.e., (2.49) and (2.50).

1.2 Trust region minimization with $f(\chi)$:

$$\tilde{\boldsymbol{\chi}}^*_{\mathcal{L}}(k+1) := \arg\min_{\tilde{\boldsymbol{\chi}}} f(\boldsymbol{\chi}) \tag{2.46a}$$

s.t. (2.44c) to (2.44g), (2.49) and (2.50)

$$||\tilde{\boldsymbol{\chi}}_{\mathcal{L}}(k+1) - \hat{\boldsymbol{\chi}}_{\mathcal{L}}(k)|| < \varphi$$

1.3 Feasible power flow projection: the next operating point $\hat{\boldsymbol{\chi}}_{\mathcal{L}}(k+1)$ is obtained by projecting the optimization results $\tilde{\boldsymbol{\chi}}^*_{\mathcal{L}}(k+1)$ to the feasible power flow solution, e.g. by using a Newton–Raphson algorithm [67].

1.4 With the previous operating point $\hat{\boldsymbol{\chi}}_{\mathcal{L}}(k)$, the approximate point $\tilde{\boldsymbol{\chi}}_{\mathcal{L}}(k+1)$ and the current operating point $\hat{\boldsymbol{\chi}}_{\mathcal{L}}(k+1)$, the following ratio is computed:

$$\sigma_(k+1) = \frac{f(\hat{\boldsymbol{\chi}}_{\mathcal{L}}(k+1)) - f(\hat{\boldsymbol{\chi}}_{\mathcal{L}}(k))}{f(\tilde{\boldsymbol{\chi}}^*_{\mathcal{L}}(k+1)) - f(\hat{\boldsymbol{\chi}}_{\mathcal{L}}(k))} \tag{2.47}$$

which represents the ratio between actual objective reduction and predicted reduction.

1.5 Trust region radii evaluation and update:

$$\varphi(k+1) = \begin{cases} \gamma\varphi_(k) & \sigma(k+1) \le \eta \\ \min\{\varphi_{\max}, 2\varphi(k)\} & \sigma(k+1) \ge (1-\eta) \\ \varphi(k) & \text{otherwise} \end{cases} \tag{2.48}$$

1.6 Trust region solution evaluation:
If $\sigma(k+1) > \beta$, solution of $\hat{\boldsymbol{\chi}}_{\mathcal{L}}(k+1)$ is accepted, otherwise rejected and $\hat{\boldsymbol{\chi}}_{\mathcal{L}}(k+1) = \hat{\boldsymbol{\chi}}_{\mathcal{L}}(k)$ is set.

1.7 Termination criteria check of trust region: $||\tilde{\boldsymbol{\chi}}_{\mathcal{L}}(k+1) - \hat{\boldsymbol{\chi}}_{\mathcal{L}}(k+1)|| < \epsilon$.

compete with each other to supply to the load located at node 2. With the marginal cost of the two energy sources, the optimal point for the minimal power procurement cost is equivalent to the problem to minimize the power losses. Note that the feasible set of control variables are defined for $(p_3, q_3) \in \mathbb{R}^2$, as the power injection at PSP can only be changed “passively”. We plot the cost function with respect to its feasible region in Fig. 2.6. It can be observed that the feasible region (p_3, q_3) is described by a non-convex set (“belt" shape in the figure). The optimal point (red

Table 2.1: Data for 3-bus network example.

Load	$1 + 1\,\jmath$ [pu]			
Line	y_{12}		y_{23}	
	$0.1 + 0.15\jmath$ [pu]		$0.1 + 0.14\jmath$ [pu]	
Generation	PSP		DG	
	capacity	price coefficient	capacity	price coefficient
	[0 inf]	10	[0 2]	10

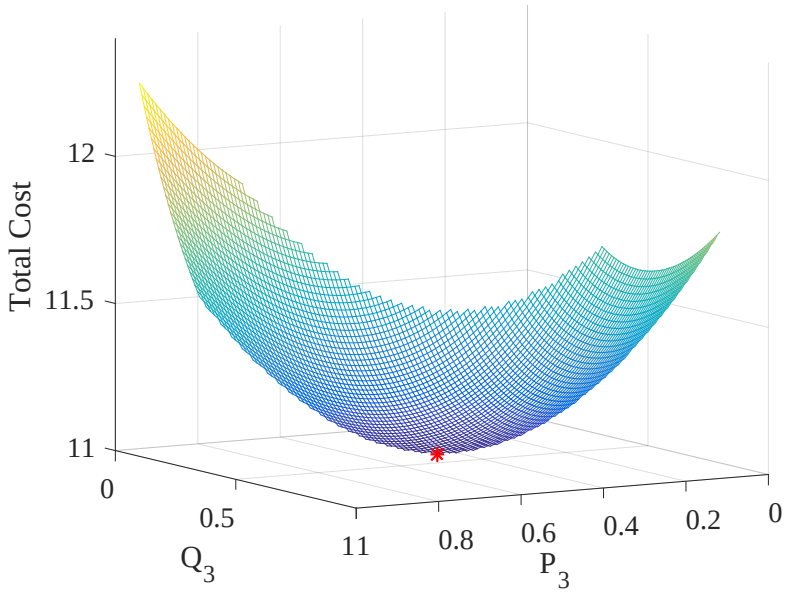

Fig. 2.6: Objective function.

dot in the figure) can be found on the boundary line of the feasible region. To this end, the target of the optimization method is to find the minimum-cost point given a starting point. The complete feasible set is defined with respect to all power flow state variables including the voltages at all buses, which can be described by the power flow manifold. In Fig. 2.7, the power flow manifold is plotted for the nodal voltage at bus 3 with respect to its active/reactive nodal injections. Particularly, one can observe the voltage lower bound of 0.90 pu.

Consider applying trust-region to solve the above test case. At each step, a trust-region is formed by obtaining the approximate model at the operating point (rectangular area). Then the direction of the arrow in Fig. 2.7 is determined by the maximal objective decent direction in the trust region algorithm step 1.2. The trust region (blue area) size is adjusted at each step based on the model accuracy measured by the error between real approximated power flow and the actual power flow solutions. The iterations repeat until a stable point (hopefully a global optimal point) is found. Note that despite the adoption of nonlinear non-convex optimal power flow models in this work, the trust-region method empirically yields the global optimal solution for the radial distribution network (in fact, for all test scenarios that have been tested in this work). At the time writing, there is no mathematical proof for this to be guaranteed. In relevance to this, similar investigations [80] for

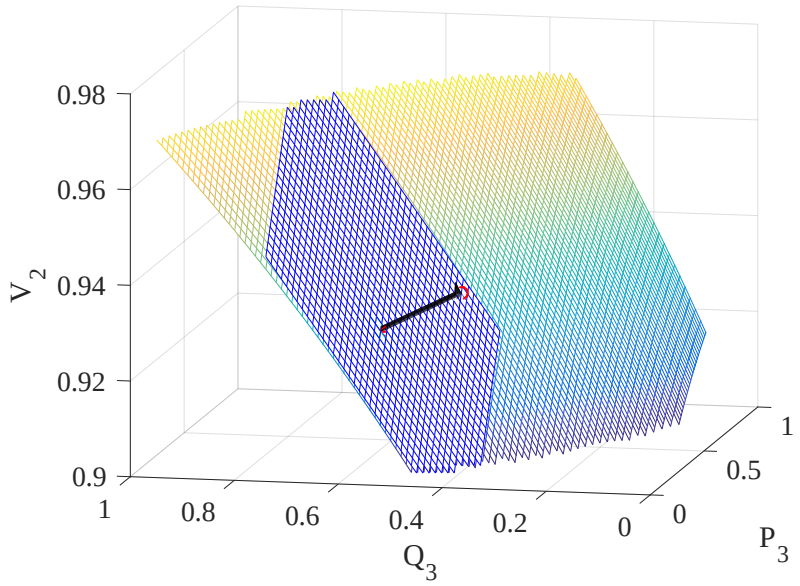

Fig. 2.7: Trust-region iterations on the power flow manifold.

convexification of optimal power flow exist in the literature.

2.4 Summary

This chapter reviews the basic modeling for electrical distribution system. As the key elements for optimal decision tools, explicit power flow linearization, optimal power flow problems and trust-region algorithm are introduced. It is important to notice that depending on the application and the real-world grid parameters, linearized power flow model provides a trade-off between the model accuracy and the computational effort, which must be taken into account to provide solutions for different applications. For example, for applications like voltage control, a linearized DistFlow model is sufficiently adequate to estimate the voltage magnitude and, hence, can be used to design distributed/centralized controller to regulate the voltage. For applications in the market design, we are more interested in the exact cost allocations. To this end, exact power flow solution and the respective solution methodologies are better suited.

Chapter 3

Spot Pricing and Distributed Optimization

Based on duality theory, the optimal spot pricing can be derived by the solution of optimal power flow problems. It results in a DLMP formulation, which follows the same form as in (1.1). The derivation of DLMP is closely related to the classical welfare theorem in microeconomics. In this chapter, we start by solving a generic optimization problem by applying the duality theory. The presentation of its mathematical formulation is aimed to provide some intuition behind the functionality of using dual variables as the optimal prices. Some of the practical aspects to implement DLMP in relevance to the research questions in chapter 1 are also addressed. The following discussion on the fundamentals of duality and pricing is inspired from the textbook [41, 81]. Sharing the same origin of using duality to solve optimization problems, distributed optimization methods are another cornerstone to enable decentralized market implementation. In the second half of this chapter, we focus on one of the methods, i.e., ADMM, which is detailed in its motivation, derivation, implementation and performance.

3.1 Market modeling

3.1.1 Fundamentals of duality

Consider a generic convex optimization in the same form of (2.45), which is referred as the primal problem in the context of duality. Lagrangian can be defined as

$$L(\mathbf{x}, \boldsymbol{\lambda}, \boldsymbol{\nu}) = f(\mathbf{x}) + \sum_{i=1}^{m} \lambda_i g_i(\mathbf{x}) + \sum_{i=1}^{p} \nu_i h_i(\mathbf{x}), \tag{3.1}$$

where $\boldsymbol{\lambda} \in \mathbb{R}^m, \boldsymbol{\nu} \in \mathbb{R}^p$ are referred as dual variable vectors for the inequality and equality constraints, respectively. To this end, the dual function can be obtained as the minimum of Lagrangian over $\mathbf{x}$

$$\mathcal{L}(\boldsymbol{\lambda}, \boldsymbol{\nu}) = \min_{\mathbf{x}} L(\mathbf{x}, \boldsymbol{\lambda}, \boldsymbol{\nu}). \tag{3.2}$$

The dual function is always a concave function, since it is the minimum of a family of affine functions. Due to its concavity, the dual function is easy to solve and proved

useful to obtain the lower bounds for the primal problem's objective. This means, for an optimal solution $p^* = f(\mathbf{x}^*)$ of problem (2.45) and a non-negative dual variable $\boldsymbol{\lambda} \geq 0$, we can obtain the lower bounds for the optimal solutions of the problem

$$\mathcal{L}(\boldsymbol{\lambda}, \boldsymbol{\nu}) \leq f(\mathbf{x}^*), \tag{3.3}$$

where its proof can be simply followed by substituting the eq. (2.45b) and (2.45c) into the Lagrangian.

This inequality condition is commonly referred as *weak duality*. To obtain the largest lower bound, the following dual problem can be defined as

$$d^* = \max_{\boldsymbol{\lambda}, \boldsymbol{\nu}} \mathcal{L}(\boldsymbol{\lambda}, \boldsymbol{\nu}) \tag{3.4a}$$

s.t.

$$\boldsymbol{\lambda} \geq 0, \tag{3.4b}$$

where, due to its concave function characteristic, the dual problem is in general easy to solve. The definition of weak duality motivates to define the concept of *strong duality* as

$$d^* = p^*. \tag{3.5}$$

Strong duality usually holds when the primal problem is convex under some mild *constraint qualification* condition. It also holds, in some rare cases, for non-convex problems. Furthermore, both primal and dual variables should satisfy the following KKT conditions if they are the optimal under the strong duality.

Karush-Kuhn-Tucker conditions

$\nabla L(\mathbf{x}, \boldsymbol{\lambda}, \boldsymbol{\nu}) = \mathbf{0}$	stationary condition	(3.6a)
$g_i(\mathbf{x}) \leq 0, , \quad i = 1, ..., m$		(3.6b)
$h_i(\mathbf{x}) = 0, \quad i = 1, ..., p$	primal feasibility	(3.6c)
$\boldsymbol{\lambda} \geq 0$	dual feasibility	(3.6d)
$\lambda_i g_i(\mathbf{x}) = 0$	complementary slackness	(3.6e)

KKT conditions are necessary conditions for optimality. In the case of convex optimization problems, they are also sufficient conditions. KKT conditions play a central role to associate the optimal power flow solutions with the optimal electricity and AS prices. Essentially, the dual variables can be devised as the optimal prices based on KKT condition. In this scope, the interpretation of dual variables as the marginal cost for electricity is important. Consider the modified generic optimization problem (2.45) to

$$\min \quad p = f(\mathbf{x}) \tag{3.7a}$$

s.t.

$$g_i(\mathbf{x}) \leq a_i, \quad i = 1, ..., m \tag{3.7b}$$
$$h_i(\mathbf{x}) = b_i, \quad i = 1, ..., p, \tag{3.7c}$$

where the right side of the equality and inequality constraints are replaced with a infinitesimal number a_i, b_i. The respective Lagrangian is obtained as

$$L(\mathbf{x}, \boldsymbol{\lambda}, \boldsymbol{\nu}) = f(\mathbf{x}) + \sum_{i=1}^{m} \lambda_i (g_i(\mathbf{x}) - a_i) + \sum_{i=1}^{p} (\nu_i h_i(\mathbf{x}) - b_i), \tag{3.8}$$

Applying the stationary condition on the infinitesimal number, the dual variables are obtained as the sensitivity of the optimal objective solution to a_i, b_i:

$$\lambda_i = -\frac{\partial p}{a_i} \quad \text{and} \quad \nu_i = -\frac{\partial p}{b_i}. \tag{3.9}$$

Hence the dual variables are obtained as the sensitivity of the total cost subject to the infinitesimal additive modification of constraint bounds, i.e., marginal cost to comply with the respective constraint. Now recall the constraints defined in the generic OPF problem. If we associate the dual variables to the grid stability constraints like voltage bound or thermal limit, the respective dual variables can be interpreted as the marginal cost to provide the ASs that maintain the stability, which gives the mathematical formulation of T&D network quality of supply premium in Eq. 1.1 in the spot pricing principles.

3.1.2 Optimal pricing

As aforementioned, for a typical optimal power flow problem, some dual variables can be interpreted as the marginal cost to maintain the grid stability. Then the question arises in how to define a market mechanism that can direct the market participants to satisfy various power system constraints in the electricity market. Consider the following problem, which can be viewed as a simplified form of optimal power flow problem,

$$\min \quad \sum_{i=1}^{n} f_i(x_i) \tag{3.10a}$$

s.t.

$$g_i(\mathbf{y}) \leq 0, \quad i = 1, ..., n \qquad : \mu_i \in \mathbb{R} \tag{3.10b}$$
$$x_i = h_i(\mathbf{y}), \quad i = 1, ..., n, \qquad : \lambda_i \in \mathbb{R} \tag{3.10c}$$

where the objective of the problem is assumed to be separable into each agent i. The objective function is further interpreted as the sum of the cost function (maximization of social-welfare) for each agent. By applying the stationary condition (3.6a) with respect to the local decision variable x_i, we obtain

$$\frac{\partial f_i(x_i)}{\partial x_i} - \lambda_i = 0. \tag{3.11}$$

The solution above is essentially equivalent for the agent i to solve the following optimization problem

$$\min \quad f_i(x_i) - \lambda_i x_i, \tag{3.12}$$

which is a cost minimization problem for agent i with λ_i given as the pre-defined price for the purchased/provided quantity x_i. Hence, if we can set the prices λ_i properly, the social-welfare problem (3.10) can be aligned to the individual problems (3.12) of agent i. The example above gives us the intuition to develop socially optimal pricing scheme for the electricity market. In the following, we introduce its adoption in the context of distribution grid market.

3.1.3 Distribution locational marginal price formulation based on spot pricing principles

In the center of the proposal for optimal electricity pricing in distribution grid, DLMPs are derived based on the social welfare maximization problem for the whole distribution system, which represents the minimization of the DSO's total cost for energy/flexibility procurement subject to all system and electric grid constraints. Mathematically speaking, the social welfare function, i.e., the difference of utility function and the cost function of all DERs, is expressed as

$$w(\mathbf{p}^{\mathsf{g}}, \mathbf{q}^{\mathsf{g}}, \mathbf{p}^{\mathsf{fl}}) = C^{\mathsf{fl}}(\mathbf{p}^{\mathsf{fl}}) - C^{\mathsf{p}}(\mathbf{p}^{\mathsf{g}}) - C^{\mathsf{q}}(\mathbf{q}^{\mathsf{g}}). \tag{3.13}$$

where the total active/reactive power nodal injections are given as

$$\mathbf{p} = \mathbf{A}^{\mathsf{g}}\mathbf{p}^{\mathsf{g}} - \mathbf{A}^{\mathsf{fl}}\mathbf{p}^{\mathsf{fl}} - \mathbf{A}^{\mathsf{sl}}\mathbf{p}^{\mathsf{sl}} \tag{3.14}$$

$$\mathbf{q} = \mathbf{A}^{\mathsf{g}}\mathbf{q}^{\mathsf{g}} - \mathbf{A}^{\mathsf{sl}}\mathbf{q}^{\mathsf{sl}} \tag{3.15}$$

with $\mathbf{A}^{\mathsf{g}} \in \mathbb{R}^{(n+1)\times g}, \mathbf{A}^{\mathsf{fl}} \in \mathbb{R}^{(n+1)\times fl}, \mathbf{A}^{\mathsf{sl}} \in \mathbb{R}^{(n+1)\times sl}$ representing the mapping matrices of DGs FLs and static loads to the grid nodes. The maximization of the overall social welfare for the whole distribution system is described by

$$\max \quad w(\mathbf{p}^{\mathsf{g}}, \mathbf{p}^{\mathsf{fl}}, \mathbf{q}^{\mathsf{g}}) \tag{3.16a}$$

s.t.

$$\mathbf{1}_{n+1}^{\mathsf{T}}\mathbf{p} = p^{\mathsf{loss}} \qquad : \lambda^{\mathsf{p}} \in \mathbb{R} \tag{3.16b}$$

$$\mathbf{1}_{n+1}^{\mathsf{T}}\mathbf{q} = q^{\mathsf{loss}} \qquad : \lambda^{\mathsf{q}} \in \mathbb{R} \tag{3.16c}$$

$$\underline{\mathbf{p}} \le \mathbf{p} \le \overline{\mathbf{p}} \qquad : \underline{\boldsymbol{\mu}}^{\mathsf{p}}, \overline{\boldsymbol{\mu}}^{\mathsf{p}} \in \mathbb{R}^n \tag{3.16d}$$

$$\underline{\mathbf{q}} \le \mathbf{q} \le \overline{\mathbf{q}} \qquad : \underline{\boldsymbol{\mu}}^{\mathsf{q}}, \overline{\boldsymbol{\mu}}^{\mathsf{q}} \in \mathbb{R}^n \tag{3.16e}$$

$$\underline{\mathbf{v}} \le \mathbf{v} \le \overline{\mathbf{v}} \qquad : \underline{\boldsymbol{\mu}}^{\mathsf{v}}, \overline{\boldsymbol{\mu}}^{\mathsf{v}} \in \mathbb{R}^n \tag{3.16f}$$

$$|\mathbf{s}^{\mathsf{f}}|^2 \le |\overline{\mathbf{s}}|^2 \qquad : \boldsymbol{\mu}^{\mathsf{sf}} \in \mathbb{R}^h \tag{3.16g}$$

$$|\mathbf{s}^{\mathsf{t}}|^2 \le |\overline{\mathbf{s}}|^2 \qquad : \boldsymbol{\mu}^{\mathsf{st}} \in \mathbb{R}^h, \tag{3.16h}$$

where constraints (3.16b) and (3.16c) are the active and reactive power balance equations. Constraints (3.16d) to (3.16h) are the box constraints for nodal power injections and voltage magnitude and bi-directional line flow. Note that constraints (3.16b) and (3.16c) contain the power flow equation implicitly. The dual variables are listed on the right side of their respecting constraints with the same dimensions.

The DLMPs are then evaluated with the respective sensitivity matrices upon the obtaining the optimal solutions. More specifically, after obtaining the optimal solutions, the DLMPs can be recovered using the KKT conditions by calculating the

first-order derivative of the Lagrangian function for nodal active power. As a result, the DLMPs for active power $\boldsymbol{\pi} \in \mathbb{R}^n$ are given as the sum of four components [35, 2]:

$$\boldsymbol{\pi} = \boldsymbol{\pi}^{\mathsf{e}} + \boldsymbol{\pi}^{\mathsf{l}} + \boldsymbol{\pi}^{\mathsf{v}} + \boldsymbol{\pi}^{\mathsf{c}}, \tag{3.17}$$

where $\boldsymbol{\pi}^{\mathsf{e}} := c^{\mathsf{p},0}\mathbf{1}_n$ is the energy component with $c^{\mathsf{p},0}$ as the active power price at PSP from the wholesale market, $\boldsymbol{\pi}^{\mathsf{l}} := -((\frac{\partial p^{\mathsf{loss}}}{\partial \mathbf{p}_{\mathcal{L}}})^{\intercal} c^{\mathsf{p},0} + (\frac{\partial q^{\mathsf{loss}}}{\partial \mathbf{p}_{\mathcal{L}}})^{\intercal} c^{\mathsf{q},0})$ is the loss component with $\frac{\partial p^{\mathsf{loss}}}{\partial \mathbf{p}_{\mathcal{L}}}, \frac{\partial q^{\mathsf{loss}}}{\partial \mathbf{p}_{\mathcal{L}}} \in \mathbb{R}^{1\times n}$ as the loss sensitivity coefficient for active/reactive power losses in respect to the nodal injections and $c^{\mathsf{q},0}$ as the reactive power price at PSP, (iii) $\boldsymbol{\pi}^{\mathsf{v}} := (\frac{\partial \mathbf{v}}{\partial \mathbf{p}_{\mathcal{L}}})^{\intercal}(\underline{\boldsymbol{\mu}}^{\mathsf{v}} - \overline{\boldsymbol{\mu}}^{\mathsf{v}})$ is the voltage support component with $\frac{\partial \mathbf{v}}{\partial \mathbf{p}_{\mathcal{L}}} \in \mathbb{R}^{n\times n}$ as the voltage sensitivity with respect to active power injections, and (iv) $\boldsymbol{\pi}^{\mathsf{c}} := (\frac{\partial |\mathbf{s}^{\mathsf{f}}|^2}{\partial \mathbf{p}_{\mathcal{L}}})^{\intercal}\boldsymbol{\mu}^{\mathsf{sf}} + (\frac{\partial |\mathbf{s}^{\mathsf{t}}|^2}{\partial \mathbf{p}_{\mathcal{L}}})^{\intercal}\boldsymbol{\mu}^{\mathsf{st}}$ is the congestion component with $\frac{\partial |\mathbf{s}^{\mathsf{f}}|^2}{\partial \mathbf{p}_{\mathcal{L}}}, \frac{\partial |\mathbf{s}^{\mathsf{t}}|^2}{\partial \mathbf{p}_{\mathcal{L}}} \in \mathbb{R}^{h\times n}$ denoting the sensitivity of the squared line flow with respect to the active power injection. Note that the DLMP representation is referred as implicit-function based decomposition in [5] that naturally lends itself into forming three different grid operation products: loss compensation, voltage support and congestion reduction for each node to contribute to the overall grid operational cost.

Options for market implementation based on DLMPs

Depending on the organization of information flow, there are two ways to organize the market using DLMPs. The first option, which is in the category of centralized control, resembles an auction-based wholesale market implementation. It can follow the following steps.

1. DGs, FLs submit their bids, energy requirements as well as the dispatch capabilities to the DSO.
2. The DSO forecasts its underlying grid demand and price for the power supply from wholesale market.
3. The DSO clears regional DLMPs to be passed on to local DGs together with their contracted energy supplies/demand.

Note that both the forward market and real-time market (for balancing) can be established in a similar manner. The second option can be categorized into decentralized control, where the DSO simply sets the price signals and DGs and FLs reacts accordingly. More specifically, the steps in this setting can be provided as follows.

1. The DSO forecasts its underlying grid demand and price for the power supply from wholesale market. The DSO either forecasts or requests the availability and supply/demand data of DGs/FLs.
2. The DSO calculates the DLMPs and publishes to DG/FL aggregators, and alternative load serving entities.

This kind of decentralized operation are proposed in a number of references including [16]. Since information privacy and autonomy is an important topic for decentralized energy management, the load aggregators tend to protect their sensitive

information such as utility function. Hence, it is worth mentioning that iterative approaches that utilizes decomposition methods, e.g., dual decomposition, ADMM, are the research interest of many proposals [82, 2]. This kind of approach generally requires the exchange of dual variables between DSO and DER aggregators, where the sensitive information like utility/cost functions, bid formulation remain locally with the DER-end. Beyond this scope, there are other occasions, where decomposition methods, or distributed optimization methods have practical use cases. We elaborate this aspect in the following section.

3.2 Distributed optimization method

As the main theme of this work is to provide the coordination scheme between market operators (DSOs), market participants (DERs), distributed optimization techniques can be found very useful in a variety of settings, e.g., formulating DER-to-DER, DSO-to-DSO coordination mechanisms. In this work, we focus on ADMM-based solution methodology, where its applications are demonstrated for a number of use cases. The arguments of the adoption of ADMM include i) implementation robustness and flexibility, ii) the interpretation as a market mechanism. Specifically, ADMM can be interpreted as a price coordination mechanism to achieve the Walrasian tâtonnement process [83], which only requires the information exchange of proxy variables without revealing the sensitive local information like utility function and constraints. It is also a robust method, which is shown in recent exposition [84] in the presence of asynchronous data update and packet loss. To this end, it makes the protocol suitable for plug & play applications.

ADMM was first introduced by Gabay, Mercier, Glowinski, and Marrocco in the mid-1970s. Since then, it has been continuously developed and intensively studied in the following decades. Only in recent years, with the emergence of large-scale data analysis techniques like artificial intelligence, it is of prime importance to develop suitable methods that can handle problem in parallel and distributed fashion, wherein the method fits well in the picture. The derivation of ADMM is deeply rooted in the duality theory that can be traced back as a variant of primal-dual method to solve convex optimization problems. In this section, we aim to provide the intuition to interlink ADMM with the duality theory, which is inspired from the Boyed's work [83].

3.2.1 Dual decomposition

Consider a generic convex optimization problem in the form of (2.45) with only equality constraint.

$$\min \quad f(\mathbf{x}) \tag{3.18a}$$

s.t.

$$\mathbf{A}\mathbf{x} = \mathbf{b}, \ : \boldsymbol{\nu}. \tag{3.18b}$$

Assuming that the strong duality holds, for a given optimal dual variable $\boldsymbol{\nu}^*$, the optimal solution $\mathbf{x}^*$ can be recovered by

$$\mathbf{x}^* = \arg\min_{\mathbf{x}} L(\boldsymbol{\nu}^*, \mathbf{x}). \tag{3.19}$$

Recall the definition of dual problem, where it can be used to find the maximal lower bound of the primal problem, a method to solve the optimization problem that is termed as *dual ascent* method, can be formulated by using the idea of gradient ascent. Recall the stationary condition in KKT conditions, where the gradient of dual function with respect to the dual variable, given as $\nabla_{\boldsymbol{\nu}}\mathcal{L} = \mathbf{A}\mathbf{x} - \mathbf{b}$, is supposed to be equal to zero. To this end, the iterative steps of dual ascent method can be given as

$$\mathbf{x}(k+1) := \arg\min_{\mathbf{x}} L(\mathbf{x}, \boldsymbol{\nu}(k)) \tag{3.20a}$$

$$\boldsymbol{\nu}(k+1) := \boldsymbol{\nu}(k) + \alpha(\mathbf{A}\mathbf{x}(k+1) - \mathbf{b}), \tag{3.20b}$$

where $\alpha > 0$ is the stepsize. Note that based on the discussion in Section 3.1.1, the dual variable $\boldsymbol{\nu}$ is the marginal cost to satisfy the equality constraint. The advantage of dual ascent method is that it can be implemented in a distributed way for some special types of problems. Consider the following case, where the objective is separable, i.e.,

$$f(\mathbf{x}) = \sum_{i=1}^{n} f_i(\mathbf{x}_i), \tag{3.21}$$

with separable constraint term $\mathbf{A}\mathbf{x} = \sum_{i=1}^{n} \mathbf{A}_i\mathbf{x}_i$. Hence, the Lagrangian is rewritten as a sum of individual terms as

$$L(\boldsymbol{\nu}, \mathbf{x}) = \sum_{i=1}^{n} L_i(\boldsymbol{\nu}_i, \mathbf{x}_i) = \sum_{i=1}^{n} \big(f_i(\mathbf{x}_i) + \boldsymbol{\nu}^{\mathsf{T}}(\mathbf{A}_i\mathbf{x}_i - \mathbf{b})\big), \tag{3.22}$$

This formulation results in a parallel-implementable dual-ascent method, which is commonly referred as *dual decomposition*, provided as

$$\mathbf{x}_i(k+1) := \arg\min_{\mathbf{x}_i} L_i(\mathbf{x}, \boldsymbol{\nu}(k)) \tag{3.23a}$$

$$\boldsymbol{\nu}(k+1) := \boldsymbol{\nu}(k) + \alpha(\mathbf{A}\mathbf{x}(k+1) - \frac{1}{n}\mathbf{b}), \tag{3.23b}$$

where step (3.23a) can be solved in parallel in n agents and step (3.23b) requires a central entity to collect the local update $\mathbf{x}_i$ and update the dual variable centrally. Then the updated dual variables will be redistributed to each agent to accomplish the next iteration. The above procedures are demonstrated in the following example.

Examples for dual decomposition

Consider a simple decomposable optimiztion problem with strict convex objective function in following form

$$\min_{x_1, x_2} \quad f(x_1, x_2) = x_1^2 + x_1 + x_2^2 + x_2 \tag{3.24a}$$

s.t.

$$x_1 + x_2 = 2, \tag{3.24b}$$

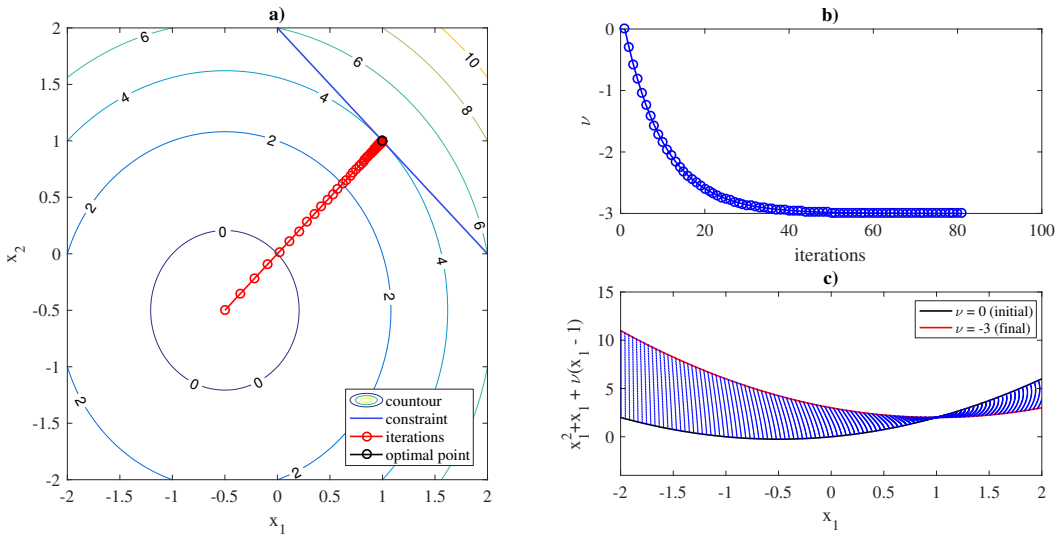

Fig. 3.1: Example for dual decomposition ($\nu(0) = 0$, $\alpha = 0.1$). Plot a) shows the contour of the objective function and the linear constraint. Plot b) shows the evolution of ν over the iterations of dual decomposition methods. Plot c) depicts the evolution of the subproblem Lagrangian over the iterations.

where the problem has a separable quadratic objective function of variables x_1, x_2 and is subject to the affine constraint. Based on the dual decomposition method, the solution can be found by the following iterations:

$$x_1(k+1) := \arg\min_{x_1} \big(x_1^2 + x_1 + \nu(x_1 - 1)\big), \tag{3.25a}$$

$$x_2(k+1) := \arg\min_{x_2} \big(x_2^2 + x_1 + \nu(x_2 - 1)\big), \tag{3.25b}$$

$$\nu(k+1) := \nu(k) + \alpha(x_1(k+1) + x_2(k+1) - 2). \tag{3.25c}$$

The evolution of the iterations are plotted in Fig. 3.1. Note that the subproblems (3.25a) and (3.25b) are unbounded in their quadratic objectives, which are trivial to solve. Hence, for the initial step, it is intuitively to find the origin of the objective function $(-0.5, -0.5)$ as the optimal point (see subplot a) in Fig. 3.1). With the increasing penalty term from decreasing ν, the origin of the Lagrangian of the subproblems are slowly shifted to the optimal point with the binding constraint. This can be observed in subplot c) of Fig. 3.1, where the origin of the quadratic Lagrangian function of the subproblem is shifted to the constraint-binding point.

Note that based on the stationary KKT condition, i.e., $\nabla L(\mathbf{x}, \boldsymbol{\lambda}, \boldsymbol{\nu}) = \mathbf{0}$, the local optimality should coincide with the global optimality, where the optimal solutions should satisfy

$$\frac{\partial f(x_1, x_2)}{\partial x_1} = -\nu, \tag{3.26a}$$

$$\frac{\partial f(x_1, x_2)}{\partial x_2} = -\nu. \tag{3.26b}$$

The overall problem is strictly convex and, hence, the solution is unique for the given example.

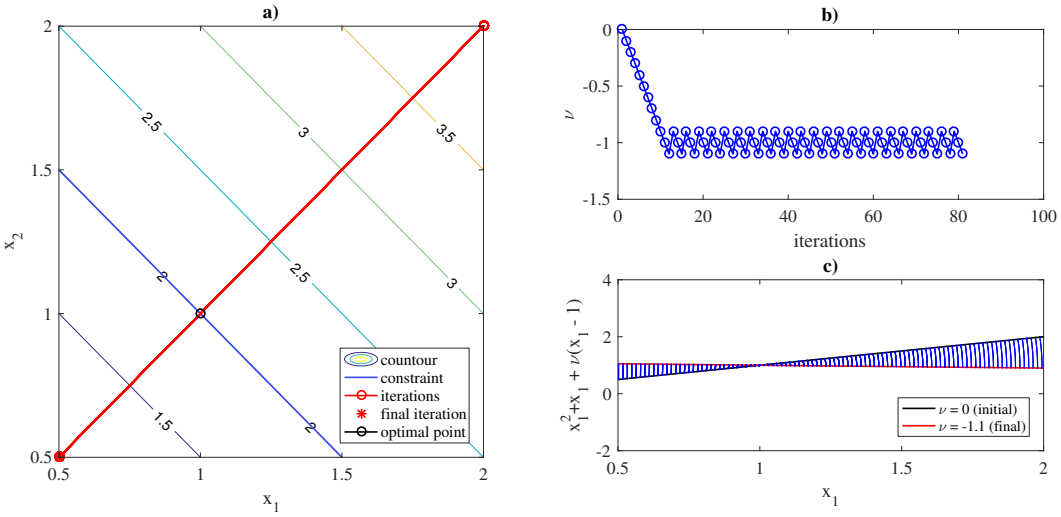

Fig. 3.2: Example for dual decomposition in an unstable scenario ($\nu(0) = 0$, $\alpha = 0.1$). Plot a) shows the contour of the linear objective function and the constraint. Plot b) shows the oscillations of ν over the iterations for the modified problem. Plot c) depicts the subproblem Lagrangian over the iterations.

In the case that the objective function is not strictly convex (even the overall problem has a unique solution), the dual ascent method has convergence issue. We illustrate by replacing objective function in problem (3.24) with an affine function as

$$\min_{x_1,x_2} \quad f(x_1, x_2) = x_1 + x_2 \tag{3.27a}$$

s.t.

$$x_1 + x_2 = 2, \tag{3.27b}$$
$$0.5 \leq x_1 \leq 2, \tag{3.27c}$$
$$0.5 \leq x_2 \leq 2. \tag{3.27d}$$

Similarly, we apply the dual decomposition method for the modified example and present the results in Fig. 3.2. One can observe from subplot a) in Fig. 3.2 that all the iterations are mostly concentrated at two end points along the decent direction of the objective (red line). This can be explained by the unbounded subproblems in plot c), where the Lagrangian for subproblem with varying ν is depicted. It can be seen that an infinitesimal change of the dual variable can lead to the change of the sign in the gradient of the Lagrangian when the iterations approaching the optimal point $(1, 1)$. For unbounded subproblems with linear objective, the change of sign will cause the "oscillation" between two end points at $(0.5, 0.5)$ and $(2, 2)$. This in turn results in the instability of the dual decomposition method for this type of problem.

3.2.2 Method of multipliers

Based on the above discussion, dual decomposition method has convergence issue when the objective function is not strictly convex. To bring robustness into the

method, the *method of multipliers* is introduced as follows. First define the *augmented Lagrangian* for problem (3.18)

$$L_\rho(\boldsymbol{\nu}, \mathbf{x}) = f(\mathbf{x}) + \boldsymbol{\nu}^\mathsf{T}(\mathbf{A}\mathbf{x} - \mathbf{b}) + \frac{1}{2}\rho||\mathbf{A}\mathbf{x} - \mathbf{b}||_2^2 \tag{3.28}$$

with a positive constant ρ, which is also termed as penalty factor. The primal problem that associated to the augmented Lagrangian is clearly equivalent to the original problem (3.18).

Example

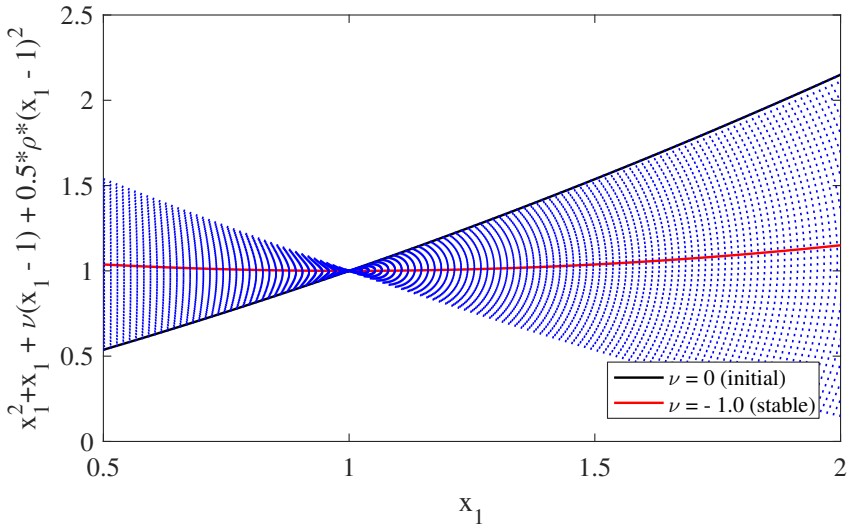

Fig. 3.3: Augmented Lagrangian for subproblem (3.25a) ($\rho = 0.3$, $\nu \in [-2, 0]$).

Consider the previous example with affine objective function in problem (3.27) as follows. We plot the associated augmented Lagrangian for the subproblem in Fig. 3.3. We can observe that the associated augmented Lagrangian is able to robustify the dual decomposition method by adding the augmented second-order term, which provides a unique solution at the optimal point $x_1 = 1$. Furthermore, the value of dual variable ν can be trivially calculated as finding the origin of the augmented Lagrangian, where $-\frac{0.7+\nu}{0.3 \cdot 0.5 \cdot 2} = 1$ gives $\nu = -1$.

In the example above, the modified Lagrangian provides the benefit that the dual function associated to the primal problem is differentiable even under rather mild conditions. Hence the underlying gradient update in the dual ascent method is more robust compared to the original dual decomposition method. The modified dual ascent method is obtained as

$$\mathbf{x}(k+1) := \arg\min_{\mathbf{x}} L_\rho(\mathbf{x}, \boldsymbol{\nu}(k)), \tag{3.29a}$$

$$\boldsymbol{\nu}(k+1) := \boldsymbol{\nu}(k) + \rho(\mathbf{A}\mathbf{x}(k+1) - \mathbf{b}), \tag{3.29b}$$

which is referred as the *method of multipliers*. The method converges under more general conditions including non-strictly-convex objective function $f(\mathbf{x})$.

Now consider the separable-objective example introduced in the dual decomposition method, where $f(\mathbf{x}) = \sum_{i=1}^{n} f_i(\mathbf{x}_i)$. We still like to achieve the similar parallel computation structure in (3.23). However, the penalty term $\frac{1}{2}\rho||\mathbf{Ax} - \mathbf{b}||_2^2$ is not separable. Hence the method of multipliers cannot be directly transformed for the decomposition purpose. In light of this, *alternating direction method of multipliers* is introduced.

3.2.3 Alternating direction method of multipliers

Consider the following problem

$$\min \quad f(\mathbf{x}) + g(\mathbf{y}) \tag{3.30a}$$

s.t.

$$\mathbf{Ax} + \mathbf{By} = \mathbf{b} \ : \boldsymbol{\nu} \in \mathbb{R}^n \tag{3.30b}$$

with variables $\mathbf{x} \in \mathbb{R}^k$, $\mathbf{y} \in \mathbb{R}^l$, mapping matrices $\mathbf{A} \in \mathbb{R}^{n\times k}, \mathbf{B} \in \mathbb{R}^{n\times l}$, and $\mathbf{b} \in \mathbb{R}^n$. It is also assumed that both $f(\mathbf{x})$ and $g(\mathbf{y})$ are convex functions. The augmented Lagrangian is defined as

$$L_\rho(\boldsymbol{\nu}, \mathbf{x}, \boldsymbol{\nu}) = f(\mathbf{x}) + g(\mathbf{y}) + \boldsymbol{\nu}^\intercal(\mathbf{Ax} + \mathbf{By} - \mathbf{b}) + \frac{1}{2}\rho||\mathbf{Ax} + \mathbf{By} - \mathbf{b}||_2^2. \tag{3.31}$$

ADMM is provided with the following steps in Algorithm 3.

Algorithm 3 ADMM algorithm

while *converged?* **do**

$$\mathbf{x}(k+1) := \arg\min_{\mathbf{x}} L_\rho(\mathbf{x}, \mathbf{y}(k), \boldsymbol{\nu}(k)) \tag{3.32}$$

$$\mathbf{y}(k+1) := \arg\min_{\mathbf{y}} L_\rho(\mathbf{x}(k+1), \mathbf{y}, \boldsymbol{\nu}(k)) \tag{3.33}$$

$$\boldsymbol{\nu}(k+1) := \boldsymbol{\nu}(k) + \rho(\mathbf{Ax}(k+1) + \mathbf{By}(k+1) - \mathbf{b}) \tag{3.34}$$

end

The generic form of ADMM algorithm works in a way that the primal variables $\mathbf{x}, \mathbf{y}$ are updated in a alternating manner (alternating direction). Then the dual variables can be updated either centrally or locally (requires different information flow). Regarding the convergence property, ADMM is able to converge to optimal solutions when $f(\mathbf{x}), g(\mathbf{y})$ are convex functions. It may even converge when the problem is nonconvex [83]. We will discuss this aspect from the application perspective in Chapter 4 and Chapter 5. Depending on the form of the problems, ADMM can be reformulated or simplified accordingly. Interested readers may refer [83] for the substantial review of these problems. To this end, we focus a special form of ADMM in solving consensus optimization problem, which is particularly interesting to formulate the electricity market coordinate scheme.

3.2.4 Consensus problem

Consider the generic consensus problem in the following form

$$\min \quad \sum_{i=1}^{n} f_i(\mathbf{x}_i) \tag{3.35a}$$

s.t.

$$\mathbf{x}_i = \mathbf{A}_i \mathbf{z} : \boldsymbol{\nu}_i \in \mathbb{R}^{n_i}, \quad i = 1, ..., n \tag{3.35b}$$

with $\mathbf{z} \in \mathbb{R}^m$ as the global variable, which the local variables $\mathbf{x}_i$ should agree upon (consensus). Matrix $\mathbf{A}_i \in \mathbb{R}^{n_i \times m}$ is the incidence matrix that projects the entries of $\mathbf{x}$ to the corresponding entries of global variable $\mathbf{z}$. We illustrate the mapping of the local variables to the global variables with Figure 3.4. It shows that one global

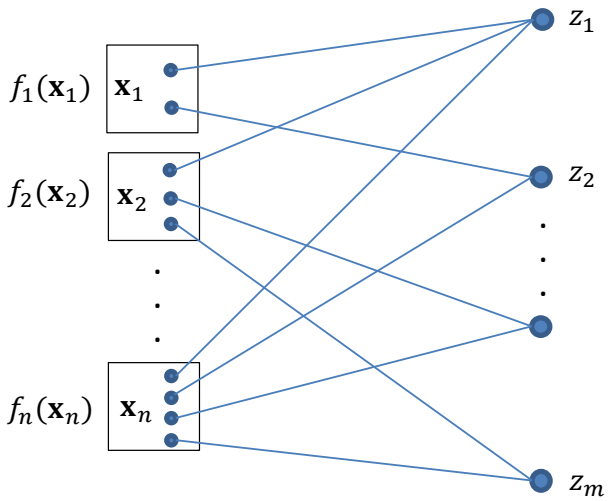

Fig. 3.4: Consensus problem.

variable can be associated to multiple local variables that the agents should agree upon. To this end, the incidence matrix to describe the mapping is defined as

$$(\mathbf{A}_i)_{k,l} = \begin{cases} 1 & \text{if} \quad (\mathbf{x}_i)_k = z_l \\ 0 & \text{if} \quad \text{others} \end{cases}. \tag{3.36}$$

Adopting Algorithm 3 to solve problem (3.35), we get the following iterations in Algorithm 4. Note that the step (3.38) is obtained from reformulating step (3.33), where the global variable $\mathbf{z}$ is updated by averaging the local variable's value $\mathbf{x}_i$. One can easily verify this by substitution of the augmented Lagrangian of consensus constraint into (3.33) and obtain the subproblem as a minimization problem of a quadratic function. The trivial solution is then obtained as the origin of the quadratic function, which is equivalent to the average values of the corresponding entries in $\mathbf{x}_i$. Interested readers may refer to [83] for substantial detail for the derivation. In terms of communication, the averaging step (3.38) can be fully decentralized into each of the components of $\mathbf{z}$ and updated at each z_i node. This provides flexibility for the practical implementation for information exchange schemes. In Chapter 4 and Chapter 5, an extended discussion on communication and information privacy will be provided from the market perspective.

Algorithm 4 Consensus-ADMM algorithm.

while *converged?* **do**

$$\mathbf{x}_i(k+1) := \arg\min_{\mathbf{x}_i} \left(f_i(\mathbf{x}_i) + \boldsymbol{\nu}_i^{\intercal}(k) \cdot \mathbf{x}_i + \frac{1}{2}\rho ||\mathbf{x}_i - \mathbf{A}_i \mathbf{z}(k)||_2^2 \right) \tag{3.37}$$

$$\mathbf{z}(k+1) := \text{diag}^{-1}(\sum_{i=1}^{n} \mathbf{A}_i^{\intercal} \mathbf{1}_{n_i \times 1}) \sum_{i=1}^{n} \mathbf{A}_i^{\intercal} \mathbf{x}_i(k+1) \tag{3.38}$$

$$\boldsymbol{\nu}_i(k+1) := \boldsymbol{\nu}_i(k) + \rho(\mathbf{x}_i(k+1) - \mathbf{A}_i \mathbf{z}(k+1)) \tag{3.39}$$

end

Remark. Based on the problem structure, a direct implementation can be formed to coordinate regional operators of power system to solve the maximize the social welfare of the overall system, as power system is de facto operated by different regional operators due to geographical restrictions. First, the power flow from one region to another should comply with physical laws. The consensus constraints regarding the physical quantities (voltage magnitude, angles) shall be enforced between regions. On the other side, we are also interested to obtain the energy/ASs exchange prices between regions. The quantity of the energy and ASs should be agreed upon on a bilateral basis and the price signals can be directly derived based on the economical perception of ADMM, where the dual variables of the consensus constraints are used as the optimal exchange prices for the respective commodities.

3.2.5 ADMM Interpretation

Competitive market mechanism

In this section, we show that the presented ADMM algorithm can be interpreted as a form of tâtonnement process that essentially adjusts the prices to achieve the market equilibrium, following the Walras theory of general equilibrium [85]. In this scope, the commodity to be exchanged is denoted by global variables $\mathbf{z}$ in the consensus problem that needs to be agreed upon the quantity among n agents. Assuming there exists a market equilibrium where the supply of the commodity meets the demand, we consider the following game with a fictitious central market operator. The game consists of three steps [86]:

(i) The central market operator announces an initial price vector $\boldsymbol{\nu}(0)$ for commodity exchange between each agent pairs.

(ii) Obtaining the price vector, each submits their supply/demand quantity based on the optimization results according to the announced price vector.

(iii) Central market operator calculates the commodity quantities excess demand and adjusts the price vector as follows: if the demand exceeds the supply, the price will be increased stepwise, otherwise reduced. The game continued until the market equilibrium price is achieved.

Now recall the dual variables in the augmented Lagrangian where ν are associated to the excess supply/demand for commodity exchange. Hence it can be readily interpreted as the market-clearing prices upon convergence of the algorithm. Then Tâtonnememnt is a process to provide the market equilibrium [86]. By comparison, the initialization of ν in Algorithm 4 and solving the local optimization problem of ADMM corresponds to trading game step (i), whereas the price adjusting step (iii) is equivalent to ADMM step 2 and 3. The penalty factor in ADMM is therefore the step size of the price adjustment. Hence, ADMM can be viewed as the algorithmic expression of the game wfithout the central market operator, i.e., a decentralized competitive market mechanism.

3.2.6 Alternative distributed optimization methods

There are alternative methods that are widely proposed for application in power system (see e.g. proximal message passing (PMP) [87], Consensus + Innovation [88], Benders decomposition, and many other methods therein). Several review works [46, 54, 3, 89, 13] exist to compare these methods in the aspect of computation, communication and organizational requirement. We briefly describe some representative methods and their advantages/disadvantages in comparison to ADMM as follows.

Benders decomposition

In the category of cutting-plane technique, Benders decomposition was initially introduced for Mixed Integer Linear Programming (MILP) [90], where the integer are handled as continuous variables and the enforcement of integer constraint is done by adding additional affine constraints from a separate process. Specifically for applying benders decomposition in solving the OPF problem, a new entity (data coordinator) is required to generate the additional constraints. The subproblems are solved in parallel by the individual agents, where the so-called “infeasibility cuts” are generated and then passed to the data coordinator. The communication structure resembles very much the structure of dual decomposition methods. In terms of computational performance, Benders decomposition yields a faster convergence rate compared to ADMM in general, whereas its organizational flexibility is less. Interested readers are encouraged to refer to our work [46] for more a detailed comparison.

KKT-condition based decomposition

Another popular category of decomposition methods is based on the solving KKT conditions in a distributed way. As described previously, KKT conditions are essentially a combination of linear equations and inequality conditions. Under the assumption that the primal problem is a convex problem, the basic idea is to use adequate protocol to find the variable values that comply with these conditions. Consensus + Innovation (C+I) protocol [91] is one of the protocol that can be adopted for this purpose, which leads to a large number of proposals for multi-agent grid management. In terms of communication structure, both ADMM and C+I can be implemented in a fully distributed way, meaning only neighbor-to-neighbor communication is necessary for implementation. From the perspective of flexibility, ADMM

is more flexible in a sense that size of the sub-problems can be constructed more flexibly than it in the case of decomposition of KKT conditions, where the decomposition is derived from a fixed number of stationary conditions and feasibility conditions. On the other hand, the convergence rate of KKT-based decomposition is substantially slower than it in ADMM. An overview of the qualitative comparison is summarized in the following table.

Method	Computation	Communication fexibility	Convergence rate
Benders	+++	+	+++
ADMM	+++	+++	++
KKT-based (C+I)	+	++	+

Table 3.1: Qualitative comparison of decomposition methods.

3.3 Summary

This chapter provides two key elements to form the market coordination scheme. Both are originated from the theory of duality. The duality theory is used to drive the optimal pricing for price-taking agents in a competitive market environment. ADMM is a competitive market mechanism as well as a robust distributed optimization method that is aimed to mitigate the convergence issue of the dual decomposition methods, which traces back to the primal-dual method of solving convex optimization problem. Note that ADMM converges under more mild conditions even for nonconvex problems. Its economical interpretations is particularly interesting to derive rules for cooperative agents to work towards a collective objective. In the next two chapters, we exploit two use cases of ADMM to organize large number of agents in electricity distribution system.

Chapter 4

Regional Distribution Grid Market Organization

This chapter presents the local distribution grid market organization including a centralized DSO-market for ASs and decentralized P2P market to accommodate the prosumer preferences. The proposed market structure ensures the prosumer autonomy and privacy while the grid stability is guaranteed. The core of the proposal focuses on the functionality of GUP (derivative of DLMP) as a coordination scheme between the two markets.

The technical contributions of this chapter are threefold. First, we propose a simultaneous market-clearing model for P2P energy trade and AS market, which utilize DLMP as a common tool to direct DERs towards “grid-friendly" behavior. This tool provides coordinated behavior between the emerging markets at the distribution grid level. Second, an interpretable and decomposable GUP scheme is derived based on implicit function formulation. The GUPs lend themselves as price signals because they are naturally decomposable into price signals for voltage support, congestion management, and loss compensation, which can be used to recover the cost of grid usage in each category. We show that the proposed GUP scheme effectively incentivize the P2P market participants to reduce the grid operation effort of the grid operators under various of scenarios. Third, to emphasize the implementation scalability and potential limitations on the privacy and communications, we propose the P2P market equilibrium to be obtained with an ADMM-based tractable solution. The obtained energy exchange prices are shown to reflect the cost allocation of ASs and peers' price differentiation based on their contribution to the grid operation for fairly large-scale systems. The main results in this chapter are included in publication [43].

4.1 DSO Market for integrated energy and ancillary services

To focus on the local distribution grid market design, following assumptions are made for the DSO-operated market. Note that the emergence of distribution grid market also involves the coordination with upstream transmission grid market, which is beyond the scope of this dissertation. First, transmission grid supplies the majority energy to the distribution grid demand. Hence the marginal cost is genuinely

determined by the price at PSP. Second, DSO Market clears before the wholesale market. The excessive energy/ASs are made available to transmission grid. Under these assumptions, the proposed distribution grid market organization is depicted in Fig. 4.1, which is operated in different time scales. Two types of markets are envisioned: i) forward market and, ii) real-time market. The forward market is a financial market, where the contractual arrangements regarding the dispatch volumes of prosumers in day-ahead and hourly-ahead manner are made. In this chapter, we focus on the (close-to) real-time (RT) market coordination, since the forward market clearing model can be formalized as a multi-time step convex optimization problem that resembles the RT-market clearing model in this proposal. Interested readers may refer [2, 35] for more details for day-ahead DSO-market clearing procedures.

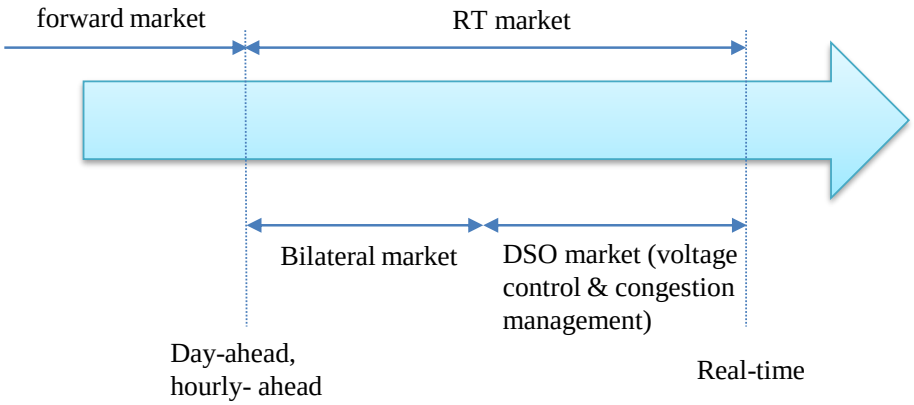

Fig. 4.1: Market organization and time scales.

As we approach the real-time operation horizon, the uncertainties due to forecast errors are assumed to be neglectable. Prior to the real-time market-clearing, the energy can either be traded based on bilateral contract or transacted in a centrally operated DSO market. Furthermore, the unbalances and grid operation contingencies are supposed to be handled by DSO, which is able to purchase additional energy and load flexibility to maintain the grid stability. This market settings entails the temporal coordination between the bilateral market (P2P market) and the DSO market. The workflow of the coordinated market-clearing model for bilateral market and DSO market can be cast as follows. First, the P2P negotiation for energy trade is initialized in fully distributed manner. Second, the GUPs are updated by DSO and communicated to peers. The negotiation steps repeat until a consensus is reached between peers regarding the trading price and quantity. The AS market that complements the P2P market is centrally operated by DSO to remove any existing violation of grid constraints during negotiations. The scope of the P2P energy trade is to settle local transactions between sellers, i.e., DGs and energy storage systems (ESSs), and buyers, i.e., FLs and conventional loads, in the distribution system. Note that the bilateral market is decoupled from the DSO market from the operational perspective, which ensures peer-centric autonomy. In light of the distribution grid market organization, we briefly describe the motivation for the inclusion of P2P market in the following.

4.2 P2P market for energy and flexibility

4.2.1 Consumer-centric market transformation

As the DSO-operated market focuses on market efficiency and grid stability, the heterogeneous preference of prosumers remains unaccommodated. According to the European Union (EU) Strategy Energy Technology Plan [92], prosumers (smart consumers) are envisioned to be at the center of the future energy system. Prosumers are defined as small-scale energy end-users with generation, energy storage and interoperable information and communication technologies (ICT), who actively manage their energy portfolio. In this scope, to encourage the transformation from passive consumers to prosumers, in some countries, e.g., Germany [93], economic incentives including feed-in tariff are provided for consumers to install the solar PV and ESSs. Feeding-into-the-grid practice, however, leads to issues of grid inertia reduction as the energy provided by renewable energy is not controllable. This in turn requires the installation of more flexible resources and flexible generations as reserves. On the other side, the fair prices for electricity become difficult to be recovered since the feed-in tariff is highly subsidized. The increasing needs for the provision of flexibility, which may potentially make it profitable for energy consumer to provide loading elasticity to the grid [30]. Proposals by California ISO consider the flexibility as fast ramping capacity to account for the uncertainty before real-time clearing (5 min) [94]. The need for flexibility essentially comes from the stochastic nature of renewable generations as well as the grid operational challenges like voltage congestion and congestion management in the future distribution grids. To this end, flexibility products are usually proposed to be procured by grid operators (TSO or DSO), and market entities (balancing responsible parties). Considering the deployment of IoT devices, the harvesting of flexibility from end-customers with limited capacity is considered to be difficult as there are no mature market models to enable this. Therefore, bi-lateral contracts can be used to procure the flexibility services and between different market layers and entities.

In view of the heterogeneous preference of the prosumers, the current power system treats electricity as a homogeneous product. A number of studies have found out that the electricity consumers are willing to pay premium based on their own preference for the generation sources e.g., local generations [95, 96]. Additional surveys also showed that people are willing to share the excess power with their community members [97]. In this scope, the P2P energy trade can be cast as an alternative way to encourage and foster the deployment of renewable energy and the exchange of green energy. In line with this, the Brooklyn microgrid has demonstrated that by establishing a small-scale P2P energy exchange market in the microgrid, profits by energy trading can be captured within the community, which in turn provides incentives for renewable generations/ESS to be deployed for balancing local supply and demand [98].

4.2.2 Market scope

In line with the discussion towards consumer-centric market organization, the P2P market model can be applied for the exchange of energy and flexibility. For illustration, consider the following example in Fig. 4.2 in an urban city, where multiple

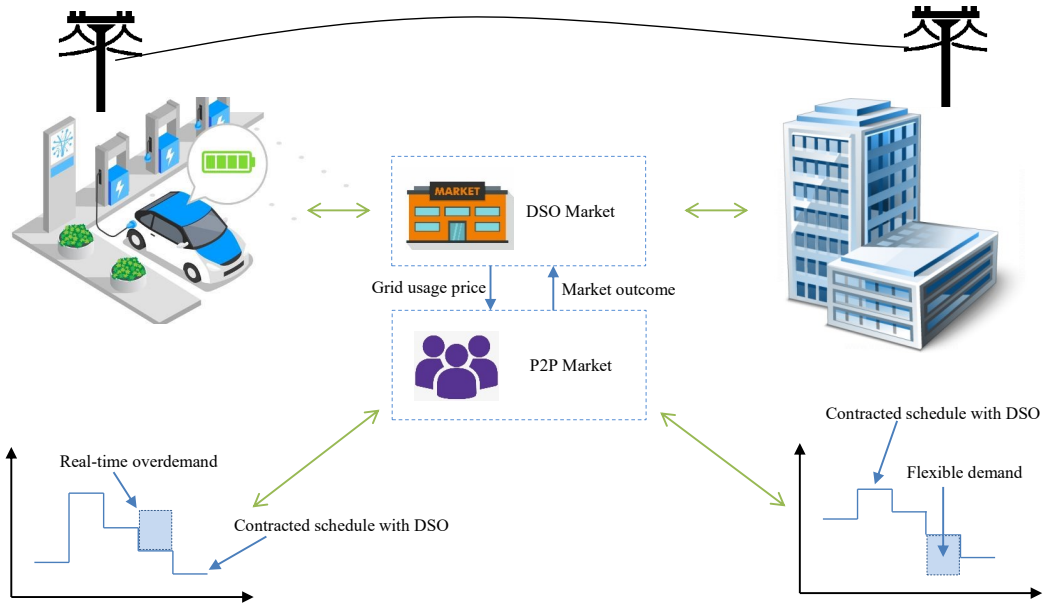

Fig. 4.2: Example for P2P trading flexibility in an urban environment.

commercial buildings and electric vehicle charging stations are located along the same distribution feeder. Suppose the DSO market has implemented a local market, where the contracted amount of energy for DER aggregators are fixed after the day-ahead market-clearing (see Section 3.1.3). Approaching the real-time operation, the car-park charging station aggregator has an over-demand of charging power that exceeds the contracted power from the day-ahead market. To avoid the penalty cost, the car-park aggregator seeks for the procurement of the additional amount of energy from alternative sources. The building aggregator may happen to have sufficient reserves to reduce its power consumption by the same amount. To this end, the selling of the flexibility from the building aggregator to the car-park charging station can take place on a bi-lateral basis without the direct involvement of the DSO. Nevertheless, the grid-usage pricing should be imposed for such a transaction to mitigate the impact on the grid operation. Note that the exchange of flexibility can also take place between two hierarchical levels, such as aggregators and end-customers, to harvest large amount of small-scale flexibility.

4.2.3 P2P market-clearing mechanism

Various market-clearing mechanisms exist in the literature, which are applicable to distinct market setting. We briefly summarize these approaches, focusing on the basic concepts of the approaches and the application perspective.

Centralized and distributed optimization

In light of economic efficiency and fairness in a market-design, optimization is perhaps the most intuitive tool to match the seller and the buyers and clear the market. The market-clearing problem can be formalized to maximize the social welfare or maximize the profit of the platform provider. This can be organized by a central

entity that collects the offers and bids from prosumers and solves the problem in a centralized manner. The optimal exchange prices can be derived based on the duality, as in primal-dual methods (see Section 3.1.2). This approach does not come without drawbacks. Indeed, the main motivation for implementing P2P energy exchange is to promote consumer-centric markets, where DERs are participating the market in an autonomously fashion. Another issue of the centralized optimization is the scalability. Considering the large number of small prosumers, centralized optimization may face bottlenecks in communication, particularly in dealing with packet losses and delays. Distributed optimization can be utilized to remove the shortcomings of the centralized organization. This is because distributed optimization preserves a P2P communication structure, which facilitate the implementation in a plug-in-and-play manner. It is also worth noticing that distributed optimization generally needs more time to converge to the optimal solution while preserving a P2P communication structure.

Game-theoretical approaches

From higher level, the game-theoretical approach is especially useful for analyzing strategic behaviors (see assumption in Section 1.5). Mathematically speaking, it comprises a broad category of games to model the decision making process in a competitive scenario. Examples can be found in the literature to model the P2P trade as non-cooperative games [99], Stackelberg game [100], and cooperative games [101, 102]. A brief introduction of these approaches is given in the following.

For non-cooperative game, it analyzes the strategic decision-making process of a number of independent players who may have partially or completely conflicting interests. It is important to note that the definition of "*non-cooperative*" does not forbid the cooperation between players. It is, rather, to emphasize that the cooperation cannot be a result of the communication or the coordination of strategic choices among the players [103]. Popular solutions for non-cooperative game includes Nash Equilibrium [104] and Variational Equilibrium [105], in which the players can not receive a better pay-off by unilaterally changing its action. Another popular non-cooperative game is Stackleberg game, which can be used to capture the strategic behavior in a hierarchical game. The game is also known as leader-follower game, where at least one player is modeled as leader to commit a strategy before other players. Then the follower players commit their strategies in response to the leader's action. This approach is particularly suitable to model the players at different hierarchical levels, e.g., aggregators and prosumers.

Another category of games is the cooperative game, which is also termed as coalitional games. Here, the focus is on designing incentives for independent players to act together as a group to improve their individual position in the game. More specifically, the study objects include the terms and conditions, under which the coalition can form, and the revenue distribution scheme to fairly allocate the revenue to the player in the coalition. A typical classification of coalitional game include three types: a coalition formation game, a coalitional graph game, and canonical coalition game [106].

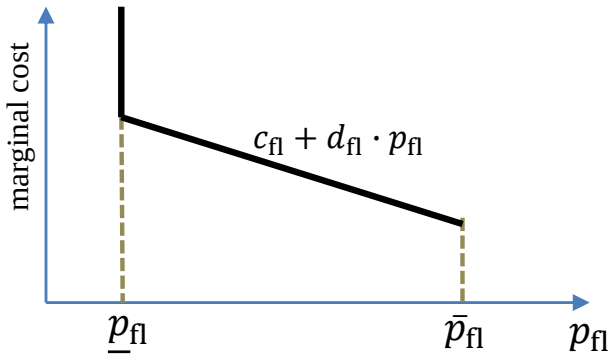

Fig. 4.3: Bid formulation for flexible loads.

Auction and transaction platforms

Alternative approaches also consider double-auction as a suitable mechanism to organize the interaction between sellers and buyers. The market-clearing process essentially establishes the merit order of the supply-side and demand-side bids and the auction price is determined by the intersection point of two curves. It resembles the organization of wholesale-market clearing. While the market-clearing mechanisms settle the market, transaction platforms and data structures provide trusted intermediary to enable the P2P trade in a decentralized manner. This was emphasized in a reasonable number of proposals, including [98, 107] to apply blockchain technologies for transactive purpose.

4.3 Coordinated market clearing

4.3.1 Bid formulation for DERs

It is assumed in this dissertation that DERs are price takers and there are sufficient market participants, which makes the DERs not be able to gain additional benefits with strategic-bidding behavior. Hence, the DERs tend to bid at the marginal cost. On the other hand, the DERs are assumed to provide price-sensitive bids for their market participation. For illustration, an example bid is is given in Fig. 4.3 for FLs. The bid consists of a baseline load $\underline{p}^{\mathrm{fl}}$ and a price-sensitive part $[\underline{\mathbf{p}}^{\mathrm{fl}}, \overline{\mathbf{p}}^{\mathrm{fl}}]$ with the marginal cost

$$\mathbf{c}^{\mathrm{fl}} + \mathrm{diag}(\mathbf{d}^{\mathrm{fl}}) \cdot \mathbf{p}^{\mathrm{fl}} \tag{4.1}$$

to represent their willingness to be curtailed depending on the market-clearing price. As aforementioned, to maximize the benefit of DERs, the DERs may want to bid at the marginal cost, which requires them being a aware of the historical data of the market-clearing price and their distribution. An example to calculate the price-sensitivity d_{fl} may be based on evaluating the merit order of the electricity supply in the market [108]. More specifically, a fit function is determined based on the historical data of the spot price at the particular node where the FL is connected. Then the coefficient d_{fl} is evaluated as the first order coefficient of the Taylor expansion

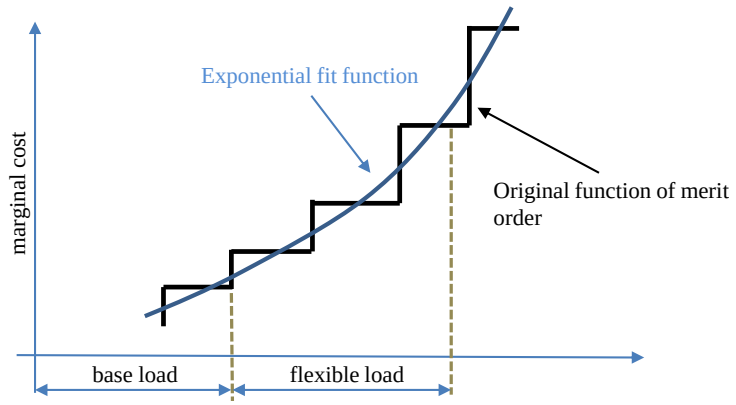

Fig. 4.4: Price sensitivity concept [36].

of the fit function. The above process is illustrated in Fig. 4.4. Note that the merit-order function of the demand side bidding is assumed to extract from historical data that are published by the DSOs.

For those FLs that provides ASs, it can be viewed as negative generators with negative baseline load, whereas a positive baseline load for FL in a conventional participation of demand side bidding. The electric power injection or consumption is limited by the respective system constraints, e.g., the curtailment capacity of a commercial building is limited by the comfort of its occupants; the reactive power injection of a DG is limited by the inverter. Such system constraints are expressed as box constraints:

$$\underline{\mathbf{p}}^{\mathsf{x}} \leq \mathbf{p}^{\mathsf{x}} \leq \overline{\mathbf{p}}^{\mathsf{x}}, \tag{4.2}$$

$$\underline{\mathbf{q}}^{\mathsf{x}} \leq \mathbf{q}^{\mathsf{x}} \leq \overline{\mathbf{q}}^{\mathsf{x}}, \quad \mathsf{x} \in \{\mathsf{g}, \mathsf{fl}\}. \tag{4.3}$$

In the context of the real-time markets, DERs, i.e., prosumers, are assumed to form their bids based on their preferences and the local system constraints and choose to submit their bids either to the P2P market or to the AS market. Note that due to the inter-temporal coupling constraints of FLs, the prosumers may need to adjust the parameters in the bid functions in different market intervals to reflect the consumption preference. This, however, does not change the convexity of the cost function formulation. Interested readers may refer to [31, 38] for more details to incorporate these inter-temporal constraints for day-ahead and real-time market coordination in P2P market and spot-market context respectively.

To this end, the cost function for DSO to procure electric power generation/flexibility from the DERs in AS market or energy procurement between DERs in a bilateral market can be expressed with a quadratic function

$$C^{\mathsf{x}}(\mathbf{p}^{\mathsf{x}}) = (\mathbf{c}^{\mathsf{x}} + \mathrm{diag}(\mathbf{d}^{\mathsf{x}}) \cdot \mathbf{p}^{\mathsf{x}})^{\intercal} \cdot \mathbf{p}^{\mathsf{x}}, \quad \mathsf{x} \in \{\mathsf{g}, \mathsf{fl}\}, \tag{4.4}$$

where $\mathbf{p}^{\mathsf{x}} \geq \mathbf{0} \in \mathbb{R}^{x}, \mathsf{x} \in \{\mathsf{g}, \mathsf{fl}\}$ is the electric power injection or consumption and $\mathbf{c}^{\mathsf{x}}, \mathbf{d}^{\mathsf{x}}, \mathsf{x} \in \{\mathsf{g}, \mathsf{fl}\}$ are the coefficients for the linear and quadratic terms. It is assumed that the cost functions are strictly convex with zero-crossing. In general, the quadratic cost function in (4.4) can be used to incorporate the prosumer preferences associated with different types of flexible resources [109]. This also makes

the cost function strictly convex and can be used to remove the multiple solution issue as discussed in [82, 16, 110], where a linear-programming based formulation may cause the divergence of centralized DSO optimization and decentralized DER optimization.

Remark (Discussions on the impact of inter-temporal constraints). In sec. II.A, one of the assumptions of the work is that the DSO operates the market in multiple-time scale including day-ahead and real-time, which necessitates the market participants like FLs to take into account the inter-temporal constraints while maximizing their surplus. Assuming the market-clearing price forecast data is available to the DERs and the DERs are price-taking agents, the participation strategy in the day-ahead market for the FLs can be based on formulating a revenue maximization problem of FLs subject to their inter-temporal constraints. Having the optimal dispatch quantity obtained, they can submit the bids to the day-ahead market. Prior to the real-time market clearing, the demand of FLs is no longer uncertain. Hence the FLs solves the revenue maximization problem in a horizon-receding manner based on their updated price/demand predictions. In the case of over-demand contracts in the day-ahead market, they may provide load reduction bids in the AS market. For the case of insufficient-demand contracts, they may seek to procure energy from P2P market.

4.3.2 Bilateral trade modeling

A P2P energy transaction is modeled with a directed graph as in Fig. 4.5. The edges $e_{i,j}, \forall i \in \mathcal{B}, j \in \mathcal{S}$ between two transactive nodes represent the active power transfer from seller to buyer. For the compact representation, the energy transfer matrix $\mathbf{E} \in \mathbb{R}^{s \times b}$ with entries $e_{i,j}$ is used to map all energy transactions. For this representation, an energy trading price $\lambda_{i,j} \in \mathbb{R}$ can be associated to each energy transfer $e_{i,j}$. Note that this representation only allows a single transaction between each seller and buyer per market interval. Since the edges are directed, this modeling forbids prosumers from selling and buying energy simultaneously.

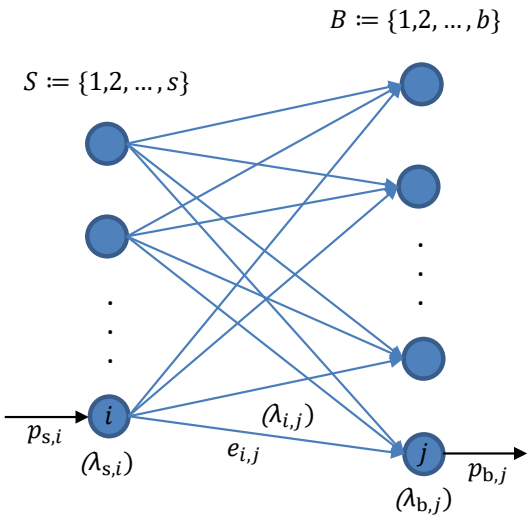

Fig. 4.5: P2P energy trade modeling.

4.3.3 Grid usage pricing

In transmission grid market, the nodal prices can be significantly different due to line congestion and losses. To this end, financial transmission right (FTR) is a tool that can be procured by market participants in a bilateral contract for energy transmissions, which can also be used to hedge against price volatility. Defining the transmission right, however, has proven not trivial. Fundamentally, this is because the power flow path due to the bilateral contract cannot be easily predetermined, particularly in the case of highly meshed transmission grid and high penetration of renewable energy. This is also part of the reasons that we only focus on the real-time market implementation as the uncertainty eliminates when operating close to real-time. In light of this, FTR is defined based on the nodal price difference for a node pair, which is a pure financial product that is always implementable, regardless of the physical consistency. By using the historical data and forecast data, FTR can be then calculated for a span of time defined by the market rules.

The GUPs are formulated based on the DLMP model in (3.17), which is considered to be updated in real-time. We term the marginal price of the transport cost as the grid usage prices (GUP). For brevity, the vectors $\boldsymbol{\pi}^{\mathsf{s}} \in \mathbb{R}^s$ and $\boldsymbol{\pi}^{\mathsf{b}} \in \mathbb{R}^b$ denote the DLMPs for all the seller nodes and buyer nodes. For each potential energy transaction $e_{i,j}, \forall i \in \mathcal{S}, j \in \mathcal{B}$, the nodal injection/consumption at the seller/buyer node results in the reward π_i^{s} for the seller and cost for the buyer π_j^{b}. The GUP for a given energy transaction $e_{i,j}$ is denoted by $\Pi_{i,j}$ and defined as

$$
\begin{aligned}
\Pi_{i,j} &= -\pi_i^{\mathsf{s}} + \pi_j^{\mathsf{b}} \\
&= -(\frac{\partial p^{\mathsf{loss}}}{\partial p_j^{\mathsf{b}}} - \frac{\partial p^{\mathsf{loss}}}{\partial p_i^{\mathsf{s}}})^{\intercal} c_0^{\mathsf{p}} - (\frac{\partial q^{\mathsf{loss}}}{\partial p_j^{\mathsf{b}}} - \frac{\partial q^{\mathsf{loss}}}{\partial p_i^{\mathsf{s}}})^{\intercal} c_0^{\mathsf{q}} \\
&+ (\frac{\partial \mathbf{v}}{\partial p_j^{\mathsf{b}}} - \frac{\partial \mathbf{v}}{\partial p_i^{\mathsf{s}}})^{\intercal} (\underline{\boldsymbol{\mu}}^{\mathsf{v}} - \overline{\boldsymbol{\mu}}^{\mathsf{v}}) + (\frac{\partial |\mathbf{s}^{\mathsf{f}}|^2}{\partial p_j^{\mathsf{b}}} - \frac{\partial |\mathbf{s}^{\mathsf{f}}|^2}{\partial p_i^{\mathsf{s}}})^{\intercal} \boldsymbol{\mu}^{\mathsf{sf}} \\
&+ (\frac{\partial |\mathbf{s}^{\mathsf{t}}|^2}{\partial p_j^{\mathsf{b}}} - \frac{\partial |\mathbf{s}^{\mathsf{t}}|^2}{\partial p_i^{\mathsf{s}}})^{\intercal} \boldsymbol{\mu}^{\mathsf{st}},
\end{aligned} \tag{4.5}
$$

where the cost of energy components is canceled by a common marginal supply unit, which is usually the active power cost of PSP for the distribution grid. We observe that the price scheme essentially includes the same grid operation products as the aforementioned DLMP decomposition, i.e. loss compensation, voltage support and congestion management. The functioning of GUPs as grid operation cost allocation and the incentive functionality is discussed in the following remarks.

Remark (Implications of decomposable GUP for cost allocations). Based on the decomposition of GUP, the active loss term $-(\frac{\partial p_{\mathsf{loss}}}{\partial p_{\mathsf{b},j}} - \frac{\partial p_{\mathsf{loss}}}{\partial p_{\mathsf{s},i}})^{\intercal} c_{\mathsf{p},0}$ and reactive loss term $(\frac{\partial q_{\mathsf{loss}}}{\partial p_{\mathsf{b},j}} - \frac{\partial q_{\mathsf{loss}}}{\partial p_{\mathsf{s},i}})^{\intercal} c_{\mathsf{q},0}$ are essentially determined by the PSP price $c_{\mathsf{p},0}, c_{\mathsf{q},0}$, where its cost can be first collected by DSOs and then passed to the loss balancing entities (TSO in this work). As for the voltage control term $(\frac{\partial \mathbf{v}}{\partial p_{\mathsf{b},j}} - \frac{\partial \mathbf{v}}{\partial p_{\mathsf{s},i}})^{\intercal} (\underline{\boldsymbol{\mu}}_{\mathsf{v}} - \overline{\boldsymbol{\mu}}_{\mathsf{v}})$ and congestion term $(\frac{\partial |\mathbf{s}_{\mathsf{f}}|^2}{\partial p_{\mathsf{b},j}} - \frac{\partial |\mathbf{s}_{\mathsf{f}}|^2}{\partial p_{\mathsf{s},i}})^{\intercal} \boldsymbol{\mu}_{\mathsf{sf}} + (\frac{\partial |\mathbf{s}_{\mathsf{t}}|^2}{\partial p_{\mathsf{b},j}} - \frac{\partial |\mathbf{s}_{\mathsf{t}}|^2}{\partial p_{\mathsf{s},i}})^{\intercal} \boldsymbol{\mu}_{\mathsf{st}}$, the associated costs are allocated to the service providers (DGs and FLs). This type of cost allocation essentially resembles the practice at the transmission grid level, where financial transmission rights (FTRs) can be procured by market participants in a bilateral

electricity trade to hedge against price volatility. FTRs are generally evaluated based on nodal price difference ($\pi_{\mathsf{b},j} - \pi_{\mathsf{s},i}$), where, by using detailed linearization of exact power flow as in Section 2.2.2, FTRs can be decoupled into loss and congestion part to construct contracts with service providers (see [111, ch. 1]).

Remark (GUP as an incentive scheme). According to the definition in (4.5), the GUP is a monotonic function of the sensitivity differences between buyer and sellers on losses, voltages and line flow. It can be interpreted as follows. Consider only the loss term; If sensitivities for nodal injections at node i and j are equal, no additional losses will be caused by the respective energy transfer due to P2P transactions. Hence the charge for losses in the GUP scheme is obtained as $\pi_j^{\mathsf{l}} - \pi_i^{\mathsf{l}} = 0$. Alternatively, the loss term is positive if losses are increased due to the P2P transaction and negative if losses are reduced because of the P2P transaction. Similar explanation holds for the functioning of GUP to reduce the voltage deviation and congestion. GUP generally serves as product differentiation price that captures regulation objectives to subsidize or penalize the energy transfer.

A compact representation of the GUP in matrix form as $\mathbf{\Pi} \in \mathbb{R}^{s \times b}$ can be given as

$$\mathbf{\Pi} = -\boldsymbol{\pi}^{\mathsf{s}} \mathbf{1}_b^{\mathsf{T}} + \mathbf{1}_s (\boldsymbol{\pi}^{\mathsf{b}})^{\mathsf{T}}, \tag{4.6}$$

which corresponds to the energy transfer matrix $\mathbf{E}$. Hence the total cost based on GUPs for all P2P energy transactions can be given as

$$\mathbf{1}_s^{\mathsf{T}} \cdot (\mathbf{\Pi} \circ \mathbf{E}) \cdot \mathbf{1}_b, \tag{4.7}$$

where $\mathbf{\Pi} \circ \mathbf{E}$ is the entrywise product of matrices $\mathbf{\Pi}$ and $\mathbf{E}$.

4.3.4 ADMM-based P2P trade matching

Different P2P matching models for P2P energy trade exist in the literature. From the communication perspective, these can be distinguished based on whether a central coordinator is required in the market-clearing process. In the category without the involvement of central coordinator, approaches can be categorized into i) distributed optimization approaches (DOA), e.g., consensus protocol [112] and ADMM [83], and ii) game-theoretical approaches, including cooperative games, e.g., [102], and non-cooperative games [104, 113].

The assumptions for the two type of approaches are generally different, where for the type of DOA prosumers are assumed to be non-strategic agents that collaboratively minimize the overall cost of the group. This can be true for the market with sufficient market participants, so that individual participants cannot improve their surplus by strategic behavior [114]. In contrast, game-theoretical approaches generally assume that the agents intend to maximize their payoffs by adjustment of their actions. To overcome the inconsistencies of the assumptions, recent expositions [115, 116] penetrate game-theoretical approaches in distributed optimization and show the compatibility of DOA as a distributed Nash equilibrium seeking method under the assumption of an imperfect local communication network. This is done by predefining the players' strategy based on the DOA protocols and each player implementing the gradient play. In this work, we adopt a similar approach for

the P2P trade context. First, the ADMM protocol is provided to solve the collective-objective (social welfare) maximization problem in (4.8). Then, the interpretation of ADMM as the solution methodology for Nash equilibrium seeking in the n-person game [113] is discussed in detail in Section 4.3.5.

To this end, the P2P market clearing, i.e. the matching of sellers and buyers, is programmed to seek the maximization of the social welfare of all P2P market participants. The social welfare optimization problem can be formulated as follows:

$$\text{max.} \quad f(\mathbf{p}^{\mathsf{s}}, \mathbf{p}^{\mathsf{b}}) := -\big(C^s(\mathbf{p}^{\mathsf{s}}) - C^{\mathsf{b}}(\mathbf{p}^{\mathsf{b}}) + \mathbf{1}_s^{\intercal} \cdot (\mathbf{\Pi} \circ \mathbf{E}) \cdot \mathbf{1}_b\big) \tag{4.8a}$$

$$\begin{aligned}
\text{s.t.} \quad & \mathbf{E}\mathbf{1}_b = \mathbf{p}^{\mathsf{s}} && : \boldsymbol{\lambda}^{\mathsf{s}} \in \mathbb{R}^s && \text{(4.8b)}\\
& \mathbf{E}^{\intercal}\mathbf{1}_s = \mathbf{p}^{\mathsf{b}} && : \boldsymbol{\lambda}^{\mathsf{b}} \in \mathbb{R}^b && \text{(4.8c)}\\
& \underline{\mathbf{p}}^{\mathsf{s}} \leq \mathbf{p}^{\mathsf{s}} \leq \overline{\mathbf{p}}^{\mathsf{s}} && : \underline{\boldsymbol{\mu}}^{\mathsf{s}}, \overline{\boldsymbol{\mu}}^{\mathsf{s}} \in \mathbb{R}^s && \text{(4.8d)}\\
& \underline{\mathbf{p}}^{\mathsf{b}} \leq \mathbf{p}^{\mathsf{b}} \leq \overline{\mathbf{p}}^{\mathsf{b}} && : \underline{\boldsymbol{\mu}}^{\mathsf{b}}, \overline{\boldsymbol{\mu}}^{\mathsf{b}} \in \mathbb{R}^b && \text{(4.8e)}\\
& \mathbf{E} \geq \mathbf{0} && : \mathbf{\Omega} \in \mathbb{R}^{s \times b} && \text{(4.8f)}
\end{aligned}$$

where the objective (4.8a) represents the social welfare consisting of sellers' revenue, buyers' cost and the grid usage cost. Constraints (4.8b) and (4.8c) provide the power balance between the power to be transferred and the power to be injected/consumed by each peer. Constraints (4.8d) and (4.8e) represent the DERs limits, respectively. Constraint (4.8f) allows for only a positive energy transfer from buyer to seller. The respective dual variables of all the constraints are listed on the right side of the equations. In general, ADMM serves as a framework for distributed optimization and is widely proposed for applications in power systems due to its scalability and robustness. To emphasize on the data privacy and scalability to solve (4.8) in a fully distributed way with only P2P communications, the ADMM-based solution methodology is adopted as follows. As a starting point, the central problem is decomposed into individual problems for seller and buyer. Therefore, the augmented Lagrangian for seller $i \in \mathcal{S}$ is formulated as

$$\begin{aligned}
L_i^{\mathsf{s,admm}}(p_i^{\mathsf{s}}, \mathbf{e}_{i,*}) =& C_i^{\mathsf{s}}(p_i^{\mathsf{s}}) + \frac{1}{2}\mathbf{e}_{i,*}\boldsymbol{\pi}_{i,*}^{\intercal} + \mathbf{\Lambda}_{i,*}(\mathbf{e}_{i,*} - \mathbf{e}_{i,*}^{+})^{\intercal}\\
&+ \frac{1}{2}\rho(\mathbf{e}_{i,*} - \mathbf{e}_{i,*}^{+})(\mathbf{e}_{i,*} - \mathbf{e}_{i,*}^{+})^{\intercal},
\end{aligned} \tag{4.9}$$

where $\mathbf{e}_{i,*}, \boldsymbol{\pi}_{i,*} \in \mathbb{R}^s$ denotes the i-th row of the matrices $\mathbf{E}$ and $\mathbf{\Pi}$. Hence, the GUP is denoted by $\frac{1}{2}\mathbf{e}_{i,*}\boldsymbol{\pi}_{i,*}^{\intercal}$, where the factor $1/2$ results from splitting the costs into two equivalent parts for seller and buyer. $\mathbf{\Lambda} \in \mathbb{R}^{s \times b}$ is the Lagrangian multiplier matrix, which essentially represents the energy trade price information (identical for seller and buyer upon consensus) for the energy transaction. In addition, a local copy is defined for the energy transfer matrix, which is denoted by $\mathbf{E}^{+}$ with their i-th row $\mathbf{e}_{i,*}^{+}$ included in (4.9). The buyer and seller are required to reach a consensus on the value of this local copy at the end of the P2P market clearing. The penalty factor is denoted by $\rho \in \mathbb{R}$, which remains constant during ADMM iterations. For

individual seller i, the constraints (4.8b) and (4.8d) are rewritten as

$$\mathbf{e}_{i,*}\mathbf{1}_b = p_i^{\mathsf{s}} \qquad : \lambda_i^{\mathsf{s}} \tag{4.10}$$

$$\underline{p}_i^{\mathsf{s}} \leq p_i^{\mathsf{s}} \leq \overline{p}_i^{\mathsf{s}} \qquad : \underline{\mu}_i^{\mathsf{s}}, \overline{\mu}_i^{\mathsf{s}} \tag{4.11}$$

$$\mathbf{e}_{i,*}^{\intercal} \geq \mathbf{0} \qquad : \mathbf{\Omega}_{i,*}. \tag{4.12}$$

For the buyer $i \in \mathcal{B}$, the augmented Lagrangian is similarly formulated as

$$\begin{aligned} L_i^{\mathsf{b,admm}}(p_i^{\mathsf{b}}, \mathbf{e}_{*,i}) = -C_i^{\mathsf{b}}(p_i^{\mathsf{b}}) + \frac{1}{2}\mathbf{e}_{*,i}^{\intercal}\boldsymbol{\pi}_{*,i} \\ + \mathbf{\Phi}_{*,i}^{\intercal}(\mathbf{e}_{*,i} - \mathbf{e}_{*,i}^{+}) + \frac{1}{2}\rho(\mathbf{e}_{*,i} - \mathbf{e}_{*,i}^{+})^{\intercal}(\mathbf{e}_{*,i} - \mathbf{e}_{*,i}^{+}) \end{aligned} \tag{4.13}$$

with $\mathbf{\Phi} \in \mathbb{R}^{s \times b}$ representing the respective Lagrangian multiplier matrix. The constraints for the individual buyer i are reformulated as

$$\mathbf{e}_{*,i}^{\intercal}\mathbf{1}_s = p_i^{\mathsf{b}} \qquad : \lambda_i^{\mathsf{b}} \tag{4.14}$$

$$\underline{p}_i^{\mathsf{b}} \leq p_i^{\mathsf{b}} \leq \overline{p}_i^{\mathsf{b}} \qquad : \underline{\mu}_i^{\mathsf{b}}, \overline{\mu}_i^{\mathsf{b}} \tag{4.15}$$

$$\mathbf{e}_{*,i} \geq \mathbf{0} \qquad : \mathbf{\Omega}_{*,i}. \tag{4.16}$$

The ADMM algorithm for P2P-market clearing is described in Algorithm 5. The algorithm consists of four main steps: i) seller/buyer individual optimization that runs in parallel in all peers, ii) broadcasting of local optimization results between buyer and seller, iii) global variable update for energy transfer, and iv) energy exchange price update. Note that only peer-to-peer communications are necessary for the negotiation process.

Remark (Convergence property). For the convergence of the ADMM-based market clearing process, the following intuitions can be provided. Assuming a static DLMP for problem (4.8), the convex problem can be solved using ADMM with global optimality guaranteed [83]. However, since the GUP is iteratively updated in the ADMM loop with GUPs (DLMPs) derived from KKT conditions, where the KKT conditions are in general non-convex [117]. It results in the non-convexity of the overall two-stage optimization problem for the coordinated-market-clearing. Hence, the ADMM-based solution methodologies may converge to KKT points without a global optimality guarantee [83].

4.3.5 The ADMM-based P2P market-clearing from game-theoretical approaches' perspective

The ADMM-based P2P market-clearing in Section 4.3.4 is based on the assumption of non-strategic and collaborative agents that maximize social welfare. In real-world applications, the selfishness of the agents and imperfect communications should be taken into account. To this end, we elaborate how to incorporate the strategic behaviors of the prosumers based on the expositions [115, 116] of penetrating DOA with game-theoretical approaches, wherein ADMM is provided as a distributed approach for Nash equilibrium seeking in a non-cooperative game.

Let $\mathcal{P} := \mathcal{S} \cup \mathcal{B}$ denote a set of players including sellers and buyers for the P2P trade. For a seller player $i \in \mathcal{S}$, its payoff function can be defined as

$$g_i(p_i^{\mathsf{s}}, \mathbf{e}_{i,*}) = -C_i^{\mathsf{s}}(p_i^{\mathsf{s}}) - \frac{1}{2}\mathbf{e}_{i,*}\boldsymbol{\pi}_{i,*}^{\intercal} - \mathbf{\Lambda}_{i,*}(\mathbf{e}_{i,*})^{\intercal}, \tag{4.17}$$

Algorithm 5 ADMM for P2P market clearing.

1: **procedure** ADMM LOOP

2: Seller/buyer peer surplus maximization (parallel in all peers),
for seller i:

$$(p_i^{\mathsf{s}})^*(k+1), \hat{\mathbf{e}}_{i,*}^*(k+1) := \arg\min L_i^{\mathsf{s,admm}}(p_i^{\mathsf{s}}, \mathbf{e}_{i,*}) \quad \text{s.t. (4.10) to (4.12)}$$

for buyer j:

$$(p_j^{\mathsf{b}})^*(k+1), \tilde{\mathbf{e}}_{*,j}^*(k+1) := \arg\min L_j^{\mathsf{b,admm}}(p_j^{\mathsf{b}}, \mathbf{e}_{*,j}) \quad \text{s.t. (4.14) to (4.16)}$$

3: Seller i broadcasts $\hat{\mathbf{e}}_{i,*}^*(k+1)$ to all buyers;
Buyer j broadcasts $\tilde{\mathbf{e}}_{*,j}^*(k+1)$ to all sellers;
Sellers/buyers Obtain new GUPs from DSO;

4: Global variable update:

$$\mathbf{e}_{i,*}^+(k+1) = \frac{1}{2}\big(\hat{\mathbf{e}}_{i,*}^*(k+1) + \tilde{\mathbf{e}}_{i,*}^*(k+1)\big)$$
$$\mathbf{e}_{*,j}^+(k+1) = \frac{1}{2}\big(\hat{\mathbf{e}}_{*,j}^*(k+1) + \tilde{\mathbf{e}}_{*,j}^*(k+1)\big)$$

5: Energy exchange price (Lagrangian multiplier) update:

$$\mathbf{\Lambda}_{i,*}(k+1) = \mathbf{\Lambda}_{i,*}(k) + \rho_i(\hat{\mathbf{e}}_{i,*}^*(k+1) - \mathbf{e}_{i,*}^+(k+1))$$
$$\mathbf{\Phi}_{*,j}(k+1) = \mathbf{\Phi}_{*,j}(k) + \rho_i(\tilde{\mathbf{e}}_{*,j}^*(k+1) - \mathbf{e}_{*,j}^+(k+1))$$

6: **end procedure**

where p_i^{s} is the local action of player i and $\mathbf{e}_{i,*}$ represents the common action with the trade partner of player i. Note that the action on $\mathbf{e}_{i,*} \in \mathbb{R}^b$ should be agreed upon by the player i and its trade partner, which creates the dependency between seller and buyer pairs. With abuse of notation the dependency reads

$$\mathbf{e}_{i,*}^{(\mathsf{s})} = \mathbf{e}_{i,*}^{(\mathsf{b})}. \tag{4.18}$$

The payoff for a single player is determined by player's own action and its trade partner's. The respective local action set for a player i is given as

$$\Delta_i = \{p_i^{\mathsf{s}} \in \mathbb{R} |\ p_i^{\mathsf{s}} \text{ satisfies (4.10) to (4.12)}\}.$$

For brevity, the payoff functions and action set for a buyer player are not listed here. Hence the game can be defined by the payoff function and the actions over the set of players $\mathcal{P}$, where each player maximizes its payoff function, i.e.,

$$\text{max.} \quad g_i(p_i^{\mathsf{s}}, \mathbf{e}_{i,*}) \tag{4.19a}$$
$$\text{s.t.} \quad p_i^{\mathsf{s}} \in \Delta_i \tag{4.19b}$$

The game is a concave n-person game with concave payoff function in local action set. *Nash equilibrium* is defined as an action profile on which no player can gain better payoff by unilateral changing its own action, i.e., we call a action profile $(p_i^{\mathsf{s}}, \mathbf{e}_{*,i})$ Nash equilibrium if [104].

$$g_i((p_i^{\mathsf{s}})^*, \mathbf{e}_{i,*}^*) \geq g_i(p_i^{\mathsf{s}}, \mathbf{e}_{i,*}^*) \tag{4.20}$$

A Nash equilibrium point that is defined by (4.8) exists for such an n-person game [113, Theorem 1]. The goal is to design the strategy for the players to find the Nash equilibrium without a central coordinator. The difficulty exists that i) each player performs the optimization (4.19) simultaneously with the dependency between solutions of (4.19), and ii) a single player may not have access to the actions of all other players considering all-to-all communication may not always be feasible.

The ADMM-based distributed Nash equilibrium seeking is then provided as follows [115]. To tackle the dependency on the energy transfer quantity of $\mathbf{E}$, local estimates are created for each player (given as local copies $\mathbf{E}^+$ in ADMM protocol). Each player follows the strategy provided in algorithm 5, i.e., i) action update based on local optimization ii) communication on the common action, iii) estimates updates, and iv) energy exchange price update. The following conditions are further required to be fulfilled.

- The communication between all players can be described by a connected undirected graph.
- The payoff function $g_i(p_i^{\mathsf{s}}, \mathbf{e}_{i,*})$ is concave in $p_{\mathsf{x},i}$ for any given $\mathbf{e}_{i,*}$; The action set Δ_i is a convex set $\in \mathbb{R}$

The convergence of the ADMM-based distributed Nash equilibrium seeking can be proven [115, Theorem 1].

AS market clearing

We first summarize the coordinated market-clearing process for P2P and ASs in Fig. 4.6. Prior to each market interval, each DER determines their participation strategy for both markets, where the submission of their respective bids to DSO are required. This is followed by the initiation of the P2P negotiation process based on the ADMM protocol. At each ADMM iteration, DSO is held responsible for the calculation of the GUP for a potential energy exchange between any P2P pairs and the process repeats until the simultaneous market-clearing process has converged.

In relevance to the DSO market for ASs, we focus on a local market to provide the two types of ancillary services: i) voltage control and ii) congestion management. Note that the AC-OPF model in (3.16) allows the market-clearing for energy and ASs in a simultaneous manner that resembles the integrated market system at the transmission grid level [11]. The market-clearing procedure for ASs can be then followed by

1. DSO predicts the loading profile and energy price from wholesale market $c_0^{\mathsf{p}}/c_0^{\mathsf{q}}$. DSO also received the bid from the DER with the DG and FL dispatch capacity.

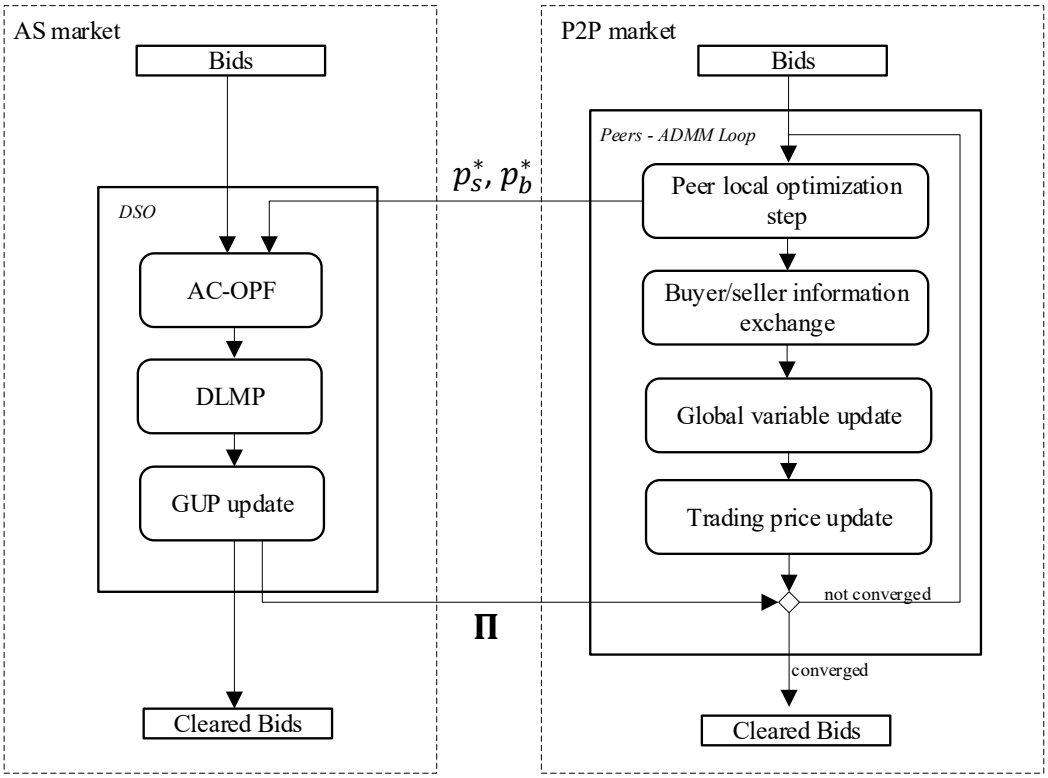

Fig. 4.6: Process diagram for the coordinated market-clearing.

2. Upon the convergence of the coordinated market-clearing in Fig. 4.6, the DLMPs are passed from DSO to DERs and DGs/FLs are rewarded with the DLMP for their scheduled dispatch amount $\mathbf{p}_{\mathsf{g}}^*, \mathbf{q}_{\mathsf{g}}^*, \mathbf{p}_{\mathsf{fl}}^*$, respectively.

Since a differentiation for conventional loads based on their geographical locations might not be acceptable in distribution grids, energy price for non-elastic loads based on uniform supply price (USP) in the distribution network zone can be given as the total energy cost divided by the total non-elastic energy consumption:

$$\text{USP} = \frac{(c_{\mathsf{p},0}, \boldsymbol{\pi}^\intercal)^\intercal \cdot \mathbf{A}_{\mathsf{sl}} \cdot \mathbf{p}_{\mathsf{sl}}}{\mathbf{p}_{\mathsf{sl}}^\intercal \cdot \mathbf{1}_{n+1}}, \tag{4.21}$$

where the energy to the end customers can be charged by introducing additional market layers, such as retailers to avoid exposing price volatility to the end customers.

Remark. Assuming the market equilibrium is obtained for the P2P energy trade, the total grid usage cost can be expressed as:

$$\mathbf{1}_s^\intercal \cdot (\boldsymbol{\Pi} \circ \mathbf{E}) \cdot \mathbf{1}_b = -(\mathbf{p}^{\mathsf{s}})^\intercal \boldsymbol{\pi}^{\mathsf{s}} + (\mathbf{p}^{\mathsf{b}})^\intercal \boldsymbol{\pi}^{\mathsf{b}} \tag{4.22}$$

The derivation is provided by substituting (4.6) into the left side of (4.22):

$$\begin{aligned} \mathbf{1}_s^\intercal \cdot (\boldsymbol{\Pi} \circ \mathbf{E}) \cdot \mathbf{1}_b &= \mathbf{1}_s^\intercal \cdot (-\boldsymbol{\pi}^{\mathsf{s}} \mathbf{1}_b^\intercal \circ \mathbf{E} + \mathbf{1}_s (\boldsymbol{\pi}^{\mathsf{b}})^\intercal \circ \mathbf{E}) \cdot \mathbf{1}_b \\ &= -\sum_{i=1}^{s} \pi_i^{\mathsf{s}} (\sum_{j=1}^{b} e_{i,j}) + \sum_{i=1}^{b} \pi_{\mathsf{b},i} (\sum_{j=1}^{s} e_{j,i}). \end{aligned} \tag{4.23}$$

By substituting (4.8b) and (4.8c) into the right side of the (4.22), we obtain the same result. This makes intuitive sense, i.e., the total grid usage cost is equal to the buyer cost (the buyer nodal consumption times the buyer DLMPs) minus the seller reward (the seller nodal injections times the buyer DLMPs).

4.3.6 Duality analysis

Upon convergence of ADMM, the obtained P2P energy trade price $\mathbf{\Lambda}$ is subjected to the following duality analysis. We first write the Lagrangian function of problem (4.8) as:

$$\begin{aligned} L = &(\mathbf{c}^{\mathsf{s}})^{\intercal}\mathbf{p}^{\mathsf{s}} + (\mathbf{p}^{\mathsf{s}})^{\intercal}\mathrm{diag}(\mathbf{d}^{\mathsf{s}})\mathbf{p}^{\mathsf{s}} - (\mathbf{c}_{\mathsf{b}})^{\intercal}\mathbf{p}^{\mathsf{b}} - (\mathbf{p}^{\mathsf{b}})^{\intercal}\mathrm{diag}(\mathbf{d}^{\mathsf{b}})\mathbf{p}^{\mathsf{b}} \\ &+ \mathbf{1}_s^{\intercal}\cdot(\mathbf{\Pi}\circ\mathbf{E})\cdot\mathbf{1}_b + (\boldsymbol{\lambda}^{\mathsf{s}})^{\intercal}(\mathbf{E}\mathbf{1}_b - \mathbf{p}^{\mathsf{s}}) + (\boldsymbol{\lambda}^{\mathsf{b}})^{\intercal}(\mathbf{E}\mathbf{1}_s - \mathbf{p}^{\mathsf{b}}) \\ &+ (\overline{\boldsymbol{\mu}}^{\mathsf{s}})^{\intercal}(\mathbf{p}^{\mathsf{s}} - \overline{\mathbf{p}}^{\mathsf{s}}) - (\underline{\boldsymbol{\mu}}^{\mathsf{s}})^{\intercal}(\mathbf{p}^{\mathsf{s}} - \underline{\mathbf{p}}^{\mathsf{s}}) + (\overline{\boldsymbol{\mu}}^{\mathsf{b}})^{\intercal}(\mathbf{p}^{\mathsf{b}} - \overline{\mathbf{p}}^{\mathsf{b}}) \\ &- (\underline{\boldsymbol{\mu}}^{\mathsf{b}})^{\intercal}(\mathbf{p}^{\mathsf{b}} - \underline{\mathbf{p}}^{\mathsf{b}}) - \mathbf{1}_s^{\intercal}\cdot(\mathbf{E}\circ\mathbf{\Omega})\cdot\mathbf{1}_b. \end{aligned} \tag{4.24}$$

The first-order optimality condition for seller nodal injections is obtained as

$$\frac{\partial L}{\partial \mathbf{p}^{\mathsf{s}}} := \mathbf{c}^{\mathsf{s}} + 2\cdot\mathrm{diag}(\mathbf{d}^{\mathsf{s}})\cdot\mathbf{p}^{\mathsf{s}} - \boldsymbol{\lambda}^{\mathsf{s}} + \overline{\boldsymbol{\mu}}^{\mathsf{s}} - \underline{\boldsymbol{\mu}}^{\mathsf{s}} = \mathbf{0}. \tag{4.25}$$

Hence, we obtain the price for the seller energy balance $\boldsymbol{\lambda}^{\mathsf{s}}$ as

$$\boldsymbol{\lambda}^{\mathsf{s}} = \mathbf{c}^{\mathsf{s}} + 2\cdot\mathrm{diag}(\mathbf{d}^{\mathsf{s}})\cdot\mathbf{p}^{\mathsf{s}} + \overline{\boldsymbol{\mu}}^{\mathsf{s}} - \underline{\boldsymbol{\mu}}^{\mathsf{s}}. \tag{4.26}$$

Now consider the KKT conditions for the individual seller/buyer problem. The Lagrangian function for seller peer i is given as

$$\begin{aligned} L_{\mathsf{s},i} =& c_i^{\mathsf{s}}p_i^{\mathsf{s}} + d_i^{\mathsf{s}}(p_i^{\mathsf{s}})^2 + \frac{1}{2}\mathbf{e}_{i,*}\boldsymbol{\pi}_{i,*}^{\intercal} + \mathbf{\Lambda}_{i,*}(\mathbf{e}_{i,*} - \mathbf{e}_{i,*}^{+})^{\intercal} \\ &+ \frac{1}{2}\rho(\mathbf{e}_{i,*} - \mathbf{e}_{i,*}^{+})(\mathbf{e}_{i,*} - \mathbf{e}_{i,*}^{+})^{\intercal} + \lambda_i^{\mathsf{s}}(\mathbf{e}_{i,*}\mathbf{1}_b - p_i^{\mathsf{s}}) \\ &+ \overline{\mu}_i^{\mathsf{s}}(p_i^{\mathsf{s}} - \overline{p}_i^{\mathsf{s}}) - \underline{\mu}_i^{\mathsf{s}}(p_i^{\mathsf{s}} - \underline{p}_i^{\mathsf{s}}) - \mathbf{e}_{i,*}\mathbf{\Omega}_{i,*}^{\intercal} \end{aligned} \tag{4.27}$$

Hence, the first-order optimality condition for energy transfer vector $\mathbf{e}_{i,*}$ of seller i is given as

$$\frac{\partial L_{s,i}}{\partial \mathbf{e}_{i,*}} := \frac{1}{2}\boldsymbol{\pi}_{i,*}^{\intercal} + \mathbf{\Lambda}_{i,*}^{\intercal} + \rho(\mathbf{e}_{i,*} - \mathbf{e}_{i,*}^{+})^{\intercal} + \lambda_i^{\mathsf{s}}\mathbf{1}_b - \mathbf{\Omega}_{i,*}^{\intercal} = \mathbf{0}. \tag{4.28}$$

Taking into account that the derivative of the second-order term is equal to zeros, i.e. $\rho(\mathbf{e}_{i,*} - \mathbf{e}_{i,*}^{+})^{\intercal} = \mathbf{0}$ upon convergence, we obtain the trading price upon market equilibrium for i as

$$\mathbf{\Lambda}_{i,*}^{\intercal} = -\frac{1}{2}\boldsymbol{\pi}_{i,*}^{\intercal} - \lambda_i^{\mathsf{s}}\mathbf{1}_b + \mathbf{\Omega}_{i,*}^{\intercal}.$$

Substitute the results of $\boldsymbol{\lambda}^{\mathsf{s}}$:

$$= -\frac{1}{2}\boldsymbol{\pi}_{i,*}^{\intercal} - (c_i^{\mathsf{s}} + 2d_i^{\mathsf{s}}\cdot p_i^{\mathsf{s}} + \overline{\mu}_i^{\mathsf{s}} - \underline{\mu}_i^{\mathsf{s}})\cdot\mathbf{1}_b + \mathbf{\Omega}_{i,*}^{\intercal}. \tag{4.29}$$

The results make intuitive sense: for a seller i, the converged trading price comprises the grid usage cost and seller generation cost. Note that for a single seller, the price differentiation to each buyer is determined by the GUPs. For the component of $\mathbf{\Omega}_{i,*}^{\mathsf{T}}$, we provide the following interpretation: constraint (4.8f) essentially forbids the reverse energy flow from buyer to seller. Hence its dual variables $\mathbf{\Omega}_{i,*}^{\mathsf{T}}$ can be interpreted as the marginal value of forbidding simultaneous buying and selling the energy in the P2P market. Note that the energy flow between buyer and seller is not constrained explicitly in this work to create congestion. Therefore, the value of $\mathbf{\Omega}_{i,*}^{\mathsf{T}}$ is expected to be neglectable, which can be verified in Section 4.4. For the energy trade price of buyer peers, a similar derivation can be followed.

4.4 Numerical examples

We test the proposed P2P algorithm on an 141-bus system [118] as illustrated

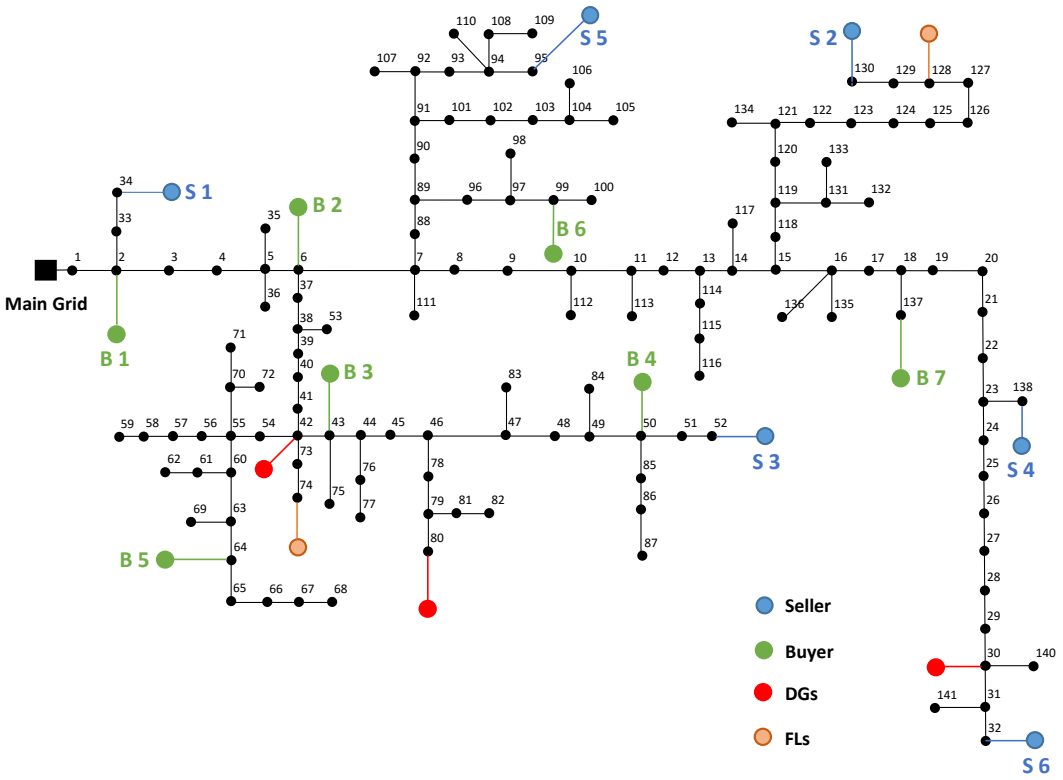

Fig. 4.7: 144-bus network [75]. P2P/AS configurations are shown in Table I/II.

in Fig. 4.7 with three test scenarios. The test system has a total static load of 11.9 MW and 7.38 MVAr. The test scenarios aim to demonstrate the effectiveness of the proposed coordinated market framework for distribution system operation, the convergence of the P2P market clearing process and the P2P energy trading price decomposition as in (4.29). Note that the AC-OPF solver is implemented with a trust-region method as in [2] to obtain the DLMPs, and the individual peer problem is implemented with YALMIP [119] and solved with GUROBI. For all test scenarios, the participants of the P2P market and AS market are described in

Table 4.1: Peer-to-peer market participants.

Participant		Seller 1	Seller 2	Seller 3	Seller 4	Seller 5	Seller 6	
Grid node index		34	130	52	138	95	32	
Injection capacity [MW]		[1 1.60]	[0 2.3]	[0 2.9]	[0 2.5]	[0 2.5]	[0 3.5]	
Price coefficient	c	3.7	4.3	3.0	4.5	3.2	3.8	
	d	0.03	0.02	0.03	0.04	0.05	0.06	
Participant		Buyer 1	Buyer 2	Buyer 3	Buyer 4	Buyer 5	Buyer 6	Buyer 7
Grid node index		2	6	43	50	64	99	137
Consumption capacity [MW]		[1.8 2.2]	[0.9 1.3]	[0.4 0.6]	[0.5 0.7]	[1.3 1.5]	[2.4 2.5]	[1.9 2.4]
Price coefficient	c	3.6	4.0	4.1	3.8	4.0	3.3	5.0
	d	-0.12	-0.21	-0.03	-0.05	-0.07	-0.09	-0.13

Table 4.2: Ancillary services market participants.

AS market	Node index	1	30	42	80	74	128
	DG/FL capability [MW]	[0 Inf]	[0 3.5]	[0 3.5]	[0 3.9]	[-0.3 0]	[-0.6 0]
	Price coefficients c [$/MW]	17	20	23	20	18	20.6
	Price coefficients d [$/MW^2]	0.01	0.02	0.01	0.01	-0.03	-0.02

Tables 4.1 and 4.2, voltage constraints are defined as $[0.95, 1.05]$ and the ADMM parameters are set as $\rho = 8 \times 10^2, \lambda_i(0) = 0, i \in \mathcal{S}, \mathcal{B}$.

4.4.1 Scenario 1 - loss reduction

The first test scenario considers only the losses without binding the voltage and line flow limits. The root node voltage is set equal to 1.05 pu. DLMPs can be used as an estimation for the GUP and an indicator for the overall grid operational cost. To demonstrate the effectiveness of the proposed P2P in the reduction of the overall operational cost, we present the DLMP results (in $/MW) in Fig. 4.8. Both curves depict the DLMPs after the P2P market is cleared, where the blue curve shows the results without considering the GUP, i.e., $\mathbf{1}_s^\intercal \cdot (\mathbf{\Pi} \circ \mathbf{E}) \cdot \mathbf{1}_b = 0$ being set for solving problem (4.8). The DLMPs result shows a clear reduction of DLMPs for the proposed P2P scheme. Note that since the DLMPs merely represent the marginal cost for the losses in this scenario, the GUP is only obtained with the loss term. By comparing the exact active power loss, we observe that the proposed P2P with GUP has obtained less loss (0.5545 MW) than the P2P scheme without GUP (0.6024 MW). We present the trade price decomposition between buyer 1 and different sellers in Fig. 4.9. It can be observed that the price decomposition of the P2P energy trade price coincides with the results obtained from ADMM, which verifies eq. (4.29). Note that the GUP is obtained as a negative cost (cost reduction) for seller 2 to 6 since these transactions have helped to reduce the losses. We also notice that the GUP (cost of losses) is small compared to the marginal generation costs of sellers.

4.4.2 Scenario 2 - voltage support

The second test scenario considers a voltage violation in which the voltage constraint is binding in this case. The associated voltage profile considering the baseload together with the P2P energy transfer is shown in Fig. 4.10, wherein a voltage violation downstream of node 37 is observed. Therefore additional ASs are procured to maintain the voltage within safe bounds. This can be observed in the DLMP result

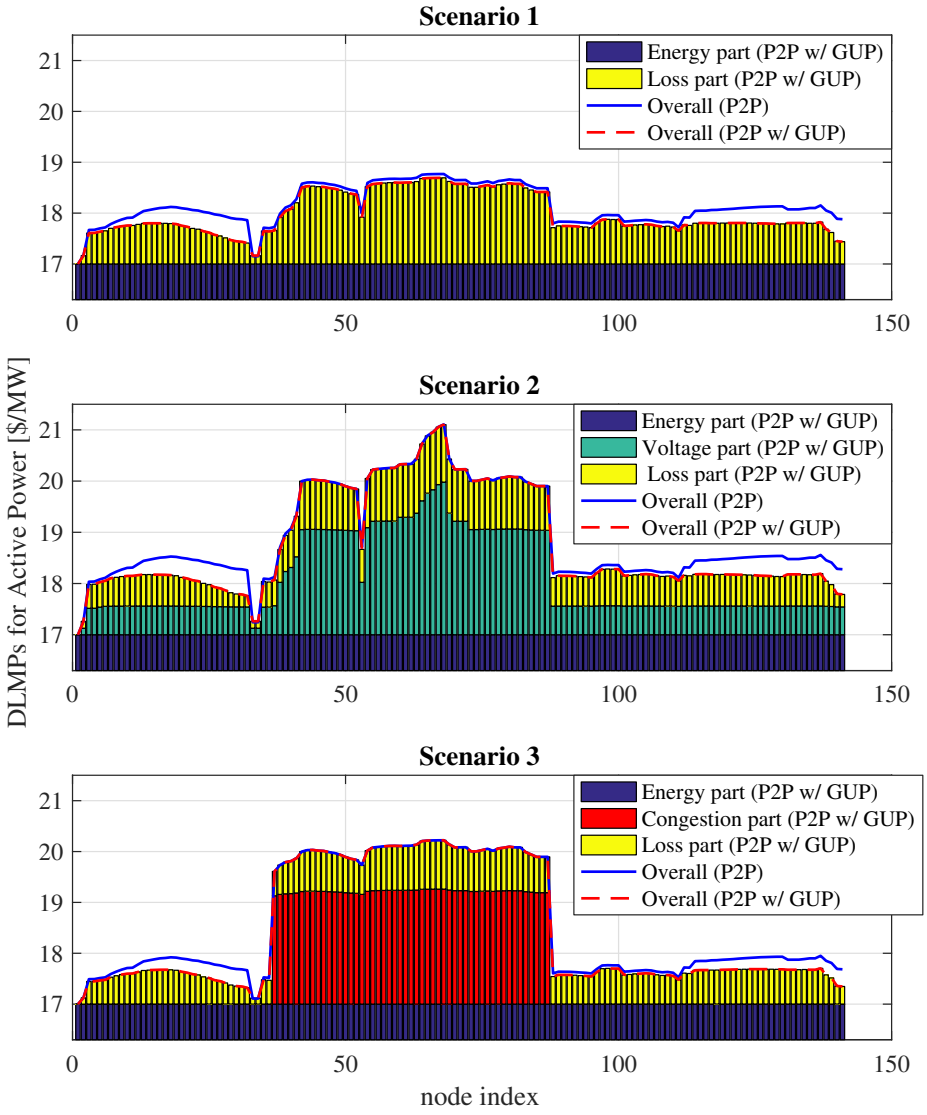

Fig. 4.8: DLMPs in all scenarios.

in Fig. 4.8, where a significant increase of DLMP between nodes 42 and node 87 is shown, which is resulted from the procurement of energy dispatch from DG at node 42 and FL unit at node 74. Note that the local voltage is globally affected by all nodal injections, which is in contrast to line flow (test scenario 3). This can be observed from the voltage charges that are applicable to all grid nodes in Fig. 4.8.

We compare two cases of i) P2P market clearing without taking into account of GUP and ii) the proposed P2P market clearing with GUP. The results show that the social welfare for the case with GUP is improved, which is reflected in the DLMPs. The associated voltage profiles for the comparison are shown in Fig. 4.10. It can be seen that the P2P with GUP market has improved the voltage profile in

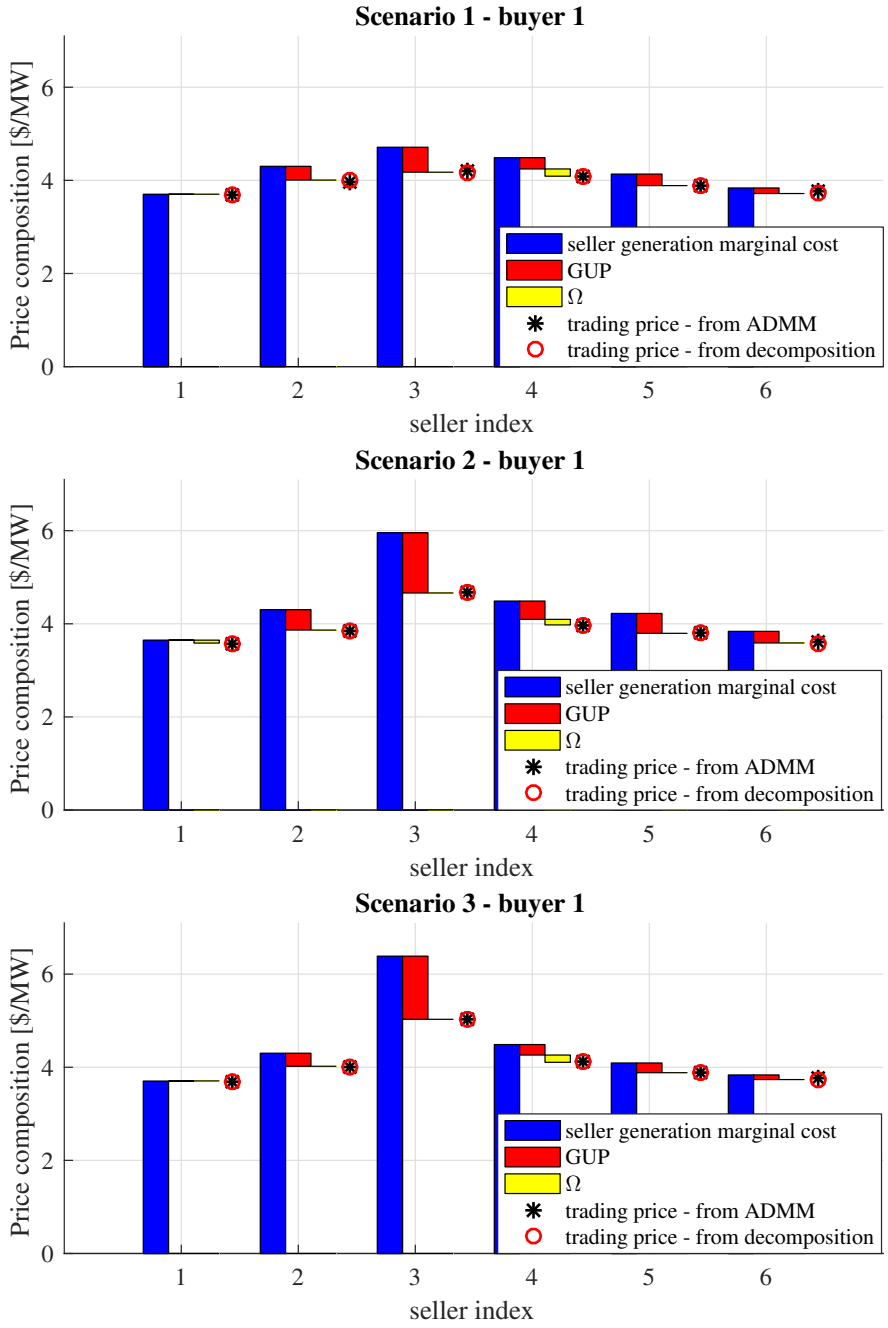

Fig. 4.9: Energy trade price decomposition for buyer 1 in all scenarios.

the sense that the voltage variations from the flat voltage have been reduced. The trade price decomposition for buyer 1 is depicted in Fig. 4.9. We observe that i) the marginal generation cost for seller 3 and 5 are further increased due to the binding constraint of the dispatch capacities; and ii) the trade price with seller 2 to 6, particularly with seller 3, has a larger reduction based on the negative GUP, which in turn incentivizes buyer 1 to procure the more energy from these sellers to improve the voltage profile.

4.4.3 Scenario 3 - congestion management

We conclude the case studies with the congestion management scenario. We

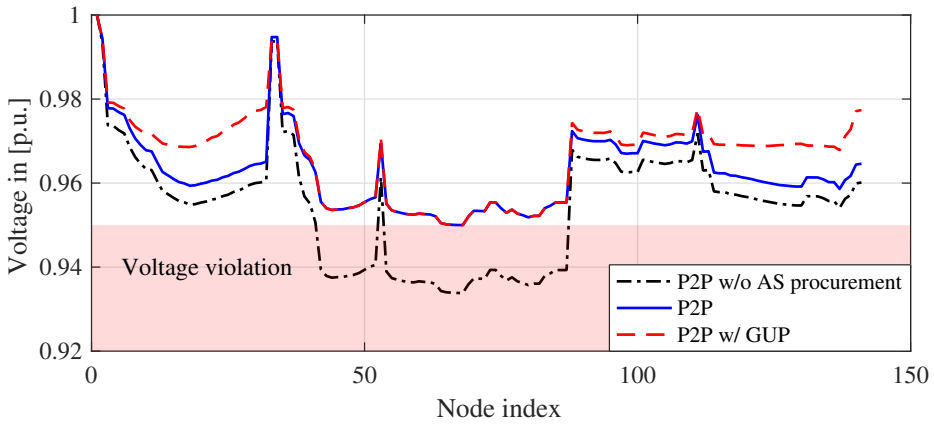

Fig. 4.10: Voltage profile for scenario 2.

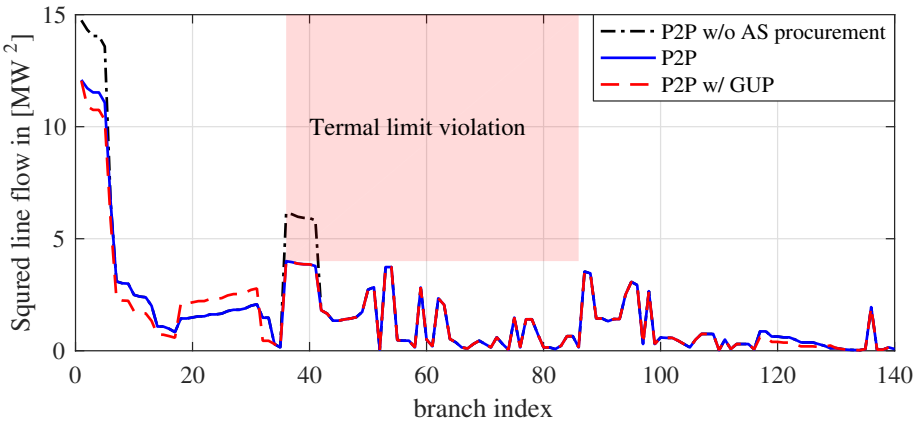

Fig. 4.11: Squared line flow for scenario 3.

add additional line flow constraints on all the lines downstream of branch between node 6 and node 37 (see Fig. 4.7) in such a way that a thermal limit of 4 MW^2 applies to the respective area in the feeder. The squared line flow profile is shown in Fig. 4.11 considering the P2P energy transfer and the existing base load, wherein the thermal limit violation for all lines between node 6 and node 42 can be observed. By procuring additional FL capacity from node 74 and generation from node 42, one can observe from Fig. 4.8 that the system has two marginal prices, i.e., the nodes in the downstream of node 37 share a common marginal cost at 20 $/MW, whereas the rest of the system has a different marginal cost at 17 $/MW (PSP). Compared to the voltage violation scenario, the line flow is rather affected by local injections (see Fig. 4.8).

When comparing the DLMP results in Fig. 4.8, the proposed P2P trade improves social welfare by obtaining lower DLMPs. For the trade price decomposition in Fig. 4.9, the P2P trade price between buyer 1 (node 43) and seller 3 (node 52)

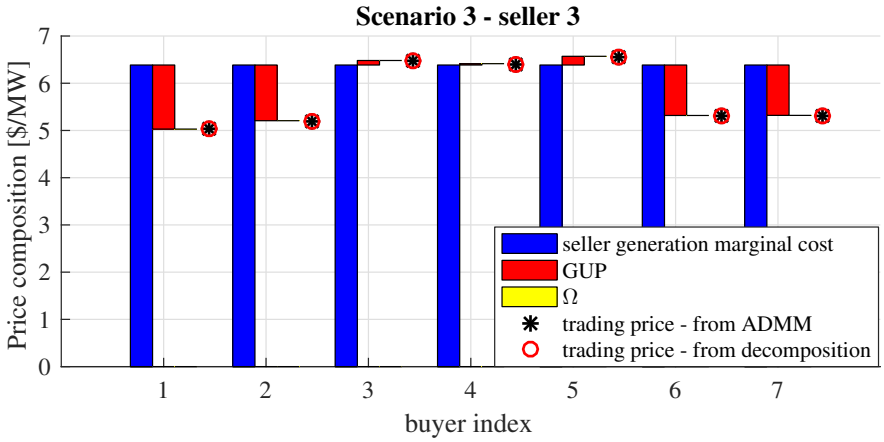

Fig. 4.12: Energy trade price decomposition for seller 3 in scenario 3.

in the congested area converges to the cost with the highest cost reduction from GUP, whereas the GUP for alternative sellers is similar to scenario 1. This is because only the injection from seller 1 can be utilized to reduce the congestion level on the branch flow between node 37 to 42 compared to scenario 2. To further reflect on this, the price decomposition for seller 3 in this scenario is depicted in Fig. 4.12, where a clear tendency for GUP to encourage the reverse power flow between non-congested area and congested area can be observed.

4.4.4 Computational performance

Finally, the convergence of the ADMM-based solution methodology is shown in Figure 4.13 together with alternative scenarios. The convergence indicator $r \in \mathbb{R}$ is given as the sum of primal residuals [83]

$$r = \mathbf{1}_s^\intercal \cdot ||\mathbf{E} - \mathbf{E}^+||_2^2 \cdot \mathbf{1}_b. \tag{4.30}$$

The simulations are performed on a personal computer with Intel i5 2.4Ghz and 8 GB RAM. In terms of computation time, the solver time for GUROBI to solve ADMM subproblems varies from 0.3 ms to 3.4 ms. Assuming the subproblem are solved in parallel, the maximal solver time determines the computation time per ADMM iteration, denoted as T_{admm}. The computation time for AS market to update GUP with the adopted trust-region AC-OPF solver varies from 0.29 s to 1.31 s, which is denoted as T_{as}. The total compuation time for the proposed simultaneous market-clearing (as depicted in Fig. 4.6) can be estimated as $n_{\text{itr}} \cdot (T_{\text{as}} + T_{\text{admm}})$, where n_{itr} is the iteration number (300 in all test scenarios).

To test the scalability of the proposed market-clearing model, we extend the test case by modifying the network size to a 564-bus network while preserving the location of PSP as reported in [34]. The number of P2P participants also is quadrupled. As a result, the solution time of AS market clearing T_{as} has increased to the range between 1.23 s and 3.31 s. The solution time of the ADMM subproblems T_{admm} remains very small in the range of 0.3 ms to 6 ms. The norms of residual versus iteration is plotted in Fig. 4.13 for the 564-bus network case with 52 P2P market participants, where with the same iteration number similar accuracy has

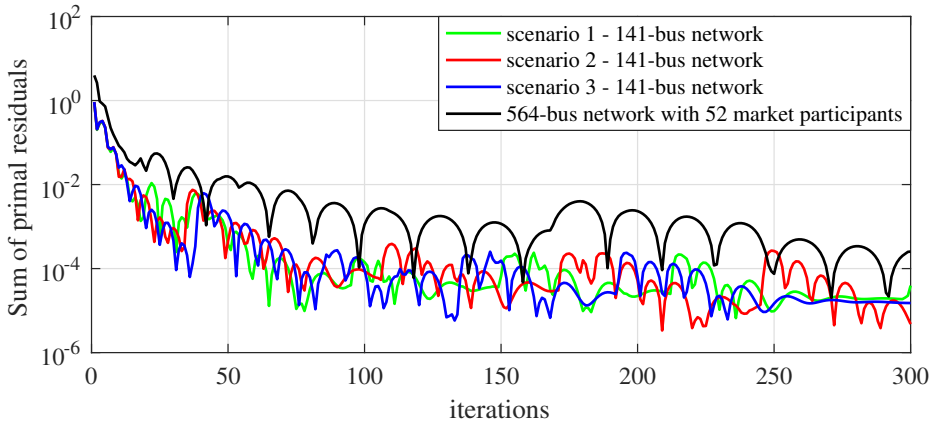

Fig. 4.13: ADMM convergence based on primal residuals for all scenarios.

been reached compared to the 141-bus network case. Hence, this shows that the proposed market-clearing model scales well with the increase in the size of the network and the number of market participants.

4.5 Summary

This chapter proposed a coordinated market design comprising a AS market and P2P market, where the DSO procures the necessary ASs to safeguard the P2P trade in distribution grids without grid constraint violations. By integrating the grid operational objectives into grid usage costs for the P2P trade, the fully distributed P2P matching process has shown to effectively converge to operating points that are beneficial for grid operation. Since the existence of multiple markets at the distribution grid level has been assumed in this work, a direct extension of the proposal is to consider the strategic-bidding behavior of DERs while achieving a stable market-clearing outcome. Another important extension of the work is to include market coordination between different time scales, which is essential to incorporate the time-coupling features of DERs and their preferences.

Chapter 5

Multi-regional Market Operation

In this chapter, we propose a method for distributed DLMP implementation in distribution grids, which provides a framework for forming multi-regional real-time markets. We adopt a similar regional concept from the transmission grid level [120, 22, 23] and apply it to the distribution grids. The proposed framework is novel in the sense that it allows the parallelization of clearing the distribution grid market while preserving solution accuracy and operation autonomy.

The key contributions of this chapter are outlined as follows. The proposed framework comes with a parallel regulation and computation architecture to overcome the computational burdens caused by the large node number in distribution grids. Furthermore, the proposed CAST algorithm possesses many other favored features, like a tractable solution and formulation to enable online implementation. The DLMP calculation has been fully distributed into each region while only limited information exchange is required. We derive the multi-regional injection sensitivity to describe the influence between regions to achieve the distributed DLMP computation. The main results in this chapter are published in work [44].

5.1 Multi-regional operation concept in distribution grids

We now envision the distribution grid to be operated by multiple regional DSOs with the market structure presented in Fig. 5.1. The goal of this framework is to coordinate the in such a way DSOs that they can maximize the overall social welfare of the distribution grid while maximizing their individual surplus. Moreover, each regional DSO must be independent in making its decision and only share physically coupled information with the neighboring regions' DSOs. Similar to the social welfare problem in 3.16, DERs (such as DGs, FLs) are assumed to be price takers and receive rewards from the associated regional DSO for power generations and load curtailments. In order to achieve the proposed distributed framework of Fig. 5.1 along with the price structure of (3.17), two research questions exist, which are answered in this chapter. First, we solve the AC-OPF problem imposed by (3.16) in a distributed way, preserving private information of the regional DSO. Second, we obtain DLMP for each region in a distributed manner with the similar decomposition structure of (3.17) and optimality of (3.16), as when solved centrally.

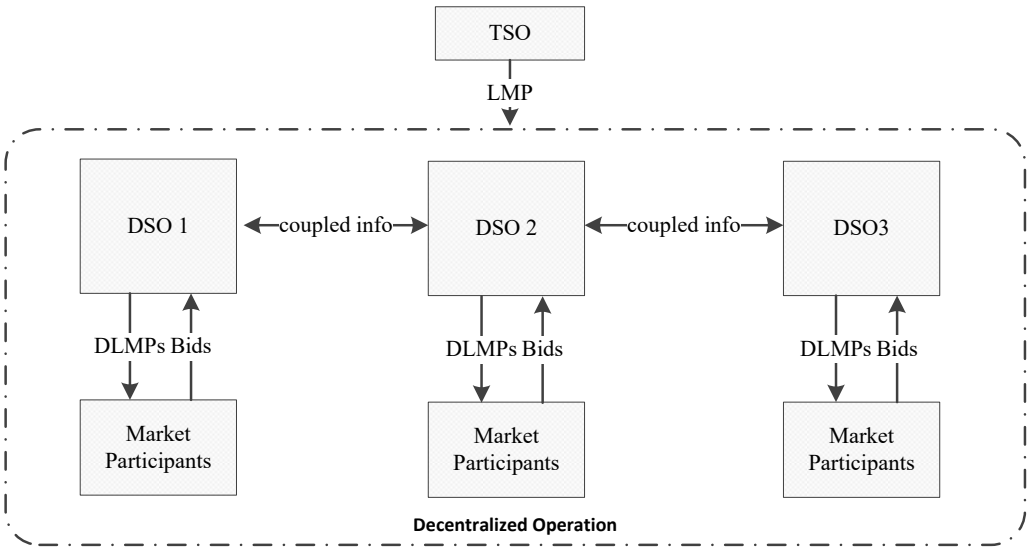

Fig. 5.1: Proposed market framework and information flow diagram.

5.2 Consensus alternating direction method of multiplier Structured Trust-Region (CAST) Algorithm

5.2.1 Network partitioning technique and consensus definition

The distribution network is partitioned into r regions where the set of regions is denoted by $\mathcal{R} = \{1, 2, ..., r\}$. Similarly, the overall PQ bus set $\mathcal{L}$ gets partitioned into r subsets, $\mathcal{L}_i := \{1_i, 2_i, ..., n_i\}$, where $i \in \mathcal{R}$. To enforce feasibility with respect to the overall grid, each region i places a reference bus (slack bus) at its physically connected neighbor. Hence, we get $\mathcal{N}_i = \mathcal{L}_i \cup \{0\}$ total nodes in the region. With this, each region i can now be represented with its local $\mathbf{Y}_i \in \mathbb{C}^{(n_i+1)\times(n_i+1)}$ and individual objective function $f_i(\mathbf{p}^{\mathsf{g}}_{\mathcal{L}_i}, \mathbf{q}^{\mathsf{g}}_{\mathcal{L}_i})$, which are the respective local versions of the overall objective function $f(\mathbf{p}^{\mathsf{g}}, \mathbf{q}^{\mathsf{g}})$ and system admittance matrix $\mathbf{Y}$.

The interconnection between regions is established by overlapping areas in which the power flow equations of each region can be interlinked. If region i is a neighbor of region j, then $\mathcal{N}_i \cap \mathcal{N}_j \neq \emptyset, \forall i, j \in \mathcal{R}$, such that $\mathcal{N}_i \cap \mathcal{N}_j$ gives a set of coupled buses that interconnects region i and region j. The set $\mathcal{C}_{ij} := \{c_{i_1} = c_{j_1}, \ldots, c_{i_k} = c_{j_k}\}$ denotes the set of k coupled buses from regions i and j (where $k < \max\{n_i, n_j\}$). In Fig. 5.2 (left), an example of a coupled bus of three regions is illustrated. The bus $c := c_1 = c_2 = c_3$ is part of region 1 (c_1), region 2 (c_2) and region 3 (c_3). Hence, $\mathcal{C}_{12} = \{c_1 = c_2\}$, $\mathcal{C}_{13} = \{c_1 = c_3\}$ and $\mathcal{C}_{23} = \{c_2 = c_3\}$.

In order to decouple the constraints for the optimization problem in (3.16) and to solve it in a distributed way, the objective and constraints are decoupled with the help of local copies of the coupled buses created for each region. To do so, we define the set of the local copies of the coupled buses in region i as $\mathcal{C}_i := \cap_{j=1}^{r} \mathcal{C}_{ij} \subset \mathcal{N}_i$. For any local copy $c_i \in \mathcal{C}_i$, the number of connected neighboring regions is specified by n_{c_i}. For example, in Fig. 5.2, three local copies of the coupled bus c are created and denoted by c_1, c_2, c_3 which gives $\mathcal{C}_1 = \{c_1, c_2, c_3\}$ and $n_{c_1} = 3$. To enforce the agreement on the power flow on the coupled buses among regions, the

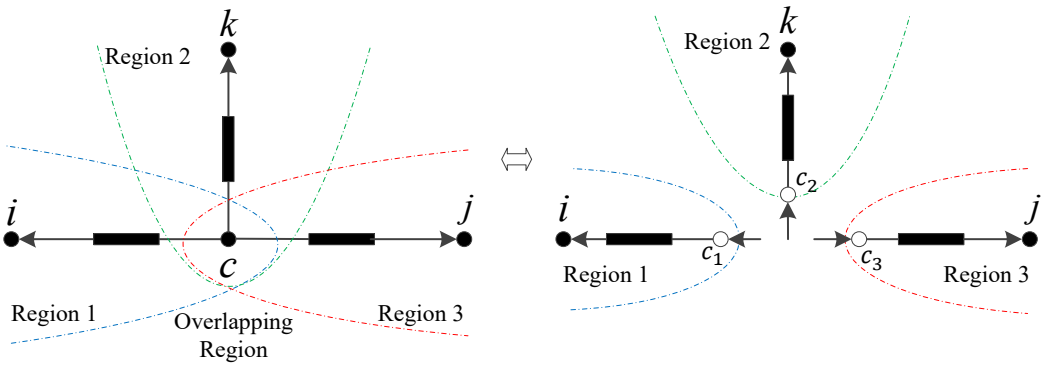

Fig. 5.2: Network-partitioning technique and consensus definition for multiple regions (dashed lines are the regions' boundary).

following consensus constraints are introduced for region $i \in \mathcal{R}$ as

$$v_{c_1} = v_{c_2} = ... = v_{c_{n_{c_i}}} \qquad c_i \in \mathcal{C}_i \tag{5.1a}$$

$$\theta_{c_1} = \theta_{c_2} = ... = \theta_{c_{n_{c_i}}} \qquad c_i \in \mathcal{C}_i \tag{5.1b}$$

$$\sum_{i=1}^{n_{c_i}} p_{c_i} = 0 \qquad c_i \in \mathcal{C}_i \tag{5.1c}$$

$$\sum_{i=1}^{n_{c_i}} q_{c_i} = 0 \qquad c_i \in \mathcal{C}_i. \tag{5.1d}$$

5.2.2 Consensus optimal power flow (Consensus OPF)

Along with the network partition, problem (3.16) is decomposed into regional subproblems (excluding the congestion constraints). For a region $i \in \mathcal{R}$, the following consensus optimization problem is defined

$$\text{max.} \quad f_i(\mathbf{p}^{\mathsf{g}}_{\mathcal{L}_i}, \mathbf{q}^{\mathsf{g}}_{\mathcal{L}_i}) \tag{5.2a}$$

s.t.

$$p_{0,i} + \mathbf{1}^{\intercal}_{n_i}\mathbf{p}^{\mathsf{g}}_{\mathcal{L}_i} - \mathbf{1}^{\intercal}_{n_i}\mathbf{p}^{\mathsf{sl}}_{\mathcal{L}_i} = p^{\mathsf{loss}}_i \qquad : \mu^{\mathsf{pl}}_i \tag{5.2b}$$

$$q_{0,i} + \mathbf{1}^{\intercal}_{n_i}\mathbf{q}^{\mathsf{g}}_{\mathcal{L}_i} - \mathbf{1}^{\intercal}_{n_i}\mathbf{q}^{\mathsf{sl}}_{\mathcal{L}_i} = q^{\mathsf{loss}}_i \qquad : \mu^{\mathsf{ql}}_i \tag{5.2c}$$

$$\underline{\mathbf{p}}_{\mathcal{L}_i} \leq \mathbf{p}^{\mathsf{g}}_{\mathcal{L}_i} \leq \overline{\mathbf{p}}_{\mathcal{L}_i} \qquad : \underline{\boldsymbol{\mu}}^{\mathsf{p}}_i, \overline{\boldsymbol{\mu}}^{\mathsf{p}}_i \tag{5.2d}$$

$$\underline{\mathbf{q}}_{\mathcal{L}_i} \leq \mathbf{q}^{\mathsf{g}}_{\mathcal{L}_i} \leq \overline{\mathbf{q}}_{\mathcal{L}_i} \qquad : \underline{\boldsymbol{\mu}}^{\mathsf{q}}_i, \overline{\boldsymbol{\mu}}^{\mathsf{q}}_i \tag{5.2e}$$

$$\underline{\mathbf{v}}_{\mathcal{L}_i} \leq \mathbf{v}_{\mathcal{L}_i} \leq \overline{\mathbf{v}}_{\mathcal{L}_i} \qquad : \underline{\boldsymbol{\mu}}^{\mathsf{v}}_i, \overline{\boldsymbol{\mu}}^{\mathsf{v}}_i \tag{5.2f}$$

and (5.1a) to (5.1d),

where the constraints (5.2b) to (5.2f) are regional representation of constraints (3.16b) to (3.16f). Consensus constraints (5.1a) to (5.1d) ensure that the power flow still holds for the global optimization problem and require each region to take into account binding its power injection at coupled buses with respect to its global

values provided from other regions. In the next section, we elaborate how to solve the consensus OPF and tackle the power flow nonlinearity in the proposed CAST algorithm.

5.2.3 Distributed solver with CAST algorithm

The proposed CAST algorithm possesses a ADMM structure with trust region (TR) algorithm embedded at each ADMM iteration as the local optimization solver. Note that each local optimization solver handles a regional subproblem with nonlinear AC power flow constraint (2.4) which is tackled by TR algorithm. The fundamental idea of the trust region algorithm is to create an approximate model (linear model) for the initial operating point within a feasible region (trust region). Then the minimization step helps to find the steepest descent direction along the objective function within the trust region. In a new iteration, the linearized model is then updated using the new operating point found in the steepest descent direction. The algorithm repeats the steps until no further improvement can be found within the next minimization step. Note that the trust region is adjusted from iteration to iteration, i.e., the trust region will be enlarged if the approximate model represents the original problem well and vice versa.

ADMM is a distributed solver mainly for convex optimization problems [83]. In principle, ADMM relies on the augmented Lagrangian to reduce the mismatch of the coupled constraints (5.1a) to (5.1d) iteratively when each local optimization solver solves the subproblem. ADMM has been proven to work well for solving AC-OPF as well as other nonlinear problems despite nonconvexity [121]. Interested readers may refer to [122] for alternative distributed AC-OPF algorithms. In this work, the proposed CAST algorithm can be considered as a variant of the distributed AC-OPF solver in [123, 121] with the main distinction of being the use of a trust-region method instead of an interior point method (IPM) as the local minimization solver. This, however, does not change the convergence guarantee nor the optimality conditions. The convergence speed of the CAST algorithm is furthermore improved by using the varying penalty (VP) method [83, 124] i.e., during the ADMM parameter update stage, by utilizing the primal/dual residual information that measures the local and global minimization progress respectively, the penalty factor will be changed accordingly at each iteration, and hence convergence performance is improved. We provide the validation of the VP method in the numerical experiment. Consider the augmented Lagrangian of a region $i \in \mathcal{R}$ as:

$$L_i^{\mathsf{ADMM}}(\tilde{\boldsymbol{\chi}}_{\mathcal{L}_i}) = f_i(\tilde{\mathbf{p}}^{\mathsf{g}}_{\mathcal{L}_i}, \tilde{\mathbf{q}}^{\mathsf{g}}_{\mathcal{L}_i}) + \boldsymbol{\lambda}_i^{\mathsf{T}}(\tilde{\boldsymbol{\chi}}_{\mathcal{C}_i} - \tilde{\boldsymbol{\chi}}^{+}_{\mathcal{C}_i}) + \frac{1}{2}\rho_i(\tilde{\boldsymbol{\chi}}_{\mathcal{C}_i} - \tilde{\boldsymbol{\chi}}^{+}_{\mathcal{C}_i})^{\mathsf{T}}(\tilde{\boldsymbol{\chi}}_{\mathcal{C}_i} - \tilde{\boldsymbol{\chi}}^{+}_{\mathcal{C}_i})$$

with decision variables for node i defined by $\boldsymbol{\chi}_i := [p_i, q_i, v_i] \in \mathbb{R}^3$, Lagrange multiplier $\boldsymbol{\lambda}_i \in \mathbb{R}^{3n_{c_i}}$ and the penalty factor $\rho_i \in \mathbb{R}$. We consider injection and voltage magnitudes as the coupling variables here, because angles for each region are implicitly updated locally with respect to the given coupled bus c_i, serving as its slack bus (see Sec. III-A on assumptions in network partitioning). Moreover, $\tilde{\boldsymbol{\chi}}^{+}_{\mathcal{C}_i} \in \mathbb{R}^{2n_{c_i}}$ denotes the global variable to be updated based on the local optimization results at each ADMM iteration. The nonlinearity in (5.2) are approximated by using (local)

linear estimates

$$\tilde{\mathbf{v}}_{\mathcal{L}_i} = \hat{\mathbf{v}}_{\mathcal{L}_i} + \mathbf{M}^{\mathsf{vp}}_{\mathcal{L}_i}\Delta\mathbf{p}_{\mathcal{L}_i} + \mathbf{M}^{\mathsf{vq}}_{\mathcal{L}_i}\Delta\mathbf{q}_{\mathcal{L}_i} + \mathbf{m}^{\mathsf{vv}}_{\mathcal{L}_i}\Delta v_{0,i} \tag{5.3}$$

$$\tilde{\boldsymbol{\theta}}_{\mathcal{L}_i} = \hat{\boldsymbol{\theta}}_{\mathcal{L}_i} + \mathbf{M}^{\theta p}_{\mathcal{L}_i}\Delta\mathbf{p}_{\mathcal{L}_i} + \mathbf{M}^{\theta\mathsf{q}}_{\mathcal{L}_i}\Delta\mathbf{q}_{\mathcal{L}_i} + \mathbf{m}^{\theta\mathsf{v}}_{\mathcal{L}_i}\Delta v_{0,i} \tag{5.4}$$

$$\tilde{p}_{0,i} = \hat{p}_{0,i} + \mathbf{m}^{\mathsf{pp}}_{\mathcal{L}_i}\Delta\mathbf{p}_{\mathcal{L}_i} + \mathbf{m}^{\mathsf{pq}}_{\mathcal{L}_i}\Delta\mathbf{q}_{\mathcal{L}_i} + m^{\mathsf{pv}}\Delta v_{0,i} \tag{5.5}$$

$$\tilde{q}_{0,i} = \hat{q}_{0,i} + \mathbf{m}^{\mathsf{qp}}_{\mathcal{L}_i}\Delta\mathbf{p}_{\mathcal{L}_i} + \mathbf{m}^{\mathsf{qq}}_{\mathcal{L}_i}\Delta\mathbf{q}_{\mathcal{L}_i} + m^{\mathsf{qv}}\Delta v_{0,i} \tag{5.6}$$

$$\tilde{v}_{0,i} = \hat{v}_{0,i} + \Delta v_{0,i}, \tag{5.7}$$

where a *new* operating point $(\tilde{\mathbf{v}}_{\mathcal{L}_i}, \tilde{\boldsymbol{\theta}}_{\mathcal{L}_i}, \tilde{p}_{0,i}, \tilde{q}_{0,i}, \tilde{v}_{0,i})$ is approximated by the given (old) operating point $(\hat{\mathbf{v}}_{\mathcal{L}_i}, \hat{\boldsymbol{\theta}}_{\mathcal{L}_i}, \hat{p}_{0,i}, \hat{q}_{0,i}, \hat{v}_{0,i})$ using the linearization coefficient matrices or vectors denoted by $\mathbf{M}^{\mathsf{vp}}_{\mathcal{L}_i}, \mathbf{M}^{\mathsf{vq}}_{\mathcal{L}_i}, \mathbf{M}^{\theta\mathsf{p}}_{\mathcal{L}_i}, \mathbf{M}^{\theta\mathsf{q}}_{\mathcal{L}_i} \in \mathbb{R}^{n_i \times n_i}$, $\mathbf{m}^{\mathsf{pp}}_{\mathcal{L}_i}, \mathbf{m}^{\mathsf{pq}}_{\mathcal{L}_i}, \mathbf{m}^{\mathsf{qp}}_{\mathcal{L}_i}, \mathbf{m}^{\mathsf{qq}}_{\mathcal{L}_i} \in \mathbb{R}^{1\times n_i}$, $\mathbf{m}^{\mathsf{vv}}_{\mathcal{L}_i}, \mathbf{m}^{\theta\mathsf{v}}_{\mathcal{L}_i} \in \mathbb{R}^{n_i\times 1}$, $m^{\mathsf{pv}}, m^{\mathsf{qv}} \in \mathbb{R}$.

The derivation of the coefficients are provided in 2.2.2. As the linearization of distribution-grid power flows is only accurate at the chosen operating point, we incorporate a trust-region algorithm to tackle the related nonlinearities [2]. Algorithm 6 explains the proposed CAST algorithm, where all computations are performed locally, except for step 2, which requires an update on the algorithm's global variables. The global variables update is followed by the averaging step of using local optimization results of the coupled variable. Interested readers may refer to [83, ch. 7] for the derivation of averaging steps in the ADMM algorithm. This update makes intuitive sense, i.e., upon convergence of CAST, the consensus power flow constraints (5.1a) to (5.1d) will be binding. Note that the parameter tuning steps for TR (step 1.4 - 1.5) and for ADMM (step 3.1 - 3.2) are carried out locally by its regional DSO. However, there are other variants of ADMM which require a central entity to update the information and coordinate the parameter tuning (see e.g., [124, 122]).

Remark (Convergence of CAST algorithm). Under the condition that the sequence of the penalties ρ_i for all $i \in \mathcal{R}$ is bounded, the convergence of the CAST algorithm can be proved using [123, Theorem 4]. In addition, upon the convergence of the CAST algorithm, the triplets $(\boldsymbol{\lambda}_i, \rho_i, \boldsymbol{\chi}_{\mathcal{L}_i})$ converge to KKT stationary points [123, Theorem 1] (i.e., local minimum for non-convex scenarios and global minimum for convex scenarios). In practice, the first two steps of CAST algorithm can take place in either order without affecting the convergence. This kind of asynchronous update has proved advantageous in dealing with communication delays and packet loss in recent expositions [125, 126].

Remark (Tractable solution and formulation to enable the online implementation). The trust region ensures a feasible load flow solution to be found at each ADMM iteration, which provides a tractable OPF solution along with the price signal in each region. This feature is favored by many online applications and can be further exploited in the provision of real-time control (see e.g., [127, 128]).

5.3 Distributed DLMP scheme

5.3.1 Regional DLMP formulation

After obtaining the optimal solution through CAST algorithm, the regional DLMP is calculated by the distributed DLMP scheme in algorithm 7. With regard to classifi-

Algorithm 6 CAST algorithm (parallelized in all regions)

Input: $\hat{\boldsymbol{\chi}}_{\mathcal{L}_i}(0)$ - initial feasible state variable, $f_i(\hat{\boldsymbol{\chi}}_{\mathcal{L}_i}(0))$ - initial local objective value
Parameters: ϵ - termination tolerance, $\varphi_i(k)$ - trust-region radius; $\varphi_{\max}$ - maximal trust-region radius; η,β,$\gamma \in (0,1)$ - trust-region constants; τ,κ - ADMM constants;

ADMM loop:

Step 1. (Local minimization with trust-region algorithm)

1.1 Choice of linearized model: to construct/update the sensitivity matrix for linearized power flow model at operating point $(\hat{u}_{\mathcal{L}_i}(k), \hat{s}_0(k))$, i.e., (5.3) to (5.6).

1.2 Trust region minimization with L_i^{ADMM}:

$$\tilde{\boldsymbol{\chi}}^*_{\mathcal{L}_i}(k+1) := \arg\min_{\tilde{\boldsymbol{\chi}}_{\mathcal{L}_i}} L_i^{\text{ADMM}} \tag{5.8a}$$

s.t. (5.2d) to (5.2f) and (5.3) to (5.6) (5.8b)

$$||\tilde{\boldsymbol{\chi}}_{\mathcal{L}_i}(k+1) - \hat{\boldsymbol{\chi}}_{\mathcal{L}_i}(k)|| < \varphi_i \tag{5.8c}$$

1.3 Feasible power flow projection: the next operating point $\hat{\boldsymbol{\chi}}_{\mathcal{L}_i}(k+1)$ is obtained by projecting the optimization results $\tilde{\boldsymbol{\chi}}^*_{\mathcal{L}_i}(k+1)$ to the feasible power flow solution, e.g. by using a Newton–Raphson algorithm [67].

1.4 With the previous operating point $\hat{\boldsymbol{\chi}}_{\mathcal{L}_i}(k)$, the approximate point $\tilde{\boldsymbol{\chi}}_{\mathcal{L}_i}(k+1)$ and the current operating point $\hat{\boldsymbol{\chi}}_{\mathcal{L}_i}(k+1)$, the following ratio is computed:

$$\sigma_i(k+1) = \frac{L_i^{\text{ADMM}}(\hat{\boldsymbol{\chi}}_{\mathcal{L}_i}(k+1)) - L_i^{\text{ADMM}}(\hat{\boldsymbol{\chi}}_{\mathcal{L}_i}(k))}{L_i^{\text{ADMM}}(\tilde{\boldsymbol{\chi}}^*_{\mathcal{L}_i}(k+1)) - L_i^{\text{ADMM}}(\hat{\boldsymbol{\chi}}_{\mathcal{L}_i}(k))} \tag{5.9}$$

which represents the ratio between actual objective reduction and predicted reduction.

1.5 Trust region radii evaluation and update:

$$\varphi_i(k+1) = \begin{cases} \gamma\varphi_i(k) & \sigma_i(k+1) \le \eta \\ \min\{\varphi_{\max}, 2\varphi_i(k)\} & \sigma_i(k+1) \ge (1-\eta) \\ \varphi_i(k) & \text{otherwise} \end{cases}$$

1.6 Trust region solution evaluation:
If $\sigma_i(k+1) > \beta$, solution of $\hat{\boldsymbol{\chi}}_{\mathcal{L}_i}(k+1)$ is accepted, otherwise rejected with $\hat{\boldsymbol{\chi}}_{\mathcal{L}_i}(k+1) = \hat{\boldsymbol{\chi}}_{\mathcal{L}_i}(k)$ being set.

1.7 Termination criteria check: $||\tilde{\boldsymbol{\chi}}_{\mathcal{L}_i}(k+1) - \hat{\boldsymbol{\chi}}_{\mathcal{L}_i}(k+1)|| < \epsilon$.

Step 2. (Global variable update)

For the coupled buses $c_i \in \mathcal{C}_i$, we have

$$\tilde{\chi}^+_{c_i}(k+1) = \sum_{i=1}^{n_{c_i}} \tilde{\chi}^*_{c_i}(k+1), \tag{5.10}$$

where the global variables are updated using the average value of the local optimization results. The step requires information exchange between regions, i.e., passing the local optimization results $\tilde{\chi}^*_{c_i}(k+1)$ to connected regions.

Step 3. (ADMM parameter update)

3.1 Primal and dual residual update:
For each region $i \in \mathcal{R}$, the squared primal residual $r_i \in \mathbb{R}$ and dual residual $s_i \in \mathbb{R}$ are updated as follows

$$r_i^2(k+1) = \|\tilde{\boldsymbol{\chi}}^*_{\mathcal{C}_i}(k+1) - \tilde{\boldsymbol{\chi}}^+_{\mathcal{C}_i}(k+1)\|_2^2 \tag{5.11}$$

$$s_i^2(k+1) = \|\tilde{\boldsymbol{\chi}}^+_{\mathcal{C}_i}(k+1) - \tilde{\boldsymbol{\chi}}^+_{\mathcal{C}_i}(k)\|_2^2. \tag{5.12}$$

3.2 Penalty factor update:

$$\rho_i(k+1) = \begin{cases} \rho_i(k)\cdot(1+\tau) & r_i(k+1) > \kappa\, s_i(k+1) \\ \rho_i(k)\cdot(1+\tau)^{-1} & r_i(k+1) < \kappa\, s_i(k+1) \\ \rho_i(k) & \text{otherwise,} \end{cases}$$

where $\rho_i \in \mathbb{R}$ is the penalty factor associated to each region $i \in \mathcal{R}$ which is changed at each iteration depending on the local and global consensus progress measured by primal and dual residuals.

3.3 Lagrangian multiplier update step:

$$\boldsymbol{\lambda}_i(k+1) = \boldsymbol{\lambda}_i(k) + \rho_i\big(\hat{\boldsymbol{\chi}}_{\mathcal{C}_i}(k+1) - \tilde{\boldsymbol{\chi}}^+_{\mathcal{C}_i}(k+1)\big). \tag{5.13}$$

cation of parent and children region in the distributed DLMP scheme, the following explanation holds. Starting from the region connected to PSP, the regions can be arranged in a sequential order. The region which has a connected downstream region serves as the parent region with its downstream region as the children region. Moreover, the children region might serve as a parent region for its further connected neighbors (children). This kind of classification generally follows the structure of the radial network nature of the distribution grid.

Algorithm 7 Distributed DLMP scheme

1.1 For any children region, the root-node price is obtained as the cleared DLMP at the respective parent region's connected node

1.2 For any parent region i, the active power regional DLMPs $\boldsymbol{\pi}_i^{\mathsf{p}}$ are given as:

$$\boldsymbol{\pi}_i^{\mathsf{p}} = \boldsymbol{\pi}_i^{\mathsf{p,e}} + \boldsymbol{\pi}_i^{\mathsf{p,l}} + \boldsymbol{\pi}_i^{\mathsf{p,v}} + \boldsymbol{\pi}_i^{\mathsf{p,ADMM}} \tag{5.14}$$

with $\boldsymbol{\pi}_i^{\mathsf{p,ADMM}} = -(\frac{\partial \mathbf{p}_{\mathcal{C}_i}}{\partial \mathbf{p}_{\mathcal{L}_i}}, \frac{\partial \mathbf{q}_{\mathcal{C}_i}}{\partial \mathbf{p}_{\mathcal{L}_i}}, \frac{\partial \mathbf{v}_{\mathcal{C}_i}}{\partial \mathbf{p}_{\mathcal{L}_i}})\boldsymbol{\lambda}_i^{\mathsf{T}}$ and $\boldsymbol{\pi}_i^{\mathsf{p,e}}$, $\boldsymbol{\pi}_i^{\mathsf{p,l}}$, $\boldsymbol{\pi}_i^{\mathsf{p,v}}$ formulated in the same way as in (3.17), $\frac{\partial \mathbf{p}_{\mathcal{C}_i}}{\partial \mathbf{p}_{\mathcal{L}_i}}, \frac{\partial \mathbf{q}_{\mathcal{C}_i}}{\partial \mathbf{p}_{\mathcal{L}_i}}, \frac{\partial \mathbf{v}_{\mathcal{C}_i}}{\partial \mathbf{p}_{\mathcal{L}_i}}$ as the cross-region injection sensitivities (Definition 1).

The proposed distributed DLMP scheme adapts to the structural changes resulted from network partitioning and the derivation is provided in the following. The Lagrangian function associated to sub-optimization problem in region i is given as

$$\begin{aligned}
L_i = {} & f_i + (\boldsymbol{\lambda}_i^{\mathsf{p}})^{\mathsf{T}}(\mathbf{p}_{\mathcal{C}_i} - \mathbf{p}_{\mathcal{C}_i}^{+}) + (\boldsymbol{\lambda}_i^{\mathsf{q}})^{\mathsf{T}}(\mathbf{q}_{\mathcal{C}_i} - \mathbf{q}_{\mathcal{C}_i}^{+}) \\
& + (\boldsymbol{\lambda}_i^{\mathsf{v}})^{\mathsf{T}}(\mathbf{v}_{\mathcal{C}_i} - \mathbf{v}_{\mathcal{C}_i}^{+}) + \frac{1}{2}\rho_i(\tilde{\mathbf{p}}_{\mathcal{C}_i} - \tilde{\mathbf{p}}_{\mathcal{C}_i}^{+})^{\mathsf{T}}(\tilde{\mathbf{p}}_{\mathcal{C}_i} - \tilde{\mathbf{p}}_{\mathcal{C}_i}^{+}) \\
& + \frac{1}{2}\rho_i(\tilde{\mathbf{q}}_{\mathcal{C}_i} - \tilde{\mathbf{q}}_{\mathcal{C}_i}^{+})^{\mathsf{T}}(\tilde{\mathbf{q}}_{\mathcal{C}_i} - \tilde{\mathbf{q}}_{\mathcal{C}_i}^{+}) + \frac{1}{2}\rho_i(\tilde{\mathbf{v}}_{\mathcal{C}_i} - \tilde{\mathbf{v}}_{\mathcal{C}_i}^{+})^{\mathsf{T}}(\tilde{\mathbf{v}}_{\mathcal{C}_i} - \tilde{\mathbf{v}}_{\mathcal{C}_i}^{+}) \\
& + \mu_i^{\mathsf{pl}}(-p_{0,i} - \mathbf{1}_{n_i}^{\mathsf{T}}\mathbf{p}_{\mathcal{L}_i}^{\mathsf{g}} + \mathbf{1}_{n_i}^{\mathsf{T}}\mathbf{p}_{\mathcal{L}_i}^{\mathsf{sl}} + p_i^{\mathsf{loss}}) \\
& + \mu_i^{\mathsf{ql}}(-q_{0,i} - \mathbf{1}_{n_i}^{\mathsf{T}}\mathbf{q}_{\mathcal{L}_i}^{\mathsf{g}} + \mathbf{1}_{n_i}^{\mathsf{T}}\mathbf{q}_{\mathcal{L}_i}^{\mathsf{sl}} + q_i^{\mathsf{loss}}) \\
& + (\overline{\boldsymbol{\mu}}_i^{\mathsf{p}})^{\mathsf{T}}(\mathbf{p}_{\mathcal{L}_i}^{\mathsf{g}} - \overline{\mathbf{p}}_{\mathcal{L}_i}) - (\underline{\boldsymbol{\mu}}_i^{\mathsf{p}})^{\mathsf{T}}(\mathbf{p}_{\mathcal{L}_i}^{\mathsf{g}} - \underline{\mathbf{p}}_{\mathcal{L}_i}) \\
& + (\overline{\boldsymbol{\mu}}_i^{\mathsf{q}})^{\mathsf{T}}(\mathbf{q}_{\mathcal{L}_i}^{\mathsf{g}} - \overline{\mathbf{q}}_{\mathcal{L}_i}) - (\underline{\boldsymbol{\mu}}_i^{\mathsf{q}})^{\mathsf{T}}(\mathbf{q}_{\mathcal{L}_i}^{\mathsf{g}} - \underline{\mathbf{q}}_{\mathcal{L}_i}) \\
& + (\overline{\boldsymbol{\mu}}_i^{\mathsf{v}})^{\mathsf{T}}(\mathbf{v}_{\mathcal{L}_i} - \overline{\mathbf{v}}_{\mathcal{L}_i}) - (\underline{\boldsymbol{\mu}}_i^{\mathsf{v}})^{\mathsf{T}}(\mathbf{v}_{\mathcal{L}_i} - \underline{\mathbf{v}}_{\mathcal{L}_i}),
\end{aligned} \tag{5.15}$$

where the Lagrangian multiplier $\boldsymbol{\lambda}_i = [\boldsymbol{\lambda}_i^{\mathsf{p}}, \boldsymbol{\lambda}_i^{\mathsf{q}}, \boldsymbol{\lambda}_i^{\mathsf{v}}]$ consisting of three parts for coupled active power and reactive power. Where $\mathbf{b}_{\mathcal{L}_i}^*, \mathbf{d}_{\mathcal{L}_i}^*$ represent the regional DLMPs for active power and reactive power respectively, the KKT conditions comprise of

first-order optimality conditions:

$$\begin{aligned}
&\mathbf{b}^*_{\mathcal{L}_i} + \mu_i^{\mathsf{pl}}(\mathbf{m}^{\mathsf{pl,p}}_{\mathcal{L}_i})^\intercal + \mu_i^{\mathsf{ql}}(\mathbf{m}^{\mathsf{ql,p}}_{\mathcal{L}_i})^\intercal + (\boldsymbol{\lambda}_i^{\mathsf{p}})^\intercal \frac{\partial \mathbf{p}_{\mathcal{C}_i}}{\partial \mathbf{p}_{\mathcal{L}_i}} + (\boldsymbol{\lambda}_i^{\mathsf{q}})^\intercal \frac{\partial \mathbf{q}_{\mathcal{C}_i}}{\partial \mathbf{p}_{\mathcal{L}_i}} \\
&+ (\boldsymbol{\lambda}_i^{\mathsf{v}})^\intercal \frac{\partial \mathbf{v}_{\mathcal{C}_i}}{\partial \mathbf{p}_{\mathcal{L}_i}} + \rho_i(\mathbf{p}_{\mathcal{C}_i} - \mathbf{p}^+_{\mathcal{C}_i}) \frac{\partial \mathbf{p}_{\mathcal{C}_i}}{\partial \mathbf{p}_{\mathcal{L}_i}} + \rho_i(\mathbf{q}_{\mathcal{C}_i} - \mathbf{q}^+_{\mathcal{C}_i}) \frac{\partial \mathbf{q}_{\mathcal{C}_i}}{\partial \mathbf{p}_{\mathcal{L}_i}} \\
&+ \mu_i^{\mathsf{pl}} + (\mathbf{M}^{\mathsf{vp}}_{\mathcal{L}_i})^\intercal(-\underline{\boldsymbol{\mu}}_i^{\mathsf{v}} + \overline{\boldsymbol{\mu}}_i^{\mathsf{v}}) = 0 \qquad (5.16) \\
&b_{0,i} + \mu_i^{\mathsf{pl}} = 0 \qquad (5.17) \\
&\mathbf{d}^*_{\mathcal{L}_i} + \mu_i^{\mathsf{pl}}(\mathbf{m}^{\mathsf{pl,q}}_{\mathcal{L}_i})^\intercal + \mu_i^{\mathsf{ql}}(\mathbf{m}^{\mathsf{ql,q}}_{\mathcal{L}_i})^\intercal + (\boldsymbol{\lambda}_i^{\mathsf{p}})^\intercal \frac{\partial \mathbf{p}_{\mathcal{C}_i}}{\partial \mathbf{q}_{\mathcal{L}_i}} + (\boldsymbol{\lambda}_i^{\mathsf{q}})^\intercal \frac{\partial \mathbf{q}_{\mathcal{C}_i}}{\partial \mathbf{q}_{\mathcal{L}_i}} \\
&+ (\boldsymbol{\lambda}_i^{\mathsf{v}})^\intercal \frac{\partial \mathbf{v}_{\mathcal{C}_i}}{\partial \mathbf{q}_{\mathcal{L}_i}} + \rho_i(\mathbf{p}_{\mathcal{C}_i} - \mathbf{p}^+_{\mathcal{C}_i}) \frac{\partial \mathbf{p}_{\mathcal{C}_i}}{\partial \mathbf{q}_{\mathcal{L}_i}} + \rho_i(\mathbf{q}_{\mathcal{C}_i} - \mathbf{q}^+_{\mathcal{C}_i}) \frac{\partial \mathbf{q}_{\mathcal{C}_i}}{\partial \mathbf{q}_{\mathcal{L}_i}} \\
&+ \mu_i^{\mathsf{pl}} + (\mathbf{M}^{\mathsf{vq}}_{\mathcal{L}_i})^\intercal(-\underline{\boldsymbol{\mu}}_i^{\mathsf{v}} + \overline{\boldsymbol{\mu}}_i^{\mathsf{v}}) = 0 \qquad (5.18) \\
&d_{0,i} + \mu_i^{\mathsf{ql}} = 0 \qquad (5.19)
\end{aligned}$$

together with complementary slackness and positive duals. Based upon the convergence of CAST, we have $\mathbf{p}_{\mathcal{C}_i} - \mathbf{p}^+_{\mathcal{C}_i} = \mathbf{0}$ and $\mathbf{q}_{\mathcal{C}_i} - \mathbf{q}^+_{\mathcal{C}_i} = \mathbf{0}$. By substituting (5.17) and (5.19) into (5.16) and (5.18), resp., we obtain the DLMPs for active power $\mathbf{b}^*_{\mathcal{L}_i}$ as in the distributed DLMP scheme, i.e.

$$\begin{aligned}
\mathbf{b}^*_{\mathcal{L}_i} &= b_{0,i} - b_{0,i}(\mathbf{m}^{\mathsf{pl,p}}_{\mathcal{L}_i})^\intercal - d_{0,i}(\mathbf{m}^{\mathsf{ql,p}}_{\mathcal{L}_i})^\intercal + (\mathbf{M}^{\mathsf{vp}}_{\mathcal{L}_i})^\intercal(\underline{\boldsymbol{\mu}}_i^{\mathsf{v}} - \overline{\boldsymbol{\mu}}_i^{\mathsf{v}}) \\
&- (\boldsymbol{\lambda}_i^{\mathsf{p}})^\intercal \frac{\partial \mathbf{p}_{\mathcal{C}_i}}{\partial \mathbf{p}_{\mathcal{L}_i}} - (\boldsymbol{\lambda}_i^{\mathsf{q}})^\intercal \frac{\partial \mathbf{q}_{\mathcal{C}_i}}{\partial \mathbf{p}_{\mathcal{L}_i}} - (\boldsymbol{\lambda}_i^{\mathsf{v}})^\intercal \frac{\partial \mathbf{v}_{\mathcal{C}_i}}{\partial \mathbf{p}_{\mathcal{L}_i}}. \qquad (5.20)
\end{aligned}$$

Definition 1: Cross-region injection sensitivities

Note that the sensitivities $\frac{\partial \mathbf{p}_{\mathcal{C}_i}}{\partial \mathbf{p}_{\mathcal{L}_i}}$ and $\frac{\partial \mathbf{q}_{\mathcal{C}_i}}{\partial \mathbf{p}_{\mathcal{L}_i}}$ capture the effect on the coupled injection change $\mathbf{p}_{\mathcal{C}_i}, \mathbf{q}_{\mathcal{C}_i}$, due to the local power injection change $\mathbf{p}_{\mathcal{L}_i}, \mathbf{q}_{\mathcal{L}_i}$. This couples the behavior of neighboring regions into local DLMP calculations. Hence, we term this as *cross-region* injection sensitivities. In region i, for a coupled bus $c_i \in \mathcal{C}_i$ connected to n_{c_i} neighboring regions, the cross-region injection sensitivity can be calculated as

$$\frac{\partial p_{c_i}}{\partial \mathbf{p}_{\mathcal{L}_i}} := \frac{\partial p_{c_i}}{\partial v_{c_i}} \frac{\partial v_{c_i}}{\partial \mathbf{p}_{\mathcal{L}_i}} = \Big(\sum_{k \neq i}^{n_{c_i}} \frac{\partial p_{c_k}}{\partial v_{c_k}}\Big) \frac{\partial v_{c_i}}{\partial \mathbf{p}_{\mathcal{L}_i}}. \qquad (5.21)$$

Some observations regarding the above definition of $\frac{\partial p_{c_i}}{\partial \mathbf{p}_{\mathcal{L}_i}}$ follow. In (5.21): (i) only voltage magnitudes are considered, as the angle differences across distribution lines are considerably smaller [5]; (ii) we incorporate information from both local $\frac{\partial v_{c_i}}{\partial \mathbf{p}_{\mathcal{L}_i}}$ and neighboring regions $\frac{\partial p_{c_k}}{\partial v_{c_k}}$; and (iii) the local sensitivities $\frac{\partial v_{c_i}}{\partial \mathbf{p}_{\mathcal{L}_i}}$ are obtained from $\mathbf{M}^{\mathsf{vp}}_{\mathcal{L}_i}$, whereas the neighboring information $\frac{\partial p_{c_k}}{\partial v_{c_k}}$ is obtained with the explicit power flow linearization in chapter 2.

The proposed market framework requires a two-way communication network for all market participants. However, the type of information to be exchanged within

a framework varies. For any regional DSO, Fig. 5.3 provides an overview of the information to be shared by a regional DSO. The communication traffic in the distributed DLMP scheme is comparably smaller than in the CAST loop since it merely requires one-time communication of passing the cleared price and cross-region injection sensitivity between regional DSOs. Note that all information except on its physically coupled buses is kept local by a regional DSO. This means that a regional DSO only needs to share information with its physically connected neighboring regional DSOs. The information needed to be revealed by any regional DSO includes physical parameters of active/reactive injections and a root-node price for its children regional DSO (only if it serves as a parent regional DSO, see Sec. IV-A for more information). This proposed information exchange framework of a regional DSO resembles a power system where multiple RTOs exist [22, 23]. Hence, the proposed framework of this paper has a high practical realization.

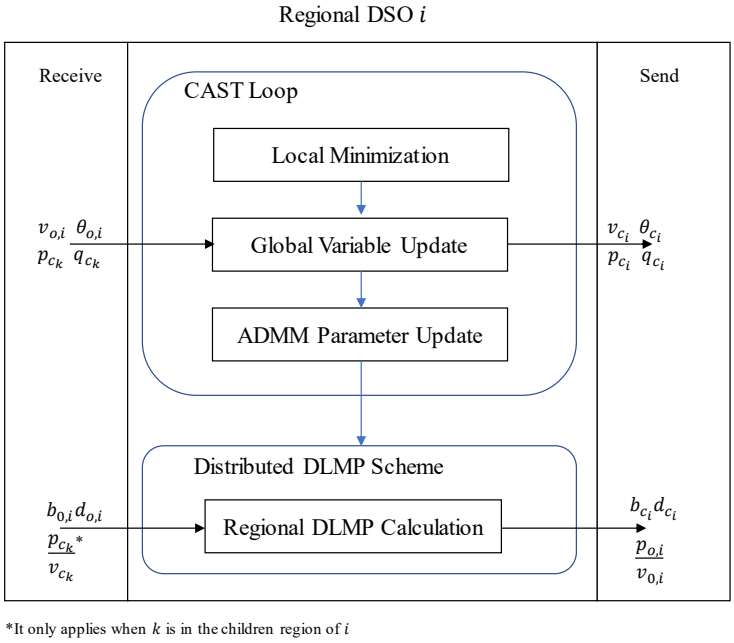

Fig. 5.3: Flowchart of the information exchange between regional DSOs.

5.3.2 Three-bus network example

We use the 3-bus network to elaborate the distributed DLMP scheme. First, consider centralized active power DLMPs (3.17) for the exemplary 3 bus system of Fig. 5.4, only with loss terms:

$$b_1 = b_0 - \frac{\partial p^{\text{loss}}}{\partial p_1} b_0 - \frac{\partial q^{\text{loss}}}{\partial p_1} d_0 \tag{5.22}$$

$$b_2 = b_0 - \frac{\partial p^{\text{loss}}}{\partial p_2} b_0 - \frac{\partial q^{\text{loss}}}{\partial p_2} d_0. \tag{5.23}$$

Now consider the network partitioned as shown in Fig. 5.4. The following two reasons prevent the adoption of the above mentioned price structure: (i) With the partitioning, note that b_0, originally the marginal price at the slack bus, is now local to

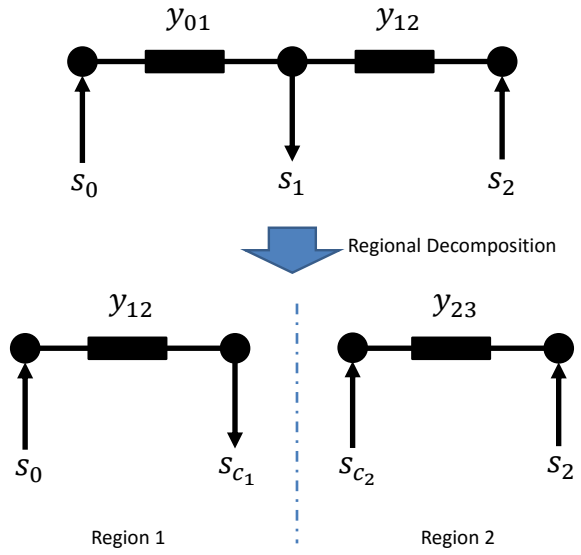

Fig. 5.4: Three-bus network example.

region 1. Moreover, region 2 has a new root-bus, i.e., bus 1. Hence, the formulation needs to be adjusted to account for these structural changes. (ii) Each region only computes local losses through local linearized terms $\mathbf{m}^{\mathsf{pl,p}}_{\mathcal{L}_1}, \mathbf{m}^{\mathsf{ql,p}}_{\mathcal{L}_1}, \mathbf{m}^{\mathsf{pl,p}}_{\mathcal{L}_2}, \mathbf{m}^{\mathsf{ql,p}}_{\mathcal{L}_2}$. However, the losses in the each region is coupled to its neigbouring region's injection through the local copy. Hence, if not accounted, this effect might induce errors in the local loss calculations and its representation in DLMPs. Hence, we derive the below pricing scheme to account for these changes and obtain a similar structure and optimality in the final price as the central method (3.17).

Region 1

The Lagrangian function associated to sub-optimization problem in region 1 is given as

$$\begin{aligned} L_1 &= f_1 + \lambda_1^p(p_{c_1} - p_{c_1}^+) + \lambda_1^q(q_{c_1} - q_{c_1}^+) \\ &+ \frac{1}{2}\rho_1(p_{c_1} - p_{c_1}^+)^2 + \frac{1}{2}\rho_1(q_{c_1} - q_{c_1}^+)^2 + \mu_1^{\mathsf{pl}}(p_0 + p_1 - p_1^{\mathsf{loss}}) \\ &+ \mu_1^{\mathsf{ql}}(q_0 + q_1 - q_1^{\mathsf{loss}}), \end{aligned} \tag{5.24}$$

where λ_1^p, λ_1^q are the augmented Lagrangian multipliers. Note that due to the network partition, the losses are automatically separated into 2 parts: p_1^{loss} and p_2^{loss} for region 1 and 2, respectively. They are related to the total loss in a way that

$$p^{\mathsf{loss}} = p_1^{\mathsf{loss}} + p_2^{\mathsf{loss}}. \tag{5.25}$$

Let b_1^*, d_1^* represent the distributed DLMPs in region 1, then the associated KKT conditions for region 1 are

$$b_1^* - \mu^{\mathsf{pl}} \frac{\partial p_1^{\mathsf{loss}}}{\partial p_1} - \mu^{\mathsf{ql}} \frac{\partial q_1^{\mathsf{loss}}}{\partial p_1} + \lambda_1^p \frac{\partial p_{c_1}}{\partial p_1} + \lambda_1^q \frac{\partial q_{c_1}}{\partial p_1}$$
$$+ \rho_i (p_{c_1} - p_{c_1}^+) \frac{\partial q_1^{\mathsf{loss}}}{\partial p_1} + \rho_i (q_{c_1} - q_{c_1}^+) \frac{\partial q_{c_1}}{\partial p_1} + \mu^{\mathsf{pl}} = 0, \tag{5.26}$$
$$b_0 + \mu^{\mathsf{pl}} = 0, \tag{5.27}$$
$$d_1^* - \mu^{\mathsf{pl}} \frac{\partial p_1^{\mathsf{loss}}}{\partial q_1} - \mu^{\mathsf{ql}} \frac{\partial q_1^{\mathsf{loss}}}{\partial q_1} + \lambda_1^p \frac{\partial p_{c_1}}{\partial q_1} + \lambda_1^q \frac{\partial q_{c_1}}{\partial q_1}$$
$$+ \rho_i (p_{c_1} - p_{c_1}^+) \frac{\partial q_1^{\mathsf{loss}}}{\partial q_1} + \rho_i (q_{c_1} - q_{c_1}^+) \frac{\partial q_{c_1}}{\partial q_1} + \mu^{\mathsf{ql}} = 0, \tag{5.28}$$
$$d_0 + \mu^{\mathsf{ql}} = 0, \tag{5.29}$$

together with the complementary slackness and positive duals. We have $p_{c_1} - p_{c_1}^+ = 0,\ q_{c_1} - q_{c_1}^+ = 0$ based upon the convergence of CAST, giving us DLMPs for node 1 in region 1 as

$$b_1^* = b_0 - b_0 \frac{\partial p_1^{\mathsf{loss}}}{\partial p_1} - d_0 \frac{\partial q_1^{\mathsf{loss}}}{\partial p_1} - \lambda_1^p \frac{\partial p_{c_1}}{\partial p_1} - \lambda_1^q \frac{\partial q_{c_1}}{\partial p_1},$$
$$d_1^* = d_0 - c_0 \frac{\partial p_1^{\mathsf{loss}}}{\partial q_1} - d_0 \frac{\partial q_1^{\mathsf{loss}}}{\partial q_1} - \lambda_1^p \frac{\partial p_{c_1}}{\partial q_1} - \lambda_1^q \frac{\partial q_{c_1}}{\partial q_1}.$$

Note that the sensitivity $\frac{\partial p_{c_1}}{\partial p_1}$, represents the effect on the coupled injection change p_{c_1}, due to the local power injection change p_1. This captures the actions of neighboring regions into local DLMP calculations. Hence, we call this term cross-region injection sensitivity. In region 1, for a coupled bus $c_1 \in \mathcal{C}_1$ connected to 1 neighboring regions, the cross-region injection sensitivity is defined by $\frac{\partial p_{c_1}}{\partial \mathbf{p}_{\mathcal{L}_1}}$ and can be calculated as

$$\frac{\partial p_{c_1}}{\partial p_1} := \frac{\partial p_{c_2}}{\partial v_{c_2}} \frac{\partial v_{c_1}}{\partial p_1}. \tag{5.30}$$

The above sensitivity only includes voltage magnitude to calculate coupled loss sensitivities, as angle difference are considerably small across lines [5]. Moreover, each part relies on the local information $\frac{\partial v_{c_1}}{\partial p_1}$ and neighbor information $\frac{\partial p_{c_2}}{\partial v_{c_{k2}}}$. Note that $\frac{\partial v_{c_1}}{\partial \mathbf{p}_{\mathcal{L}_1}}$ is part of $\mathbf{m}_{\mathcal{L}_1}^{\mathsf{PQ}}$ and $\frac{\partial p_{c_2}}{\partial v_{c_2}}$ can be either numerically or analytically calculated (refer to chapter 2).

Region 2

Recall algorithm 7, where for any children region, the root node price is obtained as the DLMP from the parent region. DLMPs for children regions are calculated in the same way as in the central scheme. To provide the derivation on the three-bus example, we first recapture the loss sensitivity decomposition chapter 2 as follows. Loss linearization can be related to slack bus injection linearization by the power

balance equations, i.e., $p_0 + \mathbf{1}_n^{\mathsf{T}} \mathbf{p}_{\mathcal{L}} = p^{\text{loss}}$. By taking first-order derivative on both sides of the equation, we obtain

$$\frac{\partial p_0}{\partial \mathbf{p}_{\mathcal{L}}} + \mathbf{1}_n = \frac{\partial p^{\text{loss}}}{\partial \mathbf{p}_{\mathcal{L}}}. \tag{5.31}$$

Intuitively, for small-scale networks, by increasing/reducing of power injections at PQ buses, similar amount of power will be reduced/increased at the slack bus, i.e., $\frac{\partial p_0}{\partial \mathbf{p}_{\mathcal{L}}} \approx -\mathbf{1}_n$ and consequently, $\frac{\partial p^{\text{loss}}}{\partial \mathbf{p}_{\mathcal{L}}}$ is close to $\mathbf{0}_n$.

Using the loss decomposition in (5.25), we obtain the following sensitivity decomposition:

$$\frac{\partial p^{\text{loss}}}{\partial p_2} = \frac{\partial p^{\text{loss}}}{\partial p_1} + \frac{\partial p_2^{\text{loss}}}{\partial p_2} \tag{5.32}$$

$$\frac{\partial q^{\text{loss}}}{\partial p_2} = \frac{\partial q^{\text{loss}}}{\partial p_1} + \frac{\partial q_2^{\text{loss}}}{\partial p_2} \tag{5.33}$$

The derivation is given as follows:

$$\begin{aligned}
\frac{\partial p^{\text{loss}}}{\partial p_2} - \frac{\partial p^{\text{loss}}}{\partial p_1} &= \frac{\partial p_1^{\text{loss}}}{\partial p_2} + \frac{\partial p_2^{\text{loss}}}{\partial p_2} - \frac{\partial p_1^{\text{loss}}}{\partial p_1} - \frac{\partial p_2^{\text{loss}}}{\partial p_1} \\
&\big(\text{with } p_1^{\text{loss}} \text{ is linked to } p_2 \text{ by } p_{c_1} \text{ and } p_{c_2}, \text{where } p_{c_1} = -p_{c_2}\big) \\
&= -\frac{\partial p_1^{\text{loss}}}{\partial p_{c_1}} \frac{\partial p_{c_2}}{\partial p_2} + \frac{\partial p_2^{\text{loss}}}{\partial p_2} - \frac{\partial p_1^{\text{loss}}}{\partial p_1} - \frac{\partial p_2^{\text{loss}}}{\partial p_1} \\
&\big(\text{Since } c_2 \text{ is the slack bus, from (2.30) we have } \frac{\partial p_{c_2}}{\partial p_2} = \frac{\partial p_2^{\text{loss}}}{\partial p_2} - 1.\big) \\
&= -\frac{\partial p_1^{\text{loss}}}{\partial p_{c_1}} (\frac{\partial p_2^{\text{loss}}}{\partial p_2} - 1) + \frac{\partial p_2^{\text{loss}}}{\partial p_2} - \frac{\partial p_1^{\text{loss}}}{\partial p_1} - \frac{\partial p_2^{\text{loss}}}{\partial p_1} \\
&= \frac{\partial p_1^{\text{loss}}}{\partial p_{c_1}} \frac{\partial p_2^{\text{loss}}}{\partial p_2} + \frac{\partial p_2^{\text{loss}}}{\partial p_2} - \frac{\partial p_2^{\text{loss}}}{\partial p_1}
\end{aligned} \tag{5.34}$$

Note that $\frac{\partial p_1^{\text{loss}}}{\partial p_{c_1}}, \frac{\partial p_2^{\text{loss}}}{\partial p_2}$ is close to 0 such that the second-order terms $\frac{\partial p_1^{\text{loss}}}{\partial p_{c_1}} \frac{\partial p_2^{\text{loss}}}{\partial p_2}$ and $\frac{\partial p_2^{\text{loss}}}{\partial p_1} = -\frac{\partial p_2^{\text{loss}}}{\partial p_{c_2}} \frac{\partial p_{c_1}}{\partial p_1}$ can be neglected. The sensitivity decomposition (5.32) and (5.33) is then obtained.

Now consider setting the root node price for region 2 using nodal price from bus 1 and calculate the DLMP locally, i.e., distributed DLMP b_2^* is calculated as

$$b_2^* = b_1 - \frac{\partial p_2^{\text{loss}}}{\partial p_2} b_1 - \frac{\partial q_2^{\text{loss}}}{\partial p_2} d_1. \tag{5.35}$$

Substitute (5.22) and $d_1 = d_0 - \frac{\partial q^{\text{loss}}}{\partial q_1} d_0 - \frac{\partial p^{\text{loss}}}{\partial q_1} b_0$, we obtain[1]

$$b_2^* = b_0 - (\frac{\partial p^{\text{loss}}}{\partial p_1} + \frac{\partial p_2^{\text{loss}}}{\partial p_2}) b_0 - (\frac{\partial q^{\text{loss}}}{\partial p_1} + \frac{\partial q_2^{\text{loss}}}{\partial p_2}) d_0 \tag{5.36}$$

using (5.32) and (5.33), we have

$$b_2^* = b_2 \tag{5.37}$$

[1] For the sake of brevity, the step of neglecting the second-order terms is skipped in the derivation

5.4 Numerical Example

We test the proposed CAST algorithm on an IEEE 33-bus system [118] with three regions as illustrated in Fig. 5.5 (see Scenario 1 & 2) and on a 144-bus network (see Scenario 3). Each region includes a DG operating locally. The test network has a total fixed load of 3.66 MW and 2.28 Mvar. In order to demonstrate the efficiency of the proposed method, we provide comparison against IPM of MATPOWER [74] for two realistic scenarios. For scenarios 1 and 2: the energy price at the PSP is kept at 30 \$/ MWh and 3 \$/ Mvar h whereas for all DGs as 20 \$/ MWh and 3 \$/ Mvar h; voltage constraints are kept as $[0.95, 1.05]$; and the ADMM and trust-region parameters are set as: $\eta = 0.1$, $\beta = 0.9$, $\gamma = 0.5$, $\tau = 0.1$, $\kappa = 10$, $\rho_i(0) = 7 \times 10^2, \lambda_i(0) = 7, i \in \mathcal{R}$. For scenario 3, the TR parameters are kept the same while the ADMM parameters are set as: $\tau = 0.1$, $\kappa = 10$, $\rho_i(0) = 1.2 \times 10^5, \lambda_i(0) = 0.5, i \in \mathcal{R}$. The simulations are performed on a personal computer with Intel i5 2.4Ghz and 8 GB RAM.

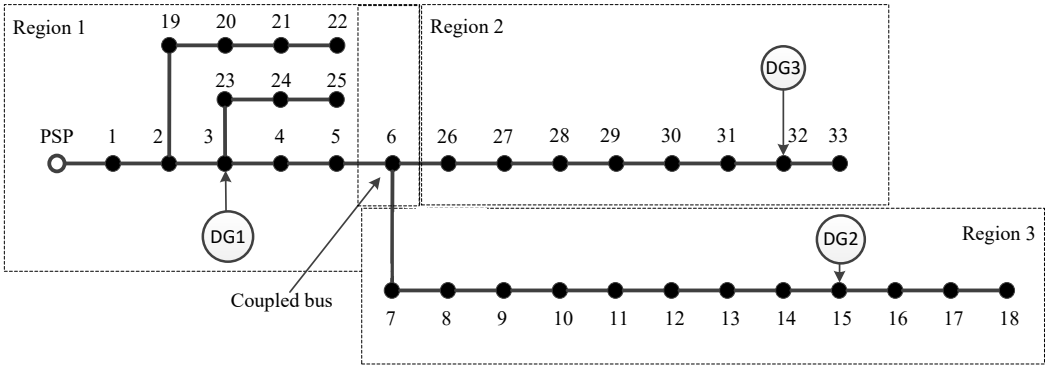

Fig. 5.5: 33-bus system with three regions.

5.4.1 Scenario 1 - lossy DLMPs

Scenario 1 considers three DGs with identical 500 kW and ± 100 kvar capacity, i.e., with modest renewable energy penetration. The convergence of the CAST algorithm with the optimal solution is illustrated in Fig. 5.6 with respect to total cost, primal gap and active/reactive power dispatch. The primal gap is defined as the sum of primal residuals in eq. (5.11) which is a measure of disagreement on the power flow parameters of the coupled buses. In order to demonstrate the VP method in the improvement of the convergence performance, we compared the situation including/excluding the varying penalty update in closing the primal gap for all three scenarios. Note that the proposed CAST algorithm achieves the exact optimal solution as the central AC-OPF (MATPOWER).

The DLMP results can be found in Fig. 5.7 and Table 5.1. Since the energy supply from DGs is cheaper than the PSP, all DGs are fully dispatched (see Table 5.2). Meanwhile, no overvoltages are caused by DGs because of the modest penetration level, keeping voltage support part of DLMP $\pi^{\text{p,v}}$ at 0. Hence, the only contribution to the overall price calculation comes from the loss component of DLMPs, penalizing nodes based on their contribution to the overall losses in the distribution grid. Regarding the coupled loss component $\pi^{\text{p,ADMM}}$, its value is comparatively small in contrast to local region losses $\pi^{\text{p,l}}$. This shows that the effect of neighboring

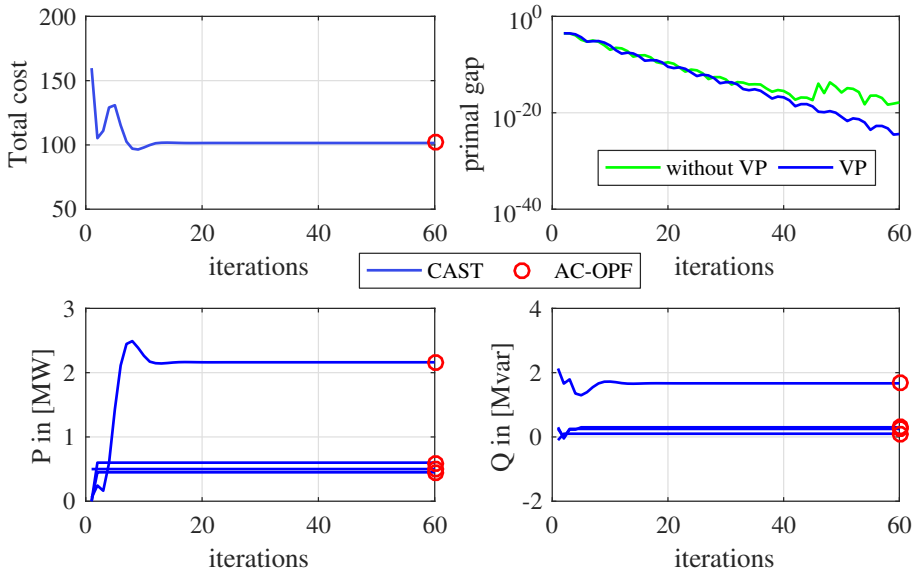

Fig. 5.6: Scenario 1: Convergence of CAST.

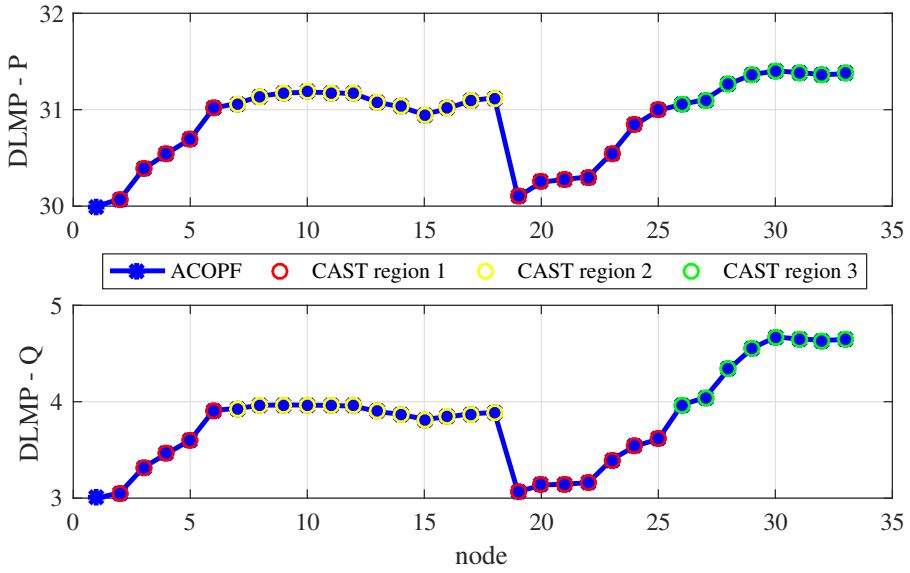

Fig. 5.7: Scenario 1: DLMP with ACOPF as benchmark.

regions in contributing to local losses is not as great. Similar to the dispatch values, the multi-regional DLMPs are also found to be similar to the central AC-OPF solution (MATPOWER).

5.4.2 Scenario 2 - binding voltage constraint

In scenario 2, a high renewables-penetration level is considered by assuming 3×3 MW DG with the nominal power factor of 0.9. As a consequence, local voltages at DG buses become binding. First, we present the convergence of CAST in Fig. 5.8

Table 5.1: Active power DLMPs for both scenarios

i		$\pi^{p,e}$	$\pi^{p,l}$	$\pi^{p,v}$	$\pi^{p,ADMM}$	π^{p} (CAST)	π^{p}(AC-OPF)
3	case 1	30	0.35	0	2.8e-3	30.39	30.39
15		31.02	-0.07	0	-	30.95	30.95
32		31.02	0.35	0	-	31.36	31.36
3	case 2	24.21	-0.064	-4.15	1.2e-3	20.00	20.00
15		20.27	-0.11	-0.159	-	20.00	20.00
32		20.27	-0.062	-0.238	-	20.00	20.00

Table 5.2: Power dispatch comparison of CAST and AC-OPF

Node		P dispatch [MW]		Q dispatch [Mvar]		Total cost [$]	
		CAST	AC-OPF	CAST	AC-OPF	CAST	AC-OPF
PSP	case 1	2.23	2.23	2.03	2.03	103.44	103.44
DG1		0.5	0.5	0.1	0.1		
DG2		0.6	0.6	0.3	0.3		
DG3		0.45	0.45	0.25	0.25		
PSP	case 2	0	0	0.95	0.95	77.302	77.302
DG1		2.34	2.34	-0.02	-0.03		
DG2		0.66	0.65	0.41	0.42		
DG3		0.69	0.69	0.94	0.94		

and dispatch values in Table 5.2. One can also observe that VP method has improved the convergence in both scenarios despite the same initial parameters. Binding voltage constraints in different regions generate more oscillations to obtain consensus among the coupled buses. The CAST settles down at a total cost of $ 77.302 which is identical to the optimal value obtained from AC-OPF.

In terms of DLMP, as compared to scenario 1, the voltage support part π^{v} is relatively high compared to other components of the DLMP that in turn reduces the DLMP at DG nodes. This penalizes DGs and reduces the local generations while maintaining the local voltage under the upper bound. Note that as nodes 15 and 32 are completely supplied by their local DGs, their cleared price $\boldsymbol{\pi}^{\mathrm{p}}$ is equal to the marginal cost of supplying power from their respective DGs, which has been set at 20 $/MWh. The dispatch results are given in Fig. 5.9, where it can be seen that the proposed distributed method achieves a similar quality to the central solution.

5.4.3 144-bus Network

In scenario 3, we extend the test case to a larger network with 144 buses [75]. The scenario considers 5 regions ($\mathcal{R} = \{1, 2, ..., 5\}$) with 7 DGs in total. The network partition is illustrated in Fig. 5.10. The price vectors for the power procurement from PSP and DGs are presented in Table 5.3. The base load of the test scenario is 11.9 MW and 7.36 Mvar. The convergence of the CAST algorithm to the optimal solution is illustrated in Fig. 5.12 with respect to total cost, primal gap and active/reactive

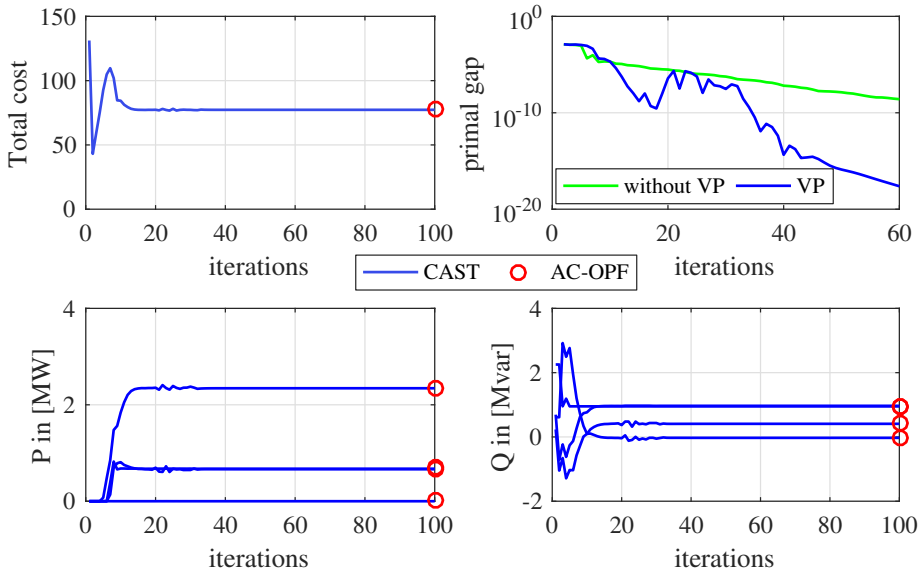

Fig. 5.8: Scenario 2: Convergence of CAST.

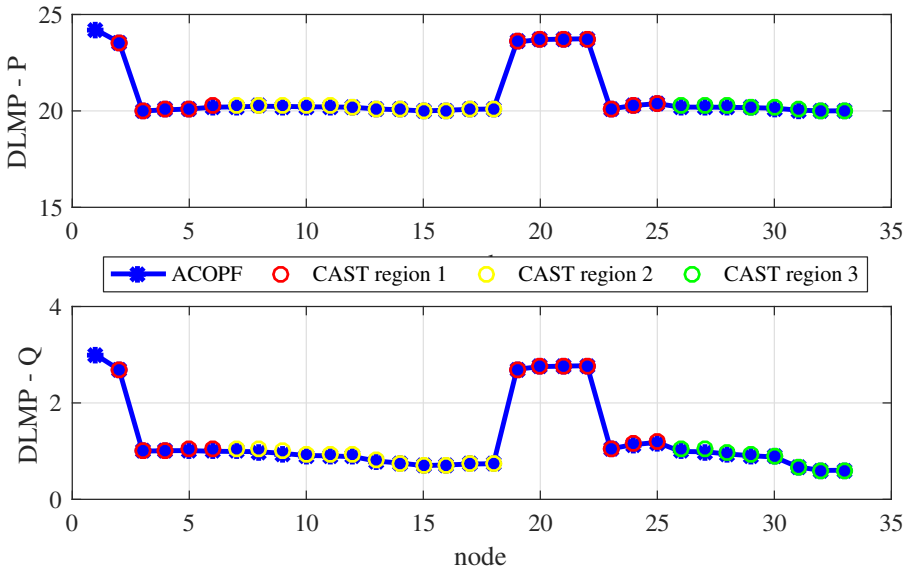

Fig. 5.9: Scenario 2: DLMP with ACOPF as benchmark.

Table 5.3: Test scenario 144-bus network: DG cost and constraints

Price vector	DG0(PSP)	DG1	DG2	DG3	DG4	DG5	DG6
P [$/MWh]	20	10	10	10	7	10	10
Q [$/Mvarh]	3	2	3	2	2.9	1.9	3.1
P Max [MWh]	-	1.5	1.5	1.9	1.2	2.3	1.5
Q Max [Mvarh]	-	+/-0.3	+/-0.3	+/-0.4	+/-0.6	+/-0.7	+/-0.9

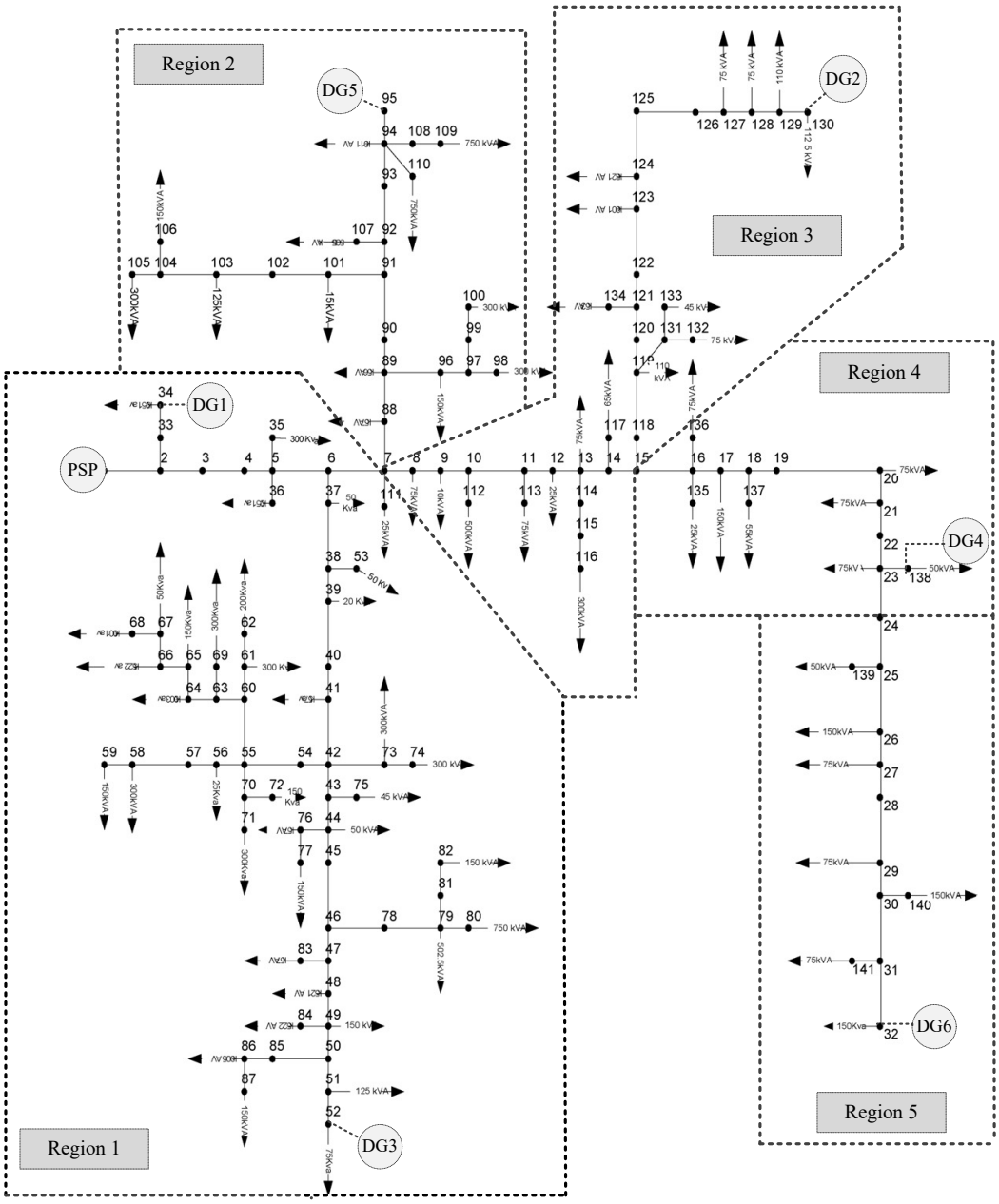

Fig. 5.10: 144-bus test case with 5 regions [75].

power dispatch. It can be seen that CAST has converged towards the same optimal solution as in ACOPF. Moreover, due to the earlier settlement for the optimal solution, one can also conclude the convergence performance is improved by VP method as well.

The test scenario considers a modest DG penetration degree, i.e., the PSP remains the primary source for the energy supply. The DLMP results for the 144-bus network can be found in Fig. 5.11. Since the PSP serves as the primary source for the energy supply, the DLMP is dominated by the root-node price accordingly. In general, one can observe the marginal price downstream of Region 1 is the

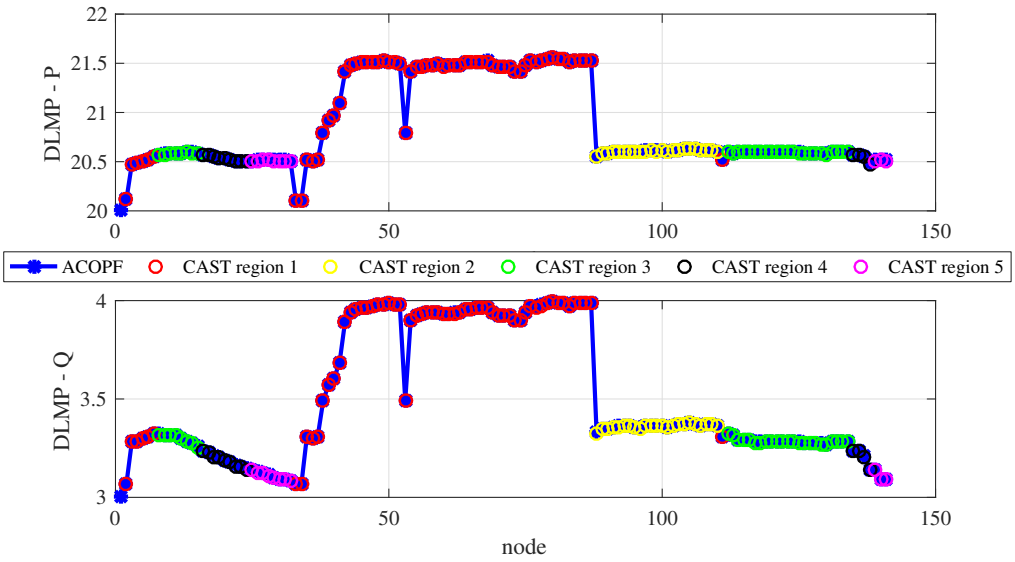

Fig. 5.11: Scenario 3: DLMP with ACOPF as benchmark.

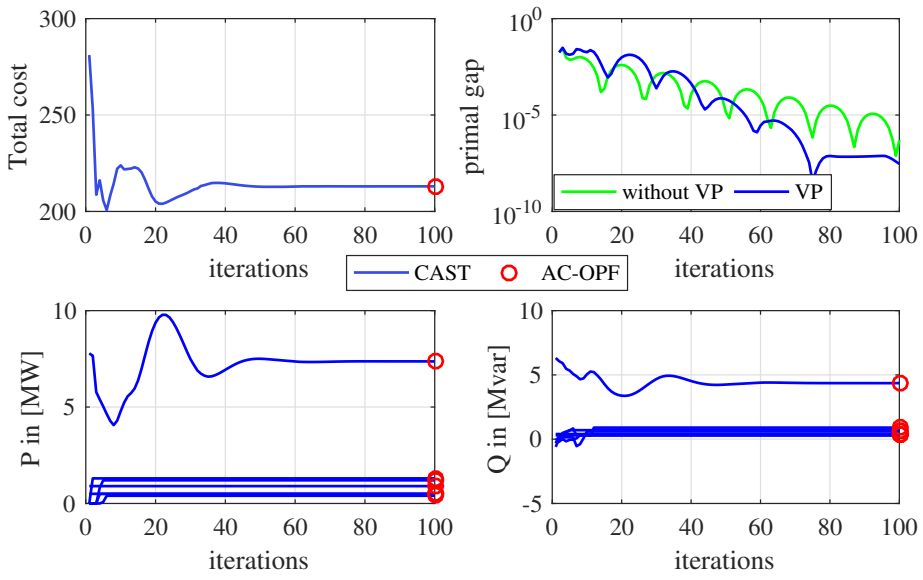

Fig. 5.12: Scenario 3: Convergence of CAST.

highest due to the higher losses. On the other hand, the distributed DLMP scheme has achieved the same price accuracy as the centralized ACOPF solution, despite multiple regions and highly coupled loss terms between the regions.

5.4.4 Computational aspects

In terms of the computation efficiency and results interpretability of the proposed

Table 5.4: Computation comparison

	TR	IPM	SDP relaxation
Global solution	✓	✓	✓
Computation time (144-bus network)	2.9 s	1.3 s	12.3 s
Implicit calculation of DLMP	✓	×	×
Tractable formulation	✓	×	×

method, we present the computational comparison of the local optimizer using TR, IPM and semi-definite-programing (SDP) relaxation methods in Table 5.4. The TR optimizer is implemented with YALMIP [119] and Gurobi [129]. The IPM and SDP are implemented with the MATPOWER interior point solver and SeDuMi [130], respectively. Note that all three solvers produce the same global solution. IPM requires less computational time than needed in TR, whereas the computational burden for SDP is the heaviest. We also notice that the computation time of TR is implementation-dependent, i.e., YALMIP consumes substantially more time in creating the model than the solver time with Gurobi. Furthermore, the DLMPs can be calculated during each iteration for the TR method, whereas it can only be recovered after finding the optimal solution for the SDP-based ACOPF and IPM-ACOPF. In this respect, a tractable formulation (i.e. a feasible power flow solution and the decomposable price signals at each iteration) can also only be provided by TR.

Since in the field deployment of CAST, each regional DSO solves the local problem in parallel, without extending the discussion of the inclusion of communication network, the overall solving time can be estimated by multiplying the iteration number by the local solver time. Recent works have reported a reasonable speedup of ADMM-based algorithm in a local simulation when a parallel computing technique is adopted [131].

5.5 Summary

In this chapter, a decentralized market framework at the distribution grid level is proposed. The main ingredients of the framework are: (i) Consensus-Alternating direction method of multipliers Structured Trust-region (CAST) solution algorithm to capture the nonconvex AC power flow in a fully distributed way and (ii) a multi-regional DLMP decomposable pricing scheme. To demonstrate the efficiency of the proposed method, three simulation scenarios are investigated on benchmark systems, and comparisons are made to the MATPOWER state-of-the-art solver. Note that the distributed DLMP scheme is only proven for the distribution grid with radial-network topology. The extension and validity to meshed network and the exact cost allocation through cross-region injection sensitivity for unbalanced network remains an open research question. On the other side, having proposed an efficient algorithm for decomposed pricing schemes, the reorganization of the existing power system in order to achieve both planning and operational efficiency still needs to be addressed in future works.

Chapter 6

Discussions and Outlook

6.1 Discussions

Building on the promise of smart distribution grid, the work at hand discusses the market frameworks to allow for greater economic efficiency, as well as continued satisfactory operation of distribution system in a decentralized fashion. This decentralized fashion is reflected in various aspects including i) reorganizing the grid and market operation to be fulfilled by collaborative regional DSOs, and ii) creating incentive-based indirect control schemes to regulate the bilateral energy exchange between prosumers at the distribution grid level.

Fundamentally, the derived pricing scheme is obtained from the Lagrangian dual of optimal power flow. Dual prices support optimal dispatch behavior of market participants if the primal problem is convex. To this end, we adopt the nonlinear programming technique to solve the optimal power flow problem and derive incentive price signals, both in centralized and decentralized fashion for the respective market environment. The electricity market and ancillary service market is supposed to be operated by the regional DSOs. At a higher level, it entails the region-to-region coordination and multi-regional market-clearing scheme that is realized by the ADMM-based solution methodology. Since the regional systems are physically coupled, the cost allocations and market settlement are in line with their physical interconnection between these regions and the cost allocations are determined by the optimal energy exchange prices and cross-region sensitivities. Specific to each regional distribution grid, the options for DERs integration exist in the participation in the centralized DSO market as well as P2P market. Both markets rely on DLMP as a common tool to derive the "grid-friendly" behavior of DERs, where GUPs are imposed for each P2P transaction.

The proposed market framework is validated by duality analysis and numerical experiments. It shows that both DLMPs and their derivative GUPs have a decomposable structure that represent incentive price signals to regulate DERs to contribute towards the grid operations. Aside from these major observations in the numerical analysis, we would like to underline the following interesting notes that may be taken into account in the market design. In algorithm 7, the energy exchange prices between regional operators revealed by ADMM include three parts: active power, reactive power and voltage. Specifically to the voltage part, it provides an economical value for not only maintaining voltages locally, but also globally. Hence,

voltage can be treated as commodities between entities like operators and prosumers. We have conducted some preliminary studies to discuss the possibility to trade voltage between interconnected microgrids by assigning voltage penalty cost in the social welfare function of the underlying system in [47]. Practically, pricing voltages is still an emerging topic, where the cost for maintaining voltages are usually considered rather as an investment problem than an operation problem. This may be subject to change as if an AC-OPF model is to be adopted by DSO. This enables a market design to be dedicated to the voltage stability on the distribution grid side, which can be potentially beneficial for obtaining short- and long-run price signals to mitigate the voltage problem in view of the integration of renewable generations.

At the time of writing, for the adoption of nonlinear programming technique the strong duality can not be guaranteed. However, it is worth mentioning that for all the radial network that have been tested in this work the global optimal solutions are obtained for different test scenarios. Mathematical insight for this phenomenon is difficult, despite the fact that some intuition can be provided from the convexity analysis for optimal power flow problem applying alternative approaches like semidefinite programming as in [80]. On the other hand, special attention should be paid to meshed network cases, which have been excluded from the discussion in this dissertation. In the practice of some countries, low-voltage radial feeders are usually interconnected to form a ring network, e.g., [132]. Meshed network generally yield multiple local optima. Hence, the convergence property and the sensitivity analysis of the proposed distributed DLMP scheme should be investigated for this context accordingly.

6.2 Future works

6.2.1 Market design considering uncertainty

We limit the majority of our discussion in this dissertation to a single-market interval. Consider of extending the bilateral programming model for DSO market and P2P market in Chapter 4 to a multi-period model, how to incorporate the stochastic nature of renewable resources in a market design determines whether the electricity market outcome is sustainable. For the practice at transmission grid level, the market are organized in a way to include multiple time scales, including day-ahead market (forward market), intra-day market (adjustment market) and real-time market (balancing market), which are viewed by many to be essential to capture the stochastic nature for the renewable integration [133]. The wholesale market generally follows the setup “supply-follows-demand" as many conventional generator types are considered dispatchable. At the distribution grid level, where the demand side is most likely to be managed, the market design can be organized in a similar way to enable a market in a “demand-follow-supply” manner, focusing on the demand-side management. To this end, the incorporating of detailed thermal load modeling, e.g., [134], further development of probabilistic DLMP and multi-period P2P market–clearing models are the essential ingredients to accommodate the uncertain nature of generations and loads in a market design.

6.2.2 Game-theoretical analysis for distribution grid market

As one of the assumptions on market participants in this work is that the DERs are price takers. It means that, there is significant competition between prosumers to prevent the market participants to improve their position through strategic price-setting behavior. However, the condition to exclude the strategic behavior are not always true and the regulation paradigm may need to take into account the prosumers that have market power. A potential solution for this is to incorporate game-theoretical approaches (e.g., [135]) to model the P2P market clearing process, where the impact on the prosumer behavior from GUP can be treated accordingly. On the other side, distribution grid market, based on some studies, are regarded as markets with lower liquidity. Hence, it is essential to design incentives to form a competitive markets that support the competitive-market assumptions of this work. In this scope, a direct extension of this work is to analyze the coordinated market design in Chapter 4 with game theoretical approach considering prosumer's spatial and temporal arbitrage as well as strategic-bidding behavior.

6.2.3 Prosumer attitudes and preferences

In line with the consideration of strategic prosumer behavior, the prosumers may have other distinguished attitudes towards risk and heterogeneous preferences. It is very common in the literature to assume that that the prosumers have identical attitudes towards risk. Therefore, the preferences for some players who are willing to accept a greater payoff volatility and risk than others are not accommodated in the market design. This may lead to conservative forward market designs and impact the market liquidity. In light of this, some existing work, e.g., [136, 137] discusses about the risk trading in the electricity market design and provides ways to develop financial hedging products for the distribution grid market context. By using historical data and long-term forecast model of the grid, hedging rights can be calculated to recover both the operating cost and investment cost. Prosumers can procure the rights beforehand to hedge against price volatility. Through this way, social welfare loss of the conservative market decision making can be avoided.

The proposal of GUP scheme requires the evaluation of the DLMP constantly for each new P2P transaction request. This is computationally expensive and the resulted GUP is volatile. Inspired by the concept of financial transmission right in transmission grid market, the solution for this is to define the financial product that can help prosumers in a P2P trade to hedge against the price volatility of GUP. This concept can be developed by using historical and forecast data of DLMP, whereby it allows for the redistribution of the merchandising surplus (MS) gathered by the DSO, who operates the coordinated market, in the form of voltage support, congestion and loss surcharge from the prosumers.

6.2.4 Further development of DLMPs

Towards the vision that the distribution grid becomes an active market place for generation and demand-side management, the DLMP scheme needs to be developed further to accommodate not only the stochastic nature of renewables but also different grid technologies, e.g., AC/DC grids. Another factor to be taken into account is the grid topology (meshed/ring topology). It is important to be aware of

that, for DLMPs calculation, the adoption of the nonlinear programming technique in combination with distributed optimization in this work requires the global optimality and strong duality that can only be shown empirically for the tested cases of radial networks. For the meshed network, the optimality can not be guaranteed. Alternative solution methodologies, such as convexified optimal power flow also face difficulty for these cases due to the lack of strong duality. Hence, designing a suitable pricing scheme for this grid setting remains as important future task.

Bibliography

[1] Klaus Schittkowski and Christian Zillober. “Nonlinear Programming: Algorithms, Software, and Applications”. In: *System Modeling and Optimization*. Ed. by John Cagnol and Jean-Paul Zolésio. Boston, MA: Springer US, 2005, pp. 73–107. ISBN: 978-0-387-23467-0.

[2] S. Hanif, K. Zhang, C. M. Hackl, M. Barati, H. B. Gooi, and T. Hamacher. “Decomposition and Equilibrium Achieving Distribution Locational Marginal Prices Using Trust-Region Method”. In: *IEEE Transactions on Smart Grid* 10.3 (May 2019), pp. 3269–3281. ISSN: 1949-3053. DOI: 10.1109/TSG.2018.2822766.

[3] D. K. Molzahn, F. Dörfler, H. Sandberg, S. H. Low, S. Chakrabarti, R. Baldick, and J. Lavaei. “A Survey of Distributed Optimization and Control Algorithms for Electric Power Systems”. In: *IEEE Transactions on Smart Grid* 8.6 (Nov. 2017), pp. 2941–2962. ISSN: 1949-3053. DOI: 10.1109/TSG.2017.2720471.

[4] D. Pudjianto, G. Strbac, and D. Boyer. “Virtual power plant: managing synergies and conflicts between transmission system operator and distribution system operator control objectives”. In: *CIRED - Open Access Proceedings Journal* 2017.1 (2017), pp. 2049–2052. ISSN: 2515-0855. DOI: 10.1049/oap-cired.2017.0829.

[5] A. Papavasiliou. “Analysis of Distribution Locational Marginal Prices”. In: *IEEE Transactions on Smart Grid* (2017), pp. 1–1. ISSN: 1949-3053. DOI: 10.1109/TSG.2017.2673860.

[6] D. Apostolopoulou, S. Bahramirad, and A. Khodaei. “The Interface of Power: Moving Toward Distribution System Operators”. In: *IEEE Power and Energy Magazine* 14.3 (May 2016), pp. 46–51. DOI: 10.1109/MPE.2016.2524960.

[7] F. Rahimi, A. Ipakchi, and F. Fletcher. “The Changing Electrical Landscape: End-to-End Power System Operation Under the Transactive Energy Paradigm”. In: *IEEE Power and Energy Magazine* 14.3 (May 2016), pp. 52–62. DOI: 10.1109/MPE.2016.2524966.

[8] F.C. Schweppe, M.C. Caramanis, R.D. Tabors, and R.E. Bohn. *Spot Pricing of Electricity*. Power Electronics and Power Systems. Springer US, 1988. ISBN: 9780898382600.

[9] M. C. Caramanis, R. E. Bohn, and F. C. Schweppe. “Optimal Spot Pricing: Practice and Theory”. In: *IEEE Transactions on Power Apparatus and Systems* PAS-101.9 (Sept. 1982), pp. 3234–3245. DOI: 10.1109/TPAS.1982.317507.

[10] A. S. Siddiqui, C. Marnay, and M. Khavkin. “Spot pricing of electricity and ancillary services in a competitive California market”. In: *Proceedings of the 34th Annual Hawaii International Conference on System Sciences*. Jan. 2001, p. 9. DOI: 10.1109/HICSS.2001.926290.

[11] Tong Wu, M. Rothleder, Z. Alaywan, and A. D. Papalexopoulos. “Pricing energy and ancillary services in integrated market systems by an optimal power flow”. In: *IEEE Transactions on Power Systems* 19.1 (Feb. 2004), pp. 339–347. ISSN: 0885-8950. DOI: 10.1109/TPWRS.2003.820701.

[12] S. Repo, S. Lu, T. Pöhö, D. D. Giustina, G. Ravera, J. M. Selga, and F. A. Figuerola. “Active distribution network concept for distributed management of low voltage network”. In: *IEEE PES ISGT Europe 2013*. Oct. 2013, pp. 1–5. DOI: 10.1109/ISGTEurope.2013.6695428.

[13] M. Caramanis, E. Ntakou, W. W. Hogan, A. Chakrabortty, and J. Schoene. “Co-Optimization of Power and Reserves in Dynamic T&D Power Markets With Nondispatchable Renewable Generation and Distributed Energy Resources”. In: *Proceedings of the IEEE* 104.4 (Apr. 2016), pp. 807–836. ISSN: 0018-9219. DOI: 10.1109/JPROC.2016.2520758.

[14] Julia Merino, Inés Gómez, Elena Turienzo, and Carlos Madina. *Ancillary service provision by RES and DSM connected at distribution level in the future power system*. Tech. rep. TECNALIA, Dec. 2016. URL: http://smartnet-project.eu/wp-content/uploads/2016/12/D1-1_20161220_V1.0.pdf.

[15] A. Papavasiliou and I. Mezghani. “Coordination Schemes for the Integration of Transmission and Distribution System Operations”. In: *2018 Power Systems Computation Conference (PSCC)*. June 2018, pp. 1–7. DOI: 10.23919/PSCC.2018.8443022.

[16] S. Huang, Q. Wu, H. Zhao, and C. Li. “Distributed Optimization based Dynamic Tariff for Congestion Management in Distribution Networks”. In: *IEEE Transactions on Smart Grid* (2018), pp. 1–1. ISSN: 1949-3053. DOI: 10.1109/TSG.2017.2735998.

[17] S. Hanif, P. Creutzburg, H. B. Gooi, and T. Hamacher. “Pricing Mechanism for Flexible Loads Using Distribution Grid Hedging Rights”. In: *IEEE Transactions on Power Systems* 34.5 (Sept. 2019), pp. 4048–4059. DOI: 10.1109/TPWRS.2018.2862149.

[18] Chris Giotitsas, Alex Pazaitis, and Vasilis Kostakis. “A peer-to-peer approach to energy production”. In: *Technology in Society* 42 (2015), pp. 28–38. ISSN: 0160-791X. DOI: https://doi.org/10.1016/j.techsoc.2015.02.002. URL: http://www.sciencedirect.com/science/article/pii/S0160791X15000251.

[19] Juhar Abdella and Khaled Shuaib. “Peer to Peer Distributed Energy Trading in Smart Grids: A Survey”. In: *Energies* 11.6 (2018). ISSN: 1996-1073. DOI: 10.3390/en11061560.

[20] Yue Zhou, Jianzhong Wu, and Chao Long. “Evaluation of peer-to-peer energy sharing mechanisms based on a multiagent simulation framework”. In: *Applied Energy* 222 (2018), pp. 993–1022. ISSN: 0306-2619. DOI: https://doi.org/10.1016/j.apenergy.2018.02.089.

[21] R. S. Fang and A. K. David. “Transmission congestion management in an electricity market”. In: *IEEE Transactions on Power Systems* 14.3 (Aug. 1999), pp. 877–883. ISSN: 0885-8950. DOI: 10.1109/59.780898.

[22] William W. Hogan. *Regional Transmission Organizations: Designing Market Institutions For Electric Network Systems*. 2000. URL: https://tinyurl.com/yaq2ezrq.

[23] USA Federal Energy Regulatory Commission: Order No. 2000. *Regional Transmission Organization*. 1999. URL: https://tinyurl.com/yaq2ezrq.

[24] F. Moret and P. Pinson. “Energy Collectives: a Community and Fairness based Approach to Future Electricity Markets”. In: *IEEE Transactions on Power Systems* (2018), pp. 1–1. ISSN: 0885-8950. DOI: 10.1109/TPWRS.2018.2808961.

[25] J. Guerrero, A. C. Chapman, and G. Verbič. “Decentralized P2P Energy Trading Under Network Constraints in a Low-Voltage Network”. In: *IEEE Transactions on Smart Grid* 10.5 (Sept. 2019), pp. 5163–5173. DOI: 10.1109/TSG.2018.2878445.

[26] Pol Olivella-Rosell, Pau Lloret-Gallego, Íngrid Munné-Collado, Roberto Villafafila-Robles, Andreas Sumper, Stig Ødegaard Ottessen, Jayaprakash Rajasekharan, and Bernt A. Bremdal. “Local flexibility market design for aggregators providing multiple flexibility services at distribution network level”. In: *Energies* 11.4 (2018), pp. 1–19. ISSN: 19961073. DOI: 10.3390/en11040822.

[27] T. Baroche, P. Pinson, R. Le Goff Latimier, and H. Ben Ahmed. “Exogenous Cost Allocation in Peer-to-Peer Electricity Markets”. In: *IEEE Transactions on Power Systems* (2019), pp. 1–1. ISSN: 0885-8950. DOI: 10.1109/TPWRS.2019.2896654.

[28] J. Kim and Y. Dvorkin. “A P2P-dominant Distribution System Architecture”. In: *IEEE Transactions on Power Systems* (2019). to be published. ISSN: 1558-0679. DOI: 10.1109/TPWRS.2019.2961330.

[29] T. Morstyn, A. Teytelboym, C. Hepburn, and M. D. McCulloch. “Integrating P2P Energy Trading with Probabilistic Distribution Locational Marginal Pricing”. In: *IEEE Transactions on Smart Grid* (2019). to be published. ISSN: 1949-3061. DOI: 10.1109/TSG.2019.2963238.

[30] T. Morstyn, A. Teytelboym, and M. D. McCulloch. “Designing Decentralized Markets for Distribution System Flexibility”. In: *IEEE Transactions on Power Systems* 34.3 (May 2019), pp. 2128–2139. ISSN: 0885-8950. DOI: 10.1109/TPWRS.2018.2886244.

[31] T. Morstyn, A. Teytelboym, and M. D. Mcculloch. “Bilateral Contract Networks for Peer-to-Peer Energy Trading”. In: *IEEE Transactions on Smart Grid* 10.2 (Mar. 2019), pp. 2026–2035. ISSN: 1949-3053. DOI: 10.1109/TSG.2017.2786668.

[32] T. Morstyn and M. D. McCulloch. “Multiclass Energy Management for Peer-to-Peer Energy Trading Driven by Prosumer Preferences”. In: *IEEE Transactions on Power Systems* 34.5 (Sept. 2019), pp. 4005–4014. ISSN: 0885-8950. DOI: 10.1109/TPWRS.2018.2834472.

[33] T. Soares, R. J. Bessa, P. Pinson, and H. Morais. “Active Distribution Grid Management Based on Robust AC Optimal Power Flow”. In: *IEEE Transactions on Smart Grid* 9.6 (Nov. 2018), pp. 6229–6241. ISSN: 1949-3053. DOI: 10.1109/TSG.2017.2707065.

[34] H. Yuan, F. Li, Y. Wei, and J. Zhu. “Novel Linearized Power Flow and Linearized OPF Models for Active Distribution Networks With Application in Distribution LMP”. In: *IEEE Transactions on Smart Grid* 9.1 (Jan. 2018), pp. 438–448. ISSN: 1949-3053. DOI: 10.1109/TSG.2016.2594814.

[35] L. Bai, J. Wang, C. Wang, C. Chen, and F. F. Li. “Distribution Locational Marginal Pricing (DLMP) for Congestion Management and Voltage Support”. In: *IEEE Transactions on Power Systems* PP.99 (2017), pp. 1–1. ISSN: 0885-8950. DOI: 10.1109/TPWRS.2017.2767632.

[36] S. Huang, Q. Wu, S. S. Oren, R. Li, and Z. Liu. “Distribution Locational Marginal Pricing Through Quadratic Programming for Congestion Management in Distribution Networks”. In: *IEEE Transactions on Power Systems* 30.4 (July 2015), pp. 2170–2178. ISSN: 0885-8950. DOI: 10.1109/TPWRS.2014.2359977.

[37] Z. Yuan, M. R. Hesamzadeh, and D. Biggar. “Distribution Locational Marginal Pricing by Convexified ACOPF and Hierarchical Dispatch”. In: *IEEE Transactions on Smart Grid* (2016), pp. 1–1. ISSN: 1949-3053. DOI: 10.1109/TSG.2016.2627139.

[38] S. Hanif, H. B. Gooi, T. Massier, T. Hamacher, and T. Reindl. “Distributed Congestion Management of Distribution Grids Under Robust Flexible Buildings Operations”. In: *IEEE Transactions on Power Systems* 32.6 (Nov. 2017), pp. 4600–4613. ISSN: 0885-8950. DOI: 10.1109/TPWRS.2017.2660065.

[39] S. Hanif, T. Massier, H. B. Gooi, T. Hamacher, and T. Reindl. “Cost Optimal Integration of Flexible Buildings in Congested Distribution Grids”. In: *IEEE Transactions on Power Systems* 32.3 (May 2017), pp. 2254–2266. ISSN: 0885-8950. DOI: 10.1109/TPWRS.2016.2605921.

[40] X. Zhou, E. Dall’Anese, L. Chen, and A. Simonetto. “An Incentive-based Online Optimization Framework for Distribution Grids”. In: *IEEE Transactions on Automatic Control* PP.99 (2017), pp. 1–1. ISSN: 0018-9286. DOI: 10.1109/TAC.2017.2760284.

[41] Joshua Adam Taylor. *Convex Optimization of Power Systems*. Cambridge University Press, 2015. DOI: 10.1017/CBO9781139924672.

[42] S. Prabhakar Karthikeyan, I. Jacob Raglend, and D.P. Kothari. “A review on market power in deregulated electricity market”. In: *International Journal of Electrical Power & Energy Systems* 48 (2013), pp. 139–147. ISSN: 0142-0615. DOI: https://doi.org/10.1016/j.ijepes.2012.11.024.

[43] K. Zhang, S. Troitzsch, S. Hanif, and T. Hamacher. “Coordinated Market Design for Peer-to-Peer Energy Trade and Ancillary Services in Distribution Grids”. In: *IEEE Transactions on Smart Grid* 11.4 (2020), pp. 2929–2941. DOI: doi:10.1109/TSG.2020.2966216.

[44] K. Zhang, S. Hanif, C. M. Hackl, and T. Hamacher. “A Framework for Multi-Regional Real-Time Pricing in Distribution Grids”. In: *IEEE Transactions on Smart Grid* 10.6 (Nov. 2019), pp. 6826–6838. DOI: 10.1109/TSG.2019.2911996.

[45] S. Troiztsch, M. Grussmann, K. Zhang, and T. Hamacher. “Distribution Locational Marginal Pricing for Combined Thermal and Electric Grid Operation”. In: *2020 IEEE Innovative Smart Grid Technologies - Europe (ISGT Europe)*. accepted. 2020.

[46] S. Candas, K. Zhang, and T. Hamacher. “A Comparative Study of Benders Decomposition and ADMM for Decentralized Optimal Power Flow”. In: *2020 IEEE Power Energy Society Innovative Smart Grid Technologies Conference (ISGT)*. to be published. 2020.

[47] K. Zhang, S. Hanif, and T. Hamacher. “Decentralized Voltage Support in a Competitive Energy Market”. In: *2019 IEEE Power Energy Society Innovative Smart Grid Technologies Conference (ISGT)*. Feb. 2019, pp. 1–5. DOI: 10.1109/ISGT.2019.8791571.

[48] S. Hanif, K. Zhang, and T. Hamacher. “Coordinated Market Mechanism for Economic Dispatch in Active Distribution Grids”. In: *2019 IEEE Power Energy Society General Meeting (PESGM)*. Aug. 2019, pp. 1–5. DOI: 10.1109/PESGM40551.2019.8973817.

[49] K. Zhang, S. Hanif, S. Troitzsch, and T. Hamacher. “Day-ahead Energy Trade Scheduling for Multiple Microgrids with Network Constraints”. In: *2019 IEEE Power Energy Society General Meeting (PESGM)*. Aug. 2019, pp. 1–5. DOI: 10.1109/PESGM40551.2019.8973609.

[50] S. Troitzsch, S. Hanif, K. Zhang, A. Trpovski, and T. Hamacher. “Flexible Distribution Grid Demonstrator (FLEDGE): Requirements and Software Architecture”. In: *2019 IEEE Power Energy Society General Meeting (PESGM)*. Aug. 2019, pp. 1–5. DOI: 10.1109/PESGM40551.2019.8973567.

[51] K. Zhang, D. Recalde, T. Massier, and T. Hamacher. “Charging Demonstrator for Ancillary Service Provision in Smart Grids”. In: *2018 IEEE Innovative Smart Grid Technologies - Asia (ISGT Asia)*. May 2018, pp. 988–993. DOI: 10.1109/ISGT-Asia.2018.8467795.

[52] K. Zhang, D. Recalde, T. Massier, and T. Hamacher. “Fast Online Distributed Voltage Support in Distribution Grids using Consensus Algorithm”. In: *2018 IEEE Innovative Smart Grid Technologies - Asia (ISGT Asia)*. May 2018, pp. 350–355. DOI: 10.1109/ISGT-Asia.2018.8467821.

[53] D. Recalde, A. Trpovski, S. Troitzsch, K. Zhang, S. Hanif, and T. Hamacher. “A Review of Operation Methods and Simulation Requirements for Future Smart Distribution Grids”. In: *2018 IEEE Innovative Smart Grid Technologies - Asia (ISGT Asia)*. May 2018, pp. 475–480. DOI: 10.1109/ISGT-Asia.2018.8467850.

[54] K. Zhang, S. Hanif, and D. Recalde. “Clustering-based decentralized optimization approaches for DC optimal power flow”. In: *2017 IEEE Innovative Smart Grid Technologies - Asia (ISGT-Asia)*. Dec. 2017, pp. 1–6. DOI: 10.1109/ISGT-Asia.2017.8378334.

[55] K. Turitsyn, P. Sulc, S. Backhaus, and M. Chertkov. “Options for Control of Reactive Power by Distributed Photovoltaic Generators”. In: *Proceedings of the IEEE* 99.6 (June 2011), pp. 1063–1073. ISSN: 0018-9219. DOI: 10.1109/JPROC.2011.2116750.

[56] Nikos Hatziargyriou. *Microgrid: Architecture and Control*. Wiley, 2014. ISBN: 9781118720684.

[57] M. Rezkallah, A. Hamadi, A. Chandra, and B. Singh. “Design and Implementation of Active Power Control With Improved P&O Method for Wind-PV-Battery-Based Standalone Generation System”. In: *IEEE Transactions on Industrial Electronics* 65.7 (July 2018), pp. 5590–5600. ISSN: 0278-0046. DOI: 10.1109/TIE.2017.2777404.

[58] V. Kekatos, G. Wang, A. J. Conejo, and G. B. Giannakis. “Stochastic Reactive Power Management in Microgrids With Renewables”. In: *IEEE Transactions on Power Systems* 30.6 (Nov. 2015), pp. 3386–3395. ISSN: 0885-8950. DOI: 10.1109/TPWRS.2014.2369452.

[59] K. Desrochers, V. Hines, F. Wallace, J. Slinkman, A. Giroux, A. Khurram, M. Amini, M. Almassalkhi, and P. D. H. Hines. “Real-world, Full-scale Validation of Power Balancing Services from Packetized Virtual Batteries”. In: *2019 IEEE Power Energy Society Innovative Smart Grid Technologies Conference (ISGT)*. Feb. 2019, pp. 1–5. DOI: 10.1109/ISGT.2019.8791628.

[60] I. Chakraborty, S. P. Nandanoori, and S. Kundu. “Virtual Battery Parameter Identification Using Transfer Learning Based Stacked Autoencoder”. In: *2018 17th IEEE International Conference on Machine Learning and Applications (ICMLA)*. Dec. 2018, pp. 1269–1274. DOI: 10.1109/ICMLA.2018.00206.

[61] J. T. Hughes, A. D. Domínguez-García, and K. Poolla. “Identification of Virtual Battery Models for Flexible Loads”. In: *IEEE Transactions on Power Systems* 31.6 (Nov. 2016), pp. 4660–4669. DOI: 10.1109/TPWRS.2015.2505645.

[62] A. Bernstein, C. Wang, E. Dall’Anese, J. Le Boudec, and C. Zhao. “Load Flow in Multiphase Distribution Networks: Existence, Uniqueness, Non-Singularity and Linear Models”. In: *IEEE Transactions on Power Systems* 33.6 (Nov. 2018), pp. 5832–5843. DOI: 10.1109/TPWRS.2018.2823277.

[63] S. Bolognani and F. Dörfler. “Fast power system analysis via implicit linearization of the power flow manifold”. In: *2015 53rd Annual Allerton Conference on Communication, Control, and Computing (Allerton)*. Sept. 2015, pp. 402–409. DOI: 10.1109/ALLERTON.2015.7447032.

[64] S. Hanif, M. Barati, A. Kargarian, H. B. Gooi, and T. Hamacher. “Multiphase Distribution Locational Marginal Prices: Approximation and Decomposition”. In: *2018 IEEE Power Energy Society General Meeting (PESGM)*. Aug. 2018, pp. 1–5. DOI: 10.1109/PESGM.2018.8585925.

[65] Sarmad Hanif. “Distribution Locational Marginal Price: Approximations, Solution Algorithm and Organization”. Dissertation. München: Technische Universität München, 2018.

[66] R. D. Zimmerman and C. E. Murillo-Sanchez. *MATPOWER User’s Manual, Version 7.0.* 2019. DOI: 10.5281/zenodo.3251118.

[67] W. F. Tinney and C. E. Hart. “Power Flow Solution by Newton’s Method”. In: *IEEE Transactions on Power Apparatus and Systems* PAS-86.11 (Nov. 1967), pp. 1449–1460. ISSN: 0018-9510. DOI: 10.1109/TPAS.1967.291823.

[68] S. Bolognani and S. Zampieri. “On the Existence and Linear Approximation of the Power Flow Solution in Power Distribution Networks”. In: *IEEE Transactions on Power Systems* 31.1 (Jan. 2016), pp. 163–172. ISSN: 0885-8950. DOI: 10.1109/TPWRS.2015.2395452.

[69] K. Christakou, J. LeBoudec, M. Paolone, and D. Tomozei. “Efficient Computation of Sensitivity Coefficients of Node Voltages and Line Currents in Unbalanced Radial Electrical Distribution Networks”. In: *IEEE Transactions on Smart Grid* 4.2 (June 2013), pp. 741–750. ISSN: 1949-3053. DOI: 10.1109/TSG.2012.2221751.

[70] M. Bazrafshan and N. Gatsis. “Comprehensive Modeling of Three-Phase Distribution Systems via the Bus Admittance Matrix”. In: *IEEE Transactions on Power Systems* 33.2 (Mar. 2018), pp. 2015–2029. DOI: 10.1109/TPWRS.2017.2728618.

[71] M. Farivar, L. Chen, and S. Low. “Equilibrium and dynamics of local voltage control in distribution systems”. In: *52nd IEEE Conference on Decision and Control*. Dec. 2013, pp. 4329–4334. DOI: 10.1109/CDC.2013.6760555.

[72] M. Farivar and S. H. Low. “Branch Flow Model: Relaxations and Convexification—Part I”. In: *IEEE Transactions on Power Systems* 28.3 (Aug. 2013), pp. 2554–2564. ISSN: 0885-8950. DOI: 10.1109/TPWRS.2013.2255317.

[73] D. Shchetinin, T. T. De Rubira, and G. Hug. “Conservative linear line flow constraints for AC optimal power flow”. In: *2017 IEEE Manchester PowerTech*. June 2017, pp. 1–6. DOI: 10.1109/PTC.2017.7981156.

[74] Daniel Zimmerman Ray, Edmundo Murillo Sanchez Carlos, and John Thomas Robert. “MATPOWER: Steady-State Operations, Planning, and Analysis Tools for Power Systems Research and Education”. In: *IEEE Transactions on Power Systems* 26.1 (2011), pp. 12–19. ISSN: 0885-8950. DOI: 10.1109/TPWRS.2010.2051168.

[75] H.M. Khodr, F.G. Olsina, P.M. De Oliveira-De Jesus, and J.M. Yusta. “Maximum savings approach for location and sizing of capacitors in distribution systems”. In: *Electric Power Systems Research* 78.7 (2008), pp. 1192–1203. ISSN: 0378-7796. DOI: https://doi.org/10.1016/j.epsr.2007.10.002.

[76] S. H. Low. “Convex Relaxation of Optimal Power Flow—Part I: Formulations and Equivalence”. In: *IEEE Transactions on Control of Network Systems* 1.1 (Mar. 2014), pp. 15–27. DOI: 10.1109/TCNS.2014.2309732.

[77] W. Wei, J. Wang, N. Li, and S. Mei. “Optimal Power Flow of Radial Networks and Its Variations: A Sequential Convex Optimization Approach”. In: *IEEE Transactions on Smart Grid* 8.6 (Nov. 2017), pp. 2974–2987. ISSN: 1949-3053. DOI: 10.1109/TSG.2017.2684183.

[78] Richard H. Byrd, Jean Charles Gilbert, and Jorge Nocedal. “A trust region method based on interior point techniques for nonlinear programming”. In: *Mathematical Programming* 89.1 (Nov. 2000), pp. 149–185. ISSN: 1436-4646. DOI: 10.1007/PL00011391.

[79] Richard H. Byrd, Mary E. Hribar, and Jorge. Nocedal. “An Interior Point Algorithm for Large-Scale Nonlinear Programming”. In: *SIAM Journal on Optimization* 9.4 (1999), pp. 877–900. DOI: 10.1137/S1052623497325107.

[80] J. Lavaei, D. Tse, and B. Zhang. “Geometry of Power Flows and Optimization in Distribution Networks”. In: *IEEE Transactions on Power Systems* 29.2 (Mar. 2014), pp. 572–583. DOI: 10.1109/TPWRS.2013.2282086.

[81] Stephen Boyd and Lieven Vandenberghe. *Convex Optimization*. Cambridge University Press, 2004. DOI: 10.1017/CBO9780511804441.

[82] R. A. Verzijlbergh, L. J. De Vries, and Z. Lukszo. “Renewable Energy Sources and Responsive Demand. Do We Need Congestion Management in the Distribution Grid?” In: *IEEE Transactions on Power Systems* 29.5 (Sept. 2014), pp. 2119–2128. DOI: 10.1109/TPWRS.2014.2300941.

[83] Stephen Boyd, Neal Parikh, Eric Chu, Borja Peleato, and Jonathan Eckstein. “Distributed Optimization and Statistical Learning via the Alternating Direction Method of Multipliers”. In: *Foundations and Trends in Machine Learning* 3.1 (2011), pp. 1–122. ISSN: 1935-8237. DOI: 10.1561/2200000016. URL: http://dx.doi.org/10.1561/2200000016.

[84] J. Xu, H. Sun, and C. J. Dent. “ADMM-Based Distributed OPF Problem Meets Stochastic Communication Delay”. In: *IEEE Transactions on Smart Grid* 10.5 (Sept. 2019), pp. 5046–5056. ISSN: 1949-3053. DOI: 10.1109/TSG.2018.2873650.

[85] Léon Walras. *Éléments d’économie politique pure, ou, Théorie de la richesse sociale*. F. Rouge, 1896.

[86] H. Uzawa. “Walras’ Tâtonnement in the Theory of Exchange”. In: *The Review of Economic Studies* 27.3 (1960), pp. 182–194. ISSN: 00346527, 1467-937X.

[87] Matt Kraning, Eric Chu, Javad Lavaei, and Stephen Boyd. “Dynamic Network Energy Management via Proximal Message Passing”. In: *Found. Trends Optim.* 1.2 (Jan. 2014), pp. 73–126. ISSN: 2167-3888. DOI: 10.1561/2400000002. URL: http://dx.doi.org/10.1561/240000-%200002.

[88] G. Hug, S. Kar, and C. Wu. “Consensus + Innovations Approach for Distributed Multiagent Coordination in a Microgrid”. In: *IEEE Transactions on Smart Grid* 6.4 (July 2015), pp. 1893–1903. DOI: 10.1109/TSG.2015.2409053.

[89] A. Kargarian, J. Mohammadi, J. Guo, S. Chakrabarti, M. Barati, G. Hug, S. Kar, and R. Baldick. “Toward Distributed/Decentralized DC Optimal Power Flow Implementation in Future Electric Power Systems”. In: *IEEE Transactions on Smart Grid* 9.4 (July 2018), pp. 2574–2594. DOI: 10.1109/TSG.2016.2614904.

[90] J. F. Benders. “Partitioning procedures for solving mixed-variables programming problems”. In: *Numerische Mathematik* 4.1 (Dec. 1962), pp. 238–252. ISSN: 0945-3245. DOI: 10.1007/BF01386316.

[91] S. Kar, J. M. F. Moura, and K. Ramanan. “Distributed Parameter Estimation in Sensor Networks: Nonlinear Observation Models and Imperfect Communication”. In: *IEEE Transactions on Information Theory* 58.6 (June 2012), pp. 3575–3605. DOI: 10.1109/TIT.2012.2191450.

[92] *The Strategic Energy Technology (SET) Plan*. Tech. rep. European Union, 2017. DOI: doi:10.2777/476339.

[93] *Merkblatt: Erneuerbare Energien "Premium"*. Tech. rep. KfW, 2020.

[94] *Flexible Ramping Product Revised Draft Final Proposal*. Tech. rep. California ISO, 2015.

[95] Alberto Longo, Anil Markandya, and Marta Petrucci. “The internalization of externalities in the production of electricity: Willingness to pay for the attributes of a policy for renewable energy”. In: *Ecological Economics* 67.1 (2008), pp. 140–152. ISSN: 0921-8009. DOI: https://doi.org/10.1016/j.ecolecon.2007.12.006. URL: http://www.sciencedirect.com/science/article/pii/S0921800907006064.

[96] Andrea Tabi, Stefanie Lena Hille, and Rolf Wüstenhagen. “What makes people seal the green power deal? — Customer segmentation based on choice experiment in Germany”. In: *Ecological Economics* 107 (2014), pp. 206–215. ISSN: 0921-8009. DOI: https://doi.org/10.1016/j.ecolecon.2014.09.004. URL: http://www.sciencedirect.com/science/article/pii/S0921800914002742.

[97] P. G. D. Silva, S. Karnouskos, and D. Ilic. “A survey towards understanding residential prosumers in smart grid neighbourhoods”. In: *2012 3rd IEEE PES Innovative Smart Grid Technologies Europe (ISGT Europe)*. Oct. 2012, pp. 1–8. DOI: 10.1109/ISGTEurope.2012.6465864.

[98] Esther Mengelkamp, Johannes Gärttner, Kerstin Rock, Scott Kessler, Lawrence Orsini, and Christof Weinhardt. “Designing microgrid energy markets: A case study: The Brooklyn Microgrid”. In: *Applied Energy* 210 (2018), pp. 870–880. ISSN: 0306-2619. DOI: https://doi.org/10.1016/j.apenergy.2017.06.054. URL: http://www.sciencedirect.com/science/article/pii/S030626191730805X.

[99] Hélène Le Cadre, Paulin Jacquot, Cheng Wan, and Clémence Alasseur. “Peer-to-peer electricity market analysis: From variational to Generalized Nash Equilibrium”. In: *European Journal of Operational Research* 282.2 (2020), pp. 753–771. ISSN: 0377-2217. DOI: https://doi.org/10.1016/j.ejor.2019.09.035.

[100] W. Tushar, W. Saad, H. V. Poor, and D. B. Smith. “Economics of Electric Vehicle Charging: A Game Theoretic Approach”. In: *IEEE Transactions on Smart Grid* 3.4 (Dec. 2012), pp. 1767–1778. ISSN: 1949-3061. DOI: 10.1109/TSG.2012.2211901.

[101] W. Tushar, T. K. Saha, C. Yuen, P. Liddell, R. Bean, and H. V. Poor. “Peer-to-Peer Energy Trading With Sustainable User Participation: A Game Theoretic Approach”. In: *IEEE Access* 6 (2018), pp. 62932–62943. ISSN: 2169-3536. DOI: 10.1109/ACCESS.2018.2875405.

[102] L. Han, T. Morstyn, and M. McCulloch. “Constructing Prosumer Coalitions for Energy Cost Savings Using Cooperative Game Theory”. In: *2018 Power Systems Computation Conference (PSCC)*. June 2018, pp. 1–7. DOI: 10.23919/PSCC.2018.8443054.

[103] W. Saad, Z. Han, H. V. Poor, and T. Basar. “Game-Theoretic Methods for the Smart Grid: An Overview of Microgrid Systems, Demand-Side Management, and Smart Grid Communications”. In: *IEEE Signal Processing Magazine* 29.5 (Sept. 2012), pp. 86–105. ISSN: 1558-0792. DOI: 10.1109/MSP.2012.2186410.

[104] John Nash. “Non-Cooperative Games”. In: *Annals of Mathematics* 54.2 (1951), pp. 286–295. ISSN: 0003486X.

[105] Francisco Facchinei and Christian Kanzow. “Generalized Nash equilibrium problems”. In: *4OR* 5.3 (Sept. 2007), pp. 173–210. ISSN: 1614-2411. DOI: 10.1007/s10288-007-0054-4. URL: https://doi.org/10.1007/s10288-007-0054-4.

[106] W. Tushar, C. Yuen, H. Mohsenian-Rad, T. Saha, H. V. Poor, and K. L. Wood. “Transforming Energy Networks via Peer-to-Peer Energy Trading: The Potential of Game-Theoretic Approaches”. In: *IEEE Signal Processing Magazine* 35.4 (July 2018), pp. 90–111. ISSN: 1558-0792. DOI: 10.1109/MSP.2018.2818327.

[107] J. Guerrero, A. C. Chapman, and G. Verbič. “Decentralized P2P Energy Trading under Network Constraints in a Low-Voltage Network”. In: *IEEE Transactions on Smart Grid* (2018), pp. 1–1. ISSN: 1949-3053. DOI: 10.1109/TSG.2018.2878445.

[108] R. A. Verzijlbergh, Z. Lukszo, and M. D. Ilić. “Comparing different EV charging strategies in liberalized power systems”. In: *2012 9th International Conference on the European Energy Market*. May 2012, pp. 1–8. DOI: 10.1109/EEM.2012.6254807.

[109] P. Samadi, A. Mohsenian-Rad, R. Schober, V. W. S. Wong, and J. Jatskevich. “Optimal Real-Time Pricing Algorithm Based on Utility Maximization for Smart Grid”. In: *2010 First IEEE International Conference on Smart Grid Communications*. Oct. 2010, pp. 415–420. DOI: 10.1109/SMARTGRID.2010.5622077.

[110] W. Liu and F. Wen. “Discussion on “Distribution Locational Marginal Pricing for Optimal Electric Vehicle Charging Management””. In: *IEEE Transactions on Power Systems* 29.4 (July 2014), pp. 1866–1866. DOI: 10.1109/TPWRS.2014.2325414.

[111] Juan Rosellón and T. Kristiansen. *Financial Transmission Rights*. Springer, 2013. DOI: 10.1007/978-1-4471-4787-9.

[112] R. Olfati-Saber, J. A. Fax, and R. M. Murray. "Consensus and Cooperation in Networked Multi-Agent Systems". In: *Proceedings of the IEEE* 95.1 (Jan. 2007), pp. 215–233. DOI: 10.1109/JPROC.2006.887293.

[113] J. B. Rosen. "Existence and Uniqueness of Equilibrium Points for Concave N-Person Games". In: *Econometrica* 33.3 (1965), pp. 520–534. ISSN: 00129682, 14680262. URL: http://www.jstor.org/stable/1911749.

[114] F. Moret, T. Baroche, E. Sorin, and P. Pinson. "Negotiation Algorithms for Peer-to-Peer Electricity Markets: Computational Properties". In: *2018 Power Systems Computation Conference (PSCC)*. June 2018, pp. 1–7. DOI: 10.23919/PSCC.2018.8442914.

[115] Farzad Salehisadaghiani and Lacra Pavel. "Distributed Nash Equilibrium Seeking via the Alternating Direction Method of Multipliers". In: *IFAC-PapersOnLine* 50.1 (2017). 20th IFAC World Congress, pp. 6166–6171. ISSN: 2405-8963. DOI: https://doi.org/10.1016/j.ifacol.2017.08.983.

[116] M. Ye and G. Hu. "Distributed Nash Equilibrium Seeking by a Consensus Based Approach". In: *IEEE Transactions on Automatic Control* 62.9 (Sept. 2017), pp. 4811–4818. DOI: 10.1109/TAC.2017.2688452.

[117] X. Han, E. G. Kardakos, and G. Hug. "Offering Strategy of a Price-Maker PV Power Plant: Multi-Stage Stochastic Programming with Probabilistic Constraints". In: *2018 Power Systems Computation Conference (PSCC)*. June 2018, pp. 1–7. DOI: 10.23919/PSCC.2018.8442698.

[118] M. E. Baran and F. F. Wu. "Network reconfiguration in distribution systems for loss reduction and load balancing". In: *IEEE Trans. Power Del.* 4.2 (Apr. 1989), pp. 1401–1407. ISSN: 0885-8977. DOI: 10.1109/61.25627.

[119] J. Löfberg. "YALMIP : A Toolbox for Modeling and Optimization in MATLAB". In: *In Proceedings of the CACSD Conference*. Taipei, Taiwan, 2004.

[120] Y. Lin, G. A. Jordan, M. O. Sanford, J. Zhu, and W. H. Babcock. "Economic Analysis of Establishing Regional Transmission Organization and Standard Market Design in the Southeast". In: *IEEE Transactions on Power Systems* 21.4 (Nov. 2006), pp. 1520–1527. ISSN: 0885-8950. DOI: 10.1109/TPWRS.2006.883690.

[121] Tomaso Erseghe. "Network reconfiguration in distribution systems for loss reduction and load balancing". In: *EURASIP Journal on Advances in Signal Processing* 2015.1 (May 2015), p. 45. ISSN: 1687-6180. DOI: 10.1186/s13634-015-0226-x.

[122] Alexander Engelmann, Tialexallmann Mühlpfordt, Yuning Jiang, Boris Houska, and Timm Faulwasser. "Distributed AC Optimal Power Flow using ALADIN". In: *IFAC-Paper- sOnLine* 50.1 (2017). 20th IFAC World Congress, pp. 5536–5541. ISSN: 2405-8963. DOI: https://doi.org/10.1016/j.ifacol.2017.08.1095.

[123] Tomaso Erseghe. “Distributed Optimal Power Flow Using ADMM”. In: *IEEE Transactions on Power Systems* 2015.5 (Sept. 2014), pp. 2370–2380. ISSN: 0885-8950. DOI: 10.1109/TPWRS.2014.2306495.

[124] Changkyu Song, Sejong Yoon, and Vladimir Pavlovic. “Fast ADMM Algorithm for Distributed Optimization with Adaptive Penalty”. In: *Proceedings of the Thirtieth AAAI Conference on Artificial Intelligence*. AAAI’16. Phoenix, Arizona: AAAI Press, 2016, pp. 753–759. URL: http://dl.acm.org/citation.cfm?id=3015812.3015924.

[125] J. Zhang, S. Nabavi, A. Chakrabortty, and Y. Xin. “ADMM Optimization Strategies for Wide-Area Oscillation Monitoring in Power Systems Under Asynchronous Communication Delays”. In: *IEEE Transactions on Smart Grid* 7.4 (July 2016), pp. 2123–2133. ISSN: 1949-3053. DOI: 10.1109/TSG.2016.2547939.

[126] J. Xu, H. Sun, and C. J. Dent. “ADMM-based Distributed OPF Problem Meets Stochastic Communication Delay”. In: *IEEE Transactions on Smart Grid* (2018), pp. 1–1. ISSN: 1949-3053. DOI: 10.1109/TSG.2018.2873650.

[127] H. J. Liu, W. Shi, and H. Zhu. “Distributed Voltage Control in Distribution Networks: Online and Robust Implementations”. In: *IEEE Transactions on Smart Grid* (2017), pp. 1–1. ISSN: 1949-3053. DOI: 10.1109/TSG.2017.2703642.

[128] L. Gan and S. H. Low. “An Online Gradient Algorithm for Optimal Power Flow on Radial Networks”. In: *IEEE Journal on Selected Areas in Communications* 34.3 (Mar. 2016), pp. 625–638. ISSN: 0733-8716. DOI: 10.1109/JSAC.2016.2525598.

[129] LLC Gurobi Optimization. *Gurobi Optimizer Reference Manual*. 2018. URL: http://www.gurobi.com.

[130] Jos F. Sturm. “Using SeDuMi 1.02, A Matlab toolbox for optimization over symmetric cones”. In: *Optimization Methods and Software* 11.1-4 (1999), pp. 625–653. DOI: 10.1080/10556789908805766. eprint: https://doi.org/10.1080/10556789908805766.

[131] Y. Liu, H. Beng Gooi, and H. Xin. “Distributed energy management for the multi-microgrid system based on ADMM”. In: *2017 IEEE Power Energy Society General Meeting*. July 2017, pp. 1–5. DOI: 10.1109/PESGM.2017.8274099.

[132] E. Veldman, M. Gibescu, and A. Postma. “Unlocking the hidden potential of electricity distribition grids”. In: *CIRED 2009 - 20th International Conference and Exhibition on Electricity Distribution - Part 1*. June 2009, pp. 1–4.

[133] Juan M. Morales, Antonio J. Conejo, Henrik Madsen, Pierre Pinson, and Marco Zugno. *Integrating Renewables in Electricity Markets*. 2014th ed. Springer, 2014.

[134] Emilio Benenati, Marcello Colombino, and Emiliano Dall’Anese. “A tractable formulation for multi-period linearized optimal power flow in presence of thermostatically controlled loads”. In: *ArXiv* abs/1908.09167 (2019).

[135] K. Anoh, S. Maharjan, A. Ikpehai, Y. Zhang, and B. Adebisi. “Energy Peer-to-Peer Trading in Virtual Microgrids in Smart Grids: A Game-Theoretic Approach”. In: *IEEE Transactions on Smart Grid* (2019). to be published. ISSN: 1949-3061. DOI: 10.1109/TSG.2019.2934830.

[136] S. Hanif, P. Creutzburg, H. B. Gooi, and T. Hamacher. “Pricing Mechanism for Flexible Loads using Distribution Grid Hedging Rights”. In: *IEEE Transactions on Power Systems* (2018), pp. 1–1. ISSN: 0885-8950. DOI: 10.1109/TPWRS.2018.2862149.

[137] Andy Philpott, Michael Ferris, and Roger Wets. “Equilibrium, uncertainty and risk in hydro-thermal electricity systems”. In: *Mathematical Programming* 157.2 (2016), pp. 483–513.